Application of Ductile Yield Link in Glulam Moment Connections

Sayed Husain Almousawi

Thesis submitted to the faculty of the Virginia Polytechnic Institute and State University in partial fulfillment of the requirements for the degree of

Master of Science
In
Civil Engineering

Matthew R. Eatherton
Daniel P. Hindman
Matthew H. Hebdon

June 8, 2018
Blacksburg, VA

Keywords: Glulam Moment Connection, Yield Link, Ductility, Stiffness

Application of Ductile Yield Link in Glulam Moment Connections

Sayed Husain Almousawi

ABSTRACT

Wood beam-column connections have traditionally been designed as simple shear connections, ignoring their potential moment capacity. A major reason for not utilizing such moment connections is linked to the brittle limit states that wood components exhibit. The purpose of this research was to develop and test a ductile and high-strength wood moment frame connection. A design procedure for such a connection is presented herein.

The proposed glulam beam-column connection utilizes an embedded steel knife plate with a reduced section that acts as a ductile yield link, thus limiting the moment that can be transferred through the connection. This configuration is intended to fail through yielding of the ductile link, thus preventing non-ductile failure mechanisms of wood from occurring. In addition, the connection provides more wood cover over the embedded steel plate, which potentially may increase the connection's fire rating as compared to typical connections.

Two specimens, based on a baseline connection developed using the design procedure presented, were monotonically loaded until failure. Unlike the first specimen, the second was reinforced in the perpendicular-to-grain direction using self-tapping screws. Failure mechanisms were analyzed, and performance characteristics related to the connection's strength, stiffness, and ductility were evaluated. Results indicated that the reinforced specimen exhibited higher strength, stiffness, and ductility compared to the unreinforced specimen. The reinforced specimen showed improvements of 9.49% and 42.2% in yielding and ultimate moment, respectively, compared to the unreinforced specimen. Moreover, an improvement of 31.3% in ductility was obtained using perpendicular-to-grain reinforcement.

Application of Ductile Yield Link in Glulam Moment Connections

Sayed Husain Almousawi

GENERAL AUDIENCE ABSTRACT

Due to the variability of wood properties and its brittle behavior, the joints of wood buildings have traditionally been designed to resist gravity loads only. These types of loads result in predictable behavior of structural wood members at the joints, which helps in simplifying the design process. However, when wood structures are subjected to lateral loads, such as earthquake and wind loads, their joints are likely to fail abruptly as the building sways, resulting in sudden, unpredictable collapse. The purpose of this research was to develop and test a high-strength wood structural joint that can fail gradually and predictably. A design procedure for such a joint is presented herein.

The proposed glue-laminated wood joint utilizes an embedded steel plate with a reduced section that acts as a ductile link. This configuration is intended to fail through gradual deformation of the ductile link, thus preventing brittle wood failure at the joint. In addition, this joint provides more wood cover over the embedded steel plate, which potentially may increase the fire resistance of the joint compared to typical configurations.

Two specimens, based on a baseline joint developed using the design procedure presented, were subjected to slowly-increasing loads until failure. Unlike the first specimen, the second specimen was reinforced in the direction perpendicular to wood grain using long screws to prevent separation of wood layers. Failure mechanisms were analyzed, and the performance characteristics of the two specimens were evaluated and compared. Results indicated that the reinforced specimen exhibited higher strength and improved ductility at failure.

ACKNOWLEDGEMENTS

I am grateful to my committee members, Dr. Eatherton, Dr. Hindman, and Dr. Hebdon, for their tremendous knowledge, contributions, encouragement, and patience. This research would not have been possible without their involvement and guidance.

I am also thankful to Dr. David Mokarem, Brett Farmer, and Dennis Huffman for their ongoing help and advice at the lab. I would also like to thank my colleagues Mahyar and Raul, as well as lab assistants Jamie, Yang, Carolyn, Eric, and Elliot for their help with the test setup preparation.

This endeavor would not have been possible without the support and patience of my wife, Dina. I also acknowledge my parents for encouraging me to take this journey toward the completion of my Master's.

Finally, I am thankful to Boise Cascade for providing the Glulam beams and columns necessary to build and test the specimens, and to Blue Ridge Timberwrights for providing me with their chain mortiser.

TABLE OF CONTENTS

LIST OF FIGURES

LIST OF TABLES

CHAPTER 1: INTRODUCTION

1.1 Motivation

Given the growing awareness of, and attention to, sustainability and energy efficiency in recent years, the interest in wood construction has increased. When harvested sustainably, this material becomes a renewable resource. In general, wood buildings consume relatively low energy (Canadian Wood Council, 2002). Additionally, wood has the ability to absorb carbon dioxide (CO_2), unlike other construction materials that often release this gas and other harmful greenhouse gases during the manufacturing process (Organschi et al., 2016).

Despite the high strength-to-weight ratio of wood, the allowable stresses of solid wood are significantly lower than those of other common structural materials due to the higher variability of mechanical properties (Milner, 2009). Light timber framing is a common construction system in North America, but it is generally limited to housing and other low-rise buildings. To utilize wood structural systems in taller and more resilient buildings, it is necessary to develop wood with less variability. Heavy timber framing allows for more capable systems, but the spans are limited, and the capacity of their connections remain a concern. Consequently, engineered wood products (EWP) with higher strengths and less variability have been developed in various forms.

Glue-laminated wood—commonly referred to as glulam—is a type of EWP that is manufactured for use in structural building systems, especially as beams and columns. Glulam is composed of wood layers adhered together with structural-grade adhesives so that all grain directions are parallel. This controlled manufacturing process results in improved structural components with higher stress grades, greater predictability in their behavior under load, and longer spans compared to solid wood components. Because glulam is manufactured in layers, higher-quality laminations can be placed in locations of higher stresses, allowing for more efficient layer distributions (Milner, 2009). Additionally, glulam components can be fabricated into large structural elements, with transportation restrictions being the major barrier.

While glulam and other engineered wood products facilitate the design of stronger wood structural systems in comparison to sawn lumber, the connections of such systems still tend to be designed as simple shear connections. That is, the relatively small moment capacity offered by these traditional connections is ignored by structural engineers. Experiments have revealed the weaknesses of such connections under bending moments, as is discussed in Chapter 2. The typical

beam-column configuration incorporates a steel plate that is embedded in both wood elements, with bolts inserted horizontally from the sides of the elements. The brittle failures often shown by these connections—namely failures due to tension perpendicular to wood grain, longitudinal shear stresses, and embedment failure—are major reasons for neglecting the moment strength (Lam et al., 2008). Typically, when such connections are subjected to large bending moments, the steel components in the beam induce high tensile stresses in the perpendicular-to-grain direction. Perpendicular-to-grain tension and longitudinal shear are known to be the weakest properties of wood, and they often occur concurrently (Lam et al., 2008; Milner, 2009). Therefore, to utilize these connections in wood moment frames, they should be designed to avoid brittle wood limit states.

While wood shear walls provide an alternative to moment frames, especially in seismic applications, their advantages come with some notable drawbacks. Shear walls lack the flexibility of moment frames since they have limitations on the dimension and placement of openings. Thus, researchers have been looking into various techniques to improve glulam beam-column moment-resisting connections because they are usually the dominant factor in the behavior of structural frames (Andreolli et al., 2011). The main purpose of these improvements is to increase strength and prevent the brittle wood limit states from governing the performance of the connection. Some researchers have attempted to strengthen wood using perpendicular-to-grain reinforcements, while others have designed steel components to yield before the wood limit states can be reached. While many of these connections provided sufficient strength, ductility, and stiffness, limitations still exist. Many joints incorporate exposed steel elements, which require fireproofing to pass certain fire-rating requirements. Other joints are intricate and may be incompatible with multi-bay moment frames. Therefore, it is necessary to develop an improved wood moment frame connection that overcomes these limitations.

1.2 Scope of Work

The purpose of this research was to develop a new type of wood moment connection. A specific configuration of this connection was designed in an attempt to overcome the limitations described in the previous section. This configuration was built and subjected to moment-resistance tests to evaluate its performance. The connection utilizes a T-shaped steel plate that is embedded inside slots in the glulam beam-column joint. The portion of the plate inside the beam has a reduced

section near the column interface. The plate is secured to the beam and column using bolts inserted through pre-drilled holes in the wood and steel components. The objectives of this connection are:

- Develop a plastic hinge in the reduced section of the steel plate when the connection approaches failure under increasing moment.
- Design the brittle wood limit states to be stronger than the strain-hardened plastic hinge in the reduced plate section.
- Embed the steel connector inside wood components for improved fire resistance and enhanced fire rating.

The *National Design Specification for Wood Construction* (American Wood Council, 2015) was used as a guide to design the connection configuration, given the properties and thickness of both the steel plate and wood components, as well as the properties and diameter of fasteners. Minimum spacing requirements for the steel plate and wood components were followed and adjusted to the required strength of the connection. The reduced portion in the steel plate was designed to a lower strength in comparison to the plate, bolts, and glulam configurations at both the beam and column. This design process enables the reduced portion to undergo plastic deformations before the brittle wood limit states occur.

The developed connection design was then used to build two similar test specimens. The second specimen utilized the same design as the first one, but included self-tapping screw reinforcement. The two specimens were subjected to monotonic tests that were performed at the Thomas M. Murray Structures Lab at Virginia Tech. The performance and behavior of the connection specimens were analyzed using test data and applicable plots. The moment capacity was compared to calculations, while ductility and failure behavior were also assessed. A comparison between the performance of the two test specimens was presented. Finally, conclusions about the performance and behavior of the tested connections are made and recommendations for future work are provided.

1.3 Thesis Organization

This thesis provides an overview of the glulam and current research related to wood moment frame connections, identifies their limitations, presents an improved connection design,

shows experimental results and conclusions, and provides recommendations for future research related to the topic. The report is organized as follows:

Chapter 1 provides a brief introduction to glue-laminated (glulam) structural components and their structural properties related to moment strength. This chapter then discusses the importance and advantages of wood moment frame connections, specifies the limitations of available moment connections, and presents the motivation for addressing these limitations and the approach taken.

Chapter 2 presents a detailed discussion of wood limit states in moment connections. It also presents the literature on traditional and modified wood connections subjected to moment tests, as well as novel connection designs with improved moment strength and ductility.

Chapter 3 presents the development of the novel connection configuration and how it addresses persistent problems found in available wood moment frame connections. Detailed calculations of the design are provided in the form of an example connection design that was called Baseline Connection.

Chapter 4 provides details regarding the test specimens, fabrication procedures, instrumentation, and testing methods.

Chapter 5 presents and discusses test results of the two specimens. Specifically, the behaviors of the specimens were examined in detail throughout the test through plots, pictures, and observations. Comparisons between the two specimens are detailed in this chapter.

Chapter 6 summarizes the research and presents concluding remarks. Recommendations and guidance for future work related to the development of this research are then provided.

CHAPTER 2: LITERATURE REVIEW

2.1 Traditional Wood Connections

Traditional wood connections generally consist of a steel plate embedded within a thin vertical cut at the support end of a wood beam, as can be seen in Figure 2.1 and Figure 2.2. This plate is welded to another perpendicular plate in a T-shape configuration attached through bolts to the side of the column facing the beam. Alternative attachment techniques also include extending the plate from the beam through a vertical slit in the column or placing the plate on the outside of the beam-column joint, as in the connection shown in Figure 2.2. Although these connections have some moment capacity, they are typically designed to resist shear only. Ignoring the moment resistance is due to the undesirable non-ductile behavior of wood near the maximum loading capacity of the connection (Lam et al., 2008).

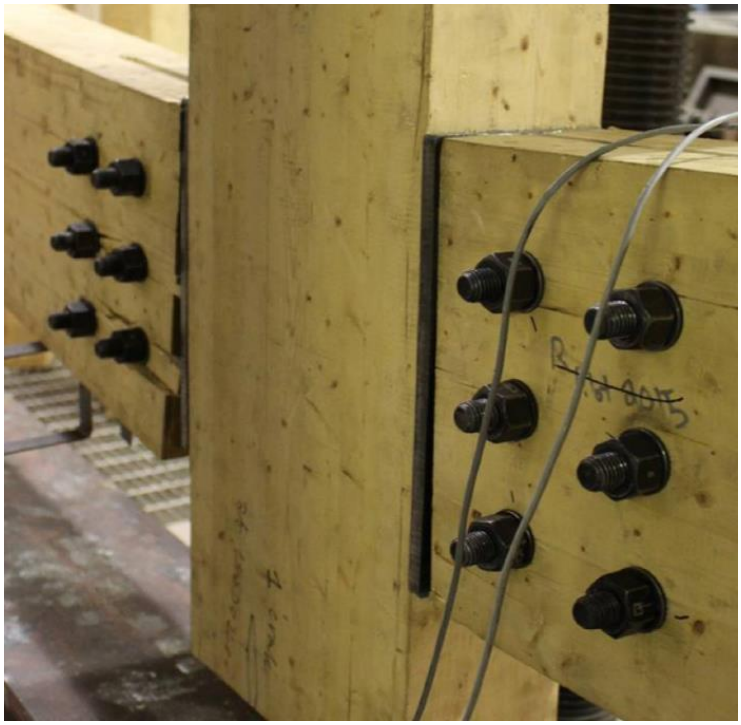

Figure 2.1 An example of a typical traditional wood connection (Salem & Petrycki, 2016).

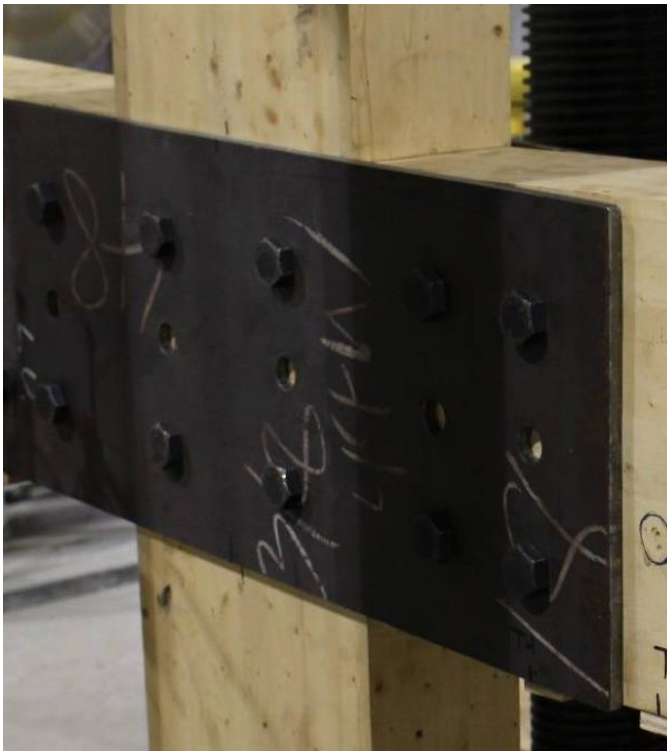

Figure 2.2 Another variation of a typical wood connection (Salem, 2016).

2.1.1 Limit States of Traditional Wood Moment Connections

As a structural material, wood features limit states that must be considered when designing moment-resisting connections. Wood components typically exhibit brittle failure mechanisms, especially at the beam-column connections in structural systems. Structures that are subjected to earthquake loading require ductile connection behavior that allows them to deform inelastically without failing.

In wood connections, there are three major brittle limit states that are commonly observed. A splitting failure limit state occurs when the tension perpendicular to wood grain exceeds the corresponding capacity. Perpendicular-to-grain tension—most commonly along the vertical axis of the beam—is one of the weakest mechanical properties of wood (Lam et al., 2008; Takač et al., 2008). When this limit state occurs, the wood separates as a crack propagates along the horizontal plane of a row of bolts. An example of this failure type can be seen in Figure 2.3.

Figure 2.3 Wood splitting failure (Karagiannis et al., 2016).

Another brittle wood limit state is row shear-out—sometimes referred to as plug shear—whereby a horizontal row of bolts tears out the block of wood along the direction of that same bolt row. In some cases, only the lowest line of bolts tears out the block of wood closer to the beam's end (Figure 2.4). In connections subjected to bending moments, this failure occurs as the longitudinal shear demand resulting from bending of the beam exceeds the shear stress capacity of wood. In this case, the block of wood that tears out fails to maintain sufficient friction with the rest of the beam. This mode of failure can often be observed in conjunction with splitting failure, as the latter may reduce the longitudinal shear strength of the wood component due to grain layers splitting (Lam et al., 2008).

Figure 2.4 Row shear-out (Salem, 2016).

The third major limit state is wood embedment failure. This limit states takes place when a wood component is subjected to high compressive stresses. A special case of this failure type—referred to as Mode I Failure—occurs when the bolts connecting the steel plate to the glulam beam or column induce high compressive stresses on the interior face of the bolt hole, crushing the wood in that region (Figure 2.5). This process often results in a loss of initial connection stiffness.

Figure 2.5 Wood embedment failure (crushing) at bolt holes (He et al., 2016).

2.1.2 Experiments on Modified Traditional Wood Connections

Over the past few years, researchers have conducted moment-resistance tests on traditional, simple wood connections with slight modifications. The purpose of these modifications was to produce better performance out of simple connections and examine their moment-resistance potential. Criteria of a higher performing connection includes improved ductility, stiffness, and moment capacity.

A number of researchers have experimented with different bolt numbers, configurations, and spacing. Yeh et al. (2008) used a flexural testing machine to evaluate moment-resistance strength of glulam beam-column connections with different combinations of 4 and 6 bolts with diameters of 15 and 18 mm. The glulam components were manufactured with Japanese Cedar (*Cryptomeria spp.*), and a 0.354-in.-thick steel plate manufactured of medium carbon structural steel was placed on the outside face of the joint (Figure 2.6). Test results indicated that, in general, increasing the number of bolts was more significant in improving connection moment capacity compared to using fewer bolts with larger diameters. The moment capacity of the joint with 6 15-mm bolts increased 67.4% from the joint with 4 bolts of the same diameter. On the other hand, when using 18-mm bolts, the moment capacity increased 53.0% as the number of bolts changed from 4 to 6. Moreover, the 6-bolt configuration with 15-mm bolt diameter showed around 7% higher ultimate (failure) moment over the joint with the same number of bolts but with diameters of 18 mm. The reason for this lower moment strength from larger bolts could possibly be due to premature wood failure induced by the larger bolts with higher yield bending moments, as suggested by Yeh et al. (2008).

Figure 2.6 The 4-bolt connection configuration tested by Yeh (2008).

Similar experiments have been conducted by Salem (2016), who varied bolt configurations and end distances. The beam-column specimens were made of black spruce (*Picea mariana spp.*) glulam with stress grade 24F-ES/NPG, which has an unadjusted bending stress of 2400 psi. The 0.5-in.-thick, 300W grade steel plate was placed on the outside of the beam-column-beam connection (Figure 2.7). End distances of 4- and 5-times bolt diameter as well as 4- and 6-bolt configurations per glulam component were varied among the specimens. The static bending test results confirmed that greater improvements in moment strength were achieved when more bolts were used in the assemblies with the smaller end distances. Specifically, in the assemblies with end distances of 4 times bolt diameter, moment strength improved 25.4% when the number of bolts was changed from 4 to 6. In comparison, moment strength improved by 20.9% when the bolts were changed from 4 to 6 in the assemblies with end distances of 5 times bolt diameter. Similarly, increasing the end distances showed greater improvement in moment strength in the 4-bolt configuration compared to the 6-bolt layout. Increasing the end distance improved the connection's moment strength by a maximum of 24.9% and 23.2% in the 4- and 6-bolt layout, respectively.

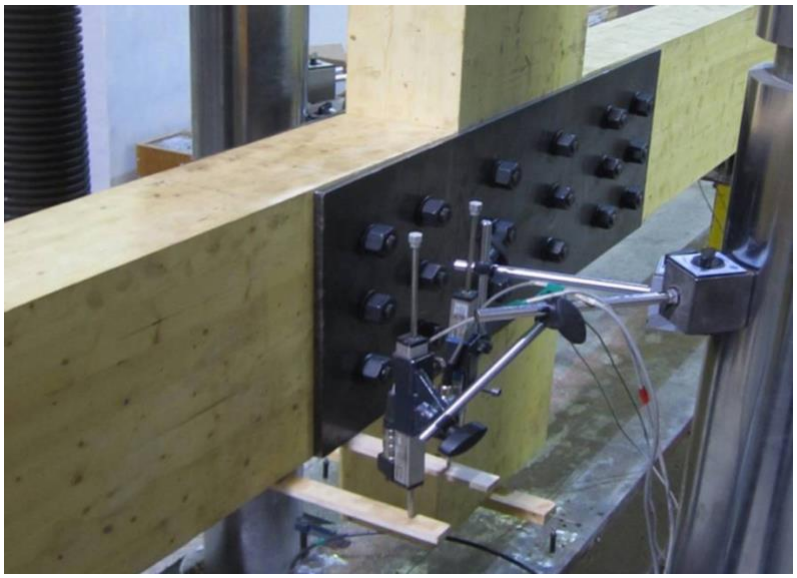

Figure 2.7 Beam-column-beam configuration tested by Salem (2016).

Salem and Petrycki (2016) also tested beam-column connections with T-stub plate connectors of the same steel material and thickness as well as the same glulam material as in the above-mentioned experiments by Salem (2016) (Figure 2.8). Parameter variations were also the same as in the experiments mentioned earlier. Test outcomes confirmed the results of the earlier tests in that greater moment capacity increase was obtained using more bolts compared to increasing the bolt's end distance, and the results were generally similar in terms of percentage improvements.

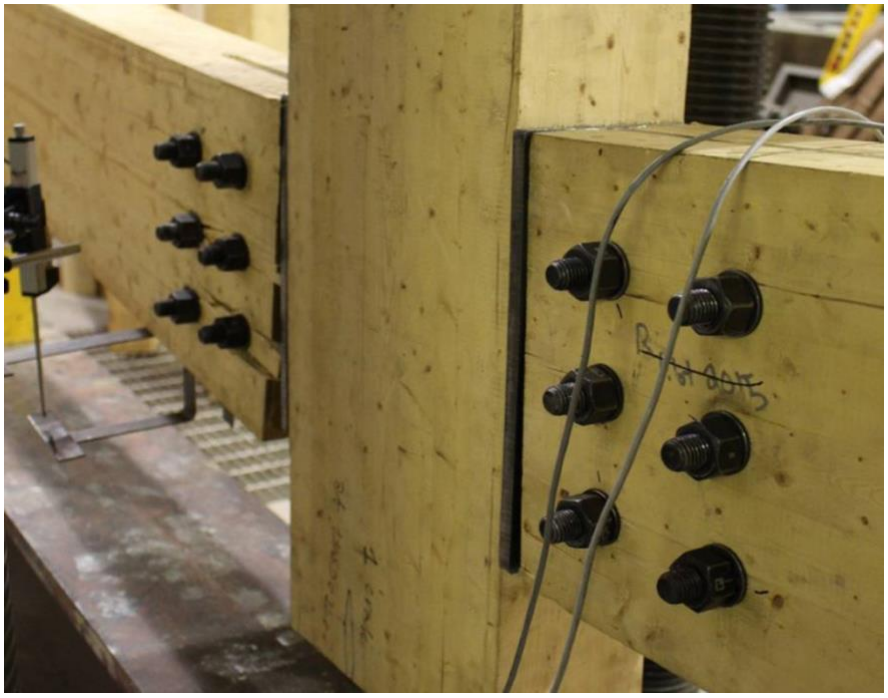

Figure 2.8 Beam-column connections with T-stub steel plates (Salem and Petrycki, 2016).

In an effort to improve the strength and capacity of traditional wood moment connections, Lam et al. (2008) carried out monotonic and reverse cyclic tests on traditional moment connections with self-tapping screw (STS) reinforcements; they then compared these connections to unreinforced specimens. The self-tapping screws were placed in the axis perpendicular to both grain and bolt directions to prevent wood splitting from occurring prematurely. The beams and columns were made from 24f-E DF-L glulam with a 0.374-in. steel plate embedded in the beam and between the double-column. The reinforced specimens utilized 300-mm (11.8-in.) long, 8-mm (0.315-in.) diameter self-tapping screws with continuous threads. The use of STS reinforcement significantly improved the performance of the moment connection. For example, the reinforced specimens achieved a moment strength improvement of 100% and 70% in monotonic and cyclic tests, respectively, over their unreinforced counterparts. The average maximum moment of the unreinforced connection was 31.49 kN-m compared to 65.88 kN-m obtained with STS reinforcement. Higher ductility was also achieved in the improved design, as the failure of the traditional connection was brittle. In fact, it was not possible to establish a ductility ratio for the traditional connections. The crack initiation due to perpendicular-to-grain tension, longitudinal

shear stresses, or a combination of both contributed to the sharp drop in moment capacity (Lam et al., 2008).

2.2 Novel Moment Connections

Novel moment connections are those uniquely designed and targeted to solve a specific set of problems. A number of researchers have developed and tested such connections, with the majority of the improvements achieved in ductility, stiffness, and moment capacity. Some of these connections were developed with new, unconventional attachment techniques that had not been utilized in structures before. The steel components of these connections were designed to predictably yield, resulting in more controlled ductile failures.

Komatsu et al. (2016) developed a portal frame connection that utilized mixed-species glulam beams and columns, composed of Douglas-fir wood (*Pseudotsuga menziesii spp.*) on the outer layers and lower strength Japanese cedar within the inner layers. The glulam beam had a steel I-beam at the supported end that was embedded in a similar manner to slotted-in steel plates. Long bolts were inserted through a bearing steel plate on the column's side opposite to the joint interface, all the way to another plate attached to the embedded I-beam (Figure 2.9). The proposed connection was designed based on contact stresses developed at the joint components and the resistance that glulam elements provided after being subjected to a bending moment. The connection specimens were assembled into portal frames and subjected to cyclic tests. Whereas the purpose of these tests was to evaluate the shear deformation performance of the semi-rigid portal frames, it is worth noting that the connections failed in a ductile manner. Moreover, the glulam components showed some deformations, as embedding occurred at the contact area of the bearing plate, which showed significant deformations.

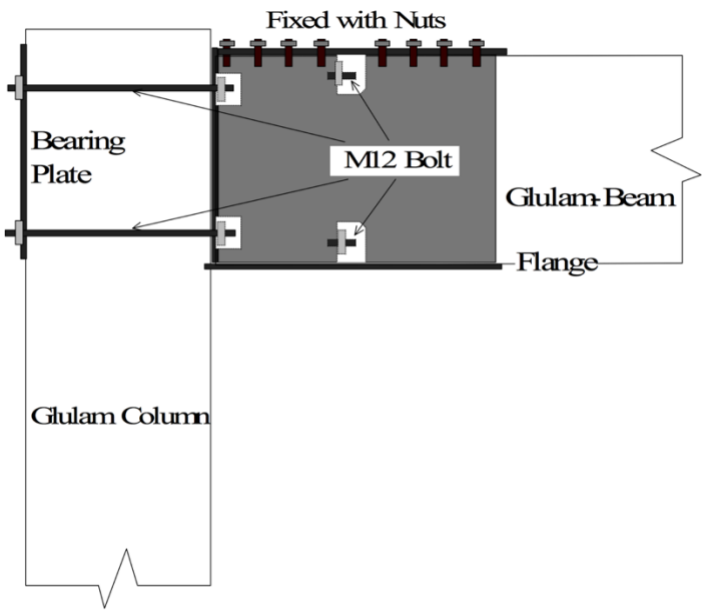

Figure 2.9 A novel moment connection developed by Komatsu et al. (2008).

In an effort to improve the performance of the above-mentioned joint as a moment-resisting connection, Komatsu et al. (2008) tested a modified version of the original design. The long bolts were replaced with lag screws and the bearing steel plate was removed. These modifications were introduced to eliminate the embedment deformation caused by the bearing plate, thus increasing the connection's stiffness and possibly maximum moment capacity. Static tests were performed on the modified beam-column joints utilizing the same glulam material as in the previous study. Stiffness and maximum moment were increased by 40% compared to the previous connection. However, ductility was reduced by 40% as a consequence of a "simple mistake in preparing test specimen[s]" (Komatsu et al., 2008). Failure occurred in the form of tearing off of the lag screws due to high tension and embedding failure was thus successfully avoided.

Another unique, yet intricate, design for a moment-resisting connection that takes advantage of a special type of lag screws was developed by Wakashima et al. (2010). The steel components were designed such that they failed through plastic deformation to prevent premature brittle wood failure. The glulam was made from red pine (*Pinus resinosa spp.*) with a flexural strength of 4350 psi. Figure 2.10 shows the complexity of the components of the two beam-column connections. These connections were subjected to cyclic tests that resulted in considerable bolt yielding and plastic deformation, yet without observable damage to the glulam components.

Maximum moments obtained were around 20 kN-m (177 kip-in.) and 40 kN-m (354 kip-in.) in C- and B-type joints, respectively.

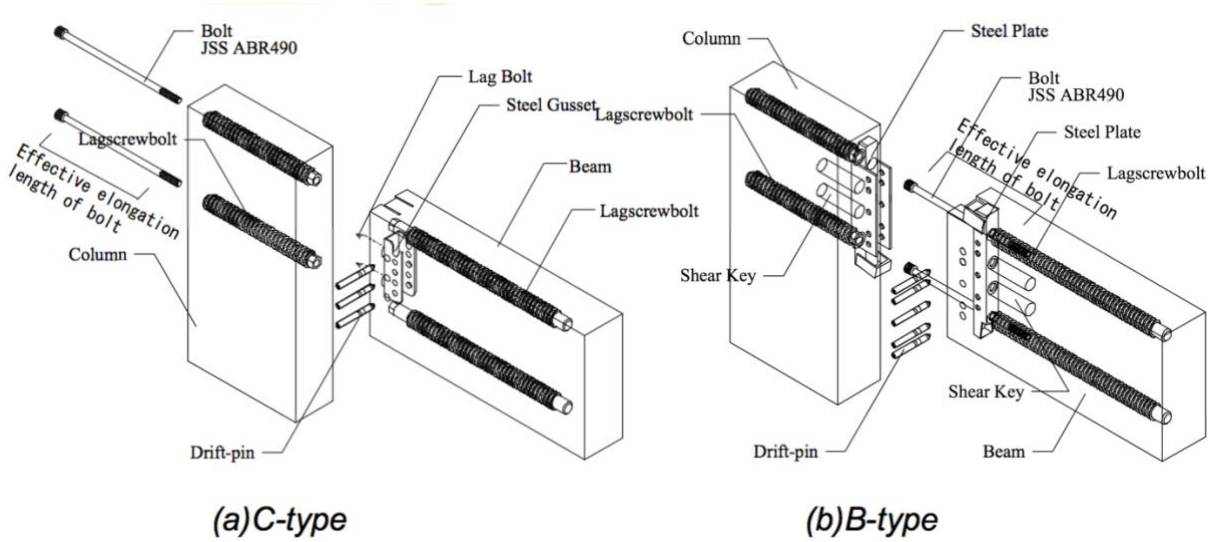

Figure 2.10 Two variations of an intricate connection (Wakashima et al., 2010).

Araki et al. (2010) took a different approach on improving moment-resisting connections. The connections—which were at the column base—utilized resin-injected, SS400 steel tubes as reinforcement for bolt holes. These tubes eliminated loss of bolt tension due to wood shrinkage; thus, no reduction in the glulam's energy dissipation capacity was observed. Instead of steel plates, the authors used 0.47-in., A2017P aluminum splice plates on both sides of the column, which dissipate energy more efficiently by sliding smoothly on the tubes. Bolts were inserted into the elongated or curved holes that allow for the rotation of the column at the base. The column was manufactured from Douglas-fir glulam with a flexural strength of 4350 psi (Figure 2.11(a)). Two variations of the connection—with 4 and 6 bolts—were subjected to quasi-static cyclic loading tests. Measured moment capacities were 26.5 kN-m (235 kip-in.) and 28.6 kN-m (253 kip-in.) for the 4- and 6-bolt configurations, respectively, which were in good agreement with test results. The connection failed in a ductile manner as demonstrated by the moment-rotation hysteresis loops (Figure 2.11(b)), which did not show a substantial drop in the restoring moment. The ratios of the actual developed flexural stress at maximum bending moment to the glulam's flexural strength were 28.3% and 30.1% for the 4- and 6-bolt configurations, respectively.

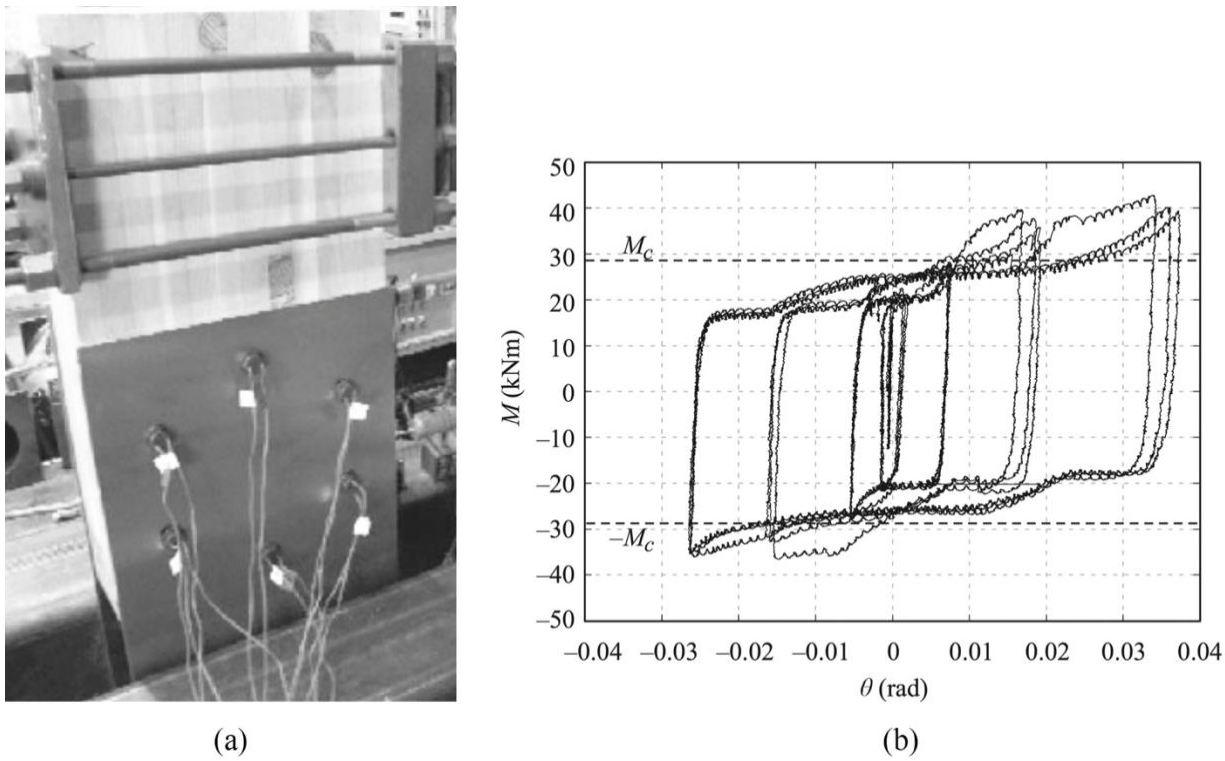

Figure 2.11 (a) 6-bolt connection and (b) its moment-rotation graph (Araki et al., 2010).

Moment connections that take advantage of tube reinforcements in bolt holes were also tested by He et al. (2016) (Figure 2.12). The glulam beams and columns were manufactured using No.2 spruce-pine-fir. The 0.63-in. embedded plate was made of Q235B steel that has a yield strength of 34.1 ksi, and the tubes were manufactured using Q345B steel with a 50.0 ksi yield strength. Some specimens also incorporated perpendicular-to-grain reinforcements using self-tapping screws. The use of the prestressed tubes notably enhanced the initial stiffness compared to the ordinary connections (without the tubes). This increase in initial stiffness was largely due to the friction generated at the interface between the steel tubes and the embedded plate accompanied by the tight fitting of the tubes in bolt holes. In particular, the tube-plate friction ensures a direct load take-up in the earlier stage of loading, which improved the connection's stiffness at that stage and before the friction resistance was exceeded (He et al., 2016). Another advantageous factor that minimizes loss of initial stiffness was the reduction of wood shrinkage imposed by bolt pretensioning, as the steel tubes resist the resulting compression.

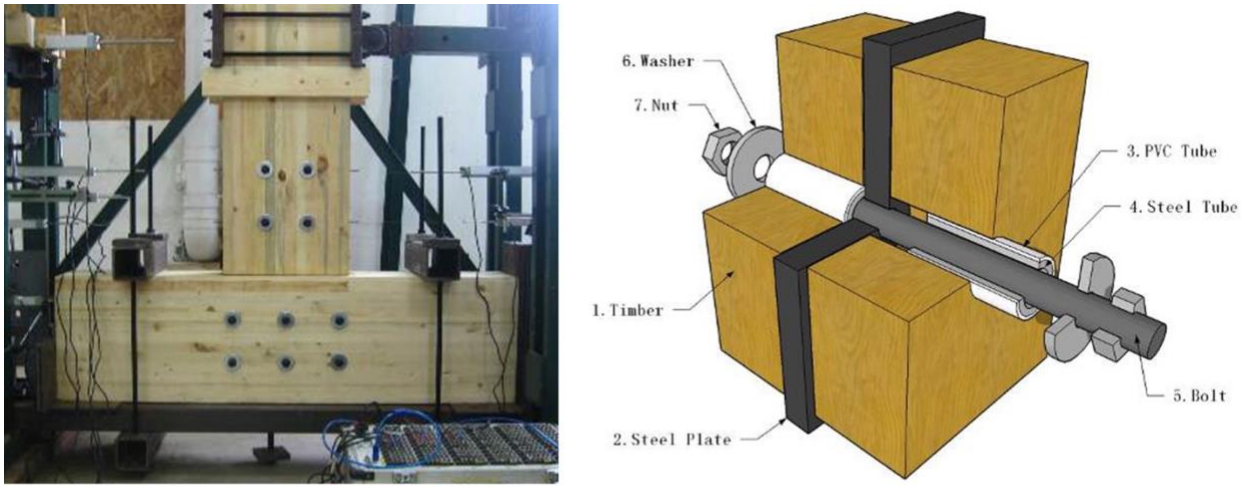

(a) (b)

Figure 2.12 Moment connection with steel tubes in bolt holes (He et al., 2016).

2.3 Summary and Limitations of Available Moment Connections

2.3.1 Summary of Improvement Methods

To overcome the limitations of traditional wood joints as moment-resisting connections, researchers have primarily focused on two different approaches to improve performance. The first is relatively straightforward and involves incorporating slight modifications to existing connections that are typically designed as shear connections. These modifications include varying the number of bolts, bolt diameter, and spacing. Experiments suggest that using more bolts with smaller diameters will result in higher ductility and strength compared to using fewer, but larger, bolts (Yeh et al., 2008). In a related study, research has shown that increasing the bolt end distances can moderately improve moment strength (Salem, 2016; Salem & Petrycki, 2016). Other more successful improvement methods have taken advantage of self-tapping screws. These screws have been shown to prevent splitting of wood in the axis that is perpendicular to grain, enabling the connection to develop higher moment strengths by preventing premature brittle wood failures (He et al., 2016; Karagiannis et al., 2016; Lam et al., 2008).

The second approach involves developing new joint components to control the failure behavior of the connection. Since wood limit states corresponding to perpendicular-to-grain tension and longitudinal shear stress are brittle and considerably inhibit the performance of the joint, researchers have sought to avoid such failures by designing the steel components to yield at

earlier stages. The use of embedded lag screws at the beam-column joint has proven to be effective, as demonstrated by the fact that performance increased while major damage to glulam components was avoided (Komatsu et al., 2008; Wakashima et al., 2010). Other improvement techniques include reinforcing bolt holes with steel tubes, which helps maintain the initial stiffness of the connection at the earlier loading stages. This initial stiffness can be preserved through the friction between the plate and tubes, as well as eliminating wood shrinkage caused by bolt pretensioning (Araki et al., 2010; He et al., 2016).

2.3.2 Identified Limitations

While reasonable advancements have been made in glulam moment frame connections, there are still a few areas where these moment-resisting joints can be improved. Some moment connections in the literature have shown brittle failures, while others have exposed steel components or are incompatible with multi-bay moment frames.

In the case of modified traditional moment connections, undesirable brittle failures are common. While Yeh et al. (2008) proved that glulam beam-column joints with more bolts showed higher strength and stiffness, the failure behavior of the tested connections was not ductile, as wood splitting occurred along the tension-side bolt line (Figure 2.13). The highest rotational stiffness achieved was 250 kN-m/rad (2213 k-in/rad), while the smallest obtained rotation was 0.07 rad, but only at 18.42 kN-m (163 k-in) of applied moment.

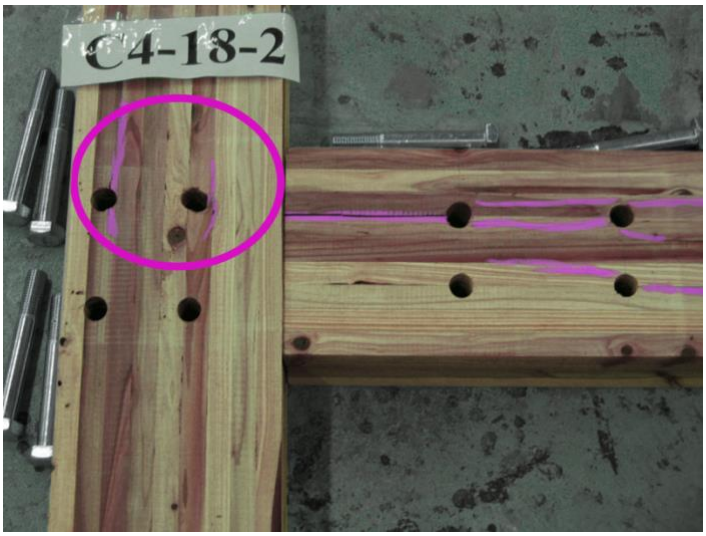

Figure 2.13 Brittle wood splitting failure (Yeh et al., 2008).

Similar results were also reported by Salem (2016), but somewhat different data was obtained. The ultimate moment and corresponding rotation using six bolts were 45.2 kN-m (400 k-in.) and 0.334 rad, respectively, whereas the smallest rotation was 0.15 rad at 37.4 kN-m (331 k-in.) of bending moment in the 4-bolt configuration. The use of larger beam and column cross-sections represents a likely reason for the higher strength in comparison to results from Yeh et al. (2008). Whereas the moment capacity increased with more bolts, the stiffness did not change (Salem, 2016). The beam-column joints showed brittle failures, supported by the fact that row shear-out—possibly accompanied by wood splitting—was observed (Figure 2.14 (a)). The moment-rotation graph for the 4- and 6-bolt configurations (Figure 2.14 (b)) showed sharp drops in load, which indicates crack initiation and an occurrence of brittle failure. Moment-rotation plots of traditional glulam moment connections generally show similar behavior (Figure 2.15).

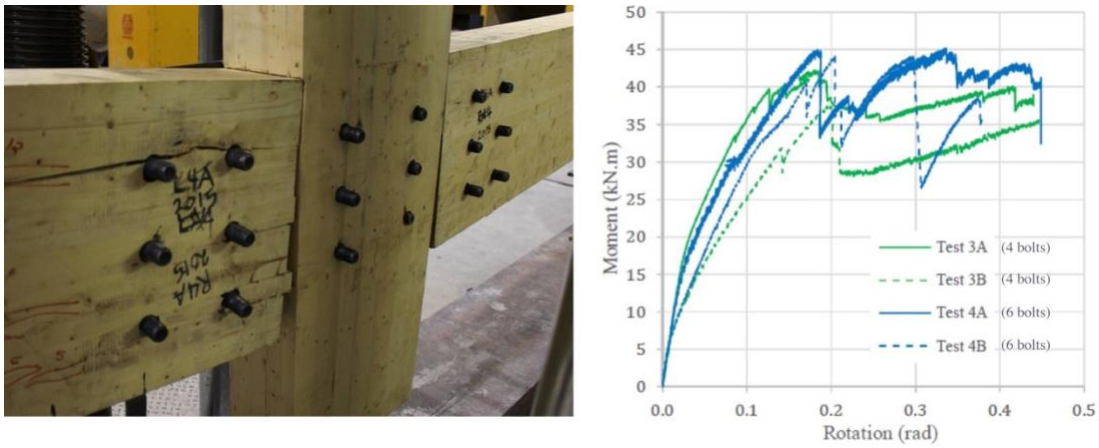

(a) (b)

Figure 2.14 (a) Row shear-out failure at two bolt lines and (b) moment-rotation graphs of the tested specimens (Salem, 2016).

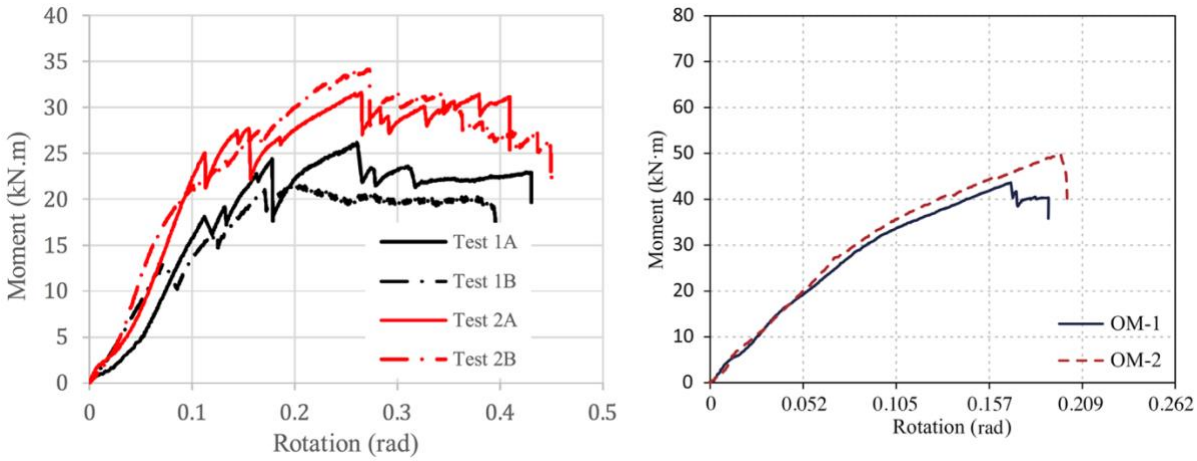

Figure 2.15 Moment-rotation graphs of traditional connections by Salem and Petrycki (2016) (left) and He et al. (2016) (right).

Most of the improved moment connections tested recently have demonstrated reasonable ductility and stiffness. In fact, self-tapping screw reinforcement showed ductile failure mechanisms (He et al., 2016; Lam et al., 2008; Wakashima et al., 2010), as can be seen in Figure 2.16. Mild row shear-out failure was observed with some bending in the bolts with one plastic hinge (Mode II failure) and heavy crushing of wood at bolt holes.

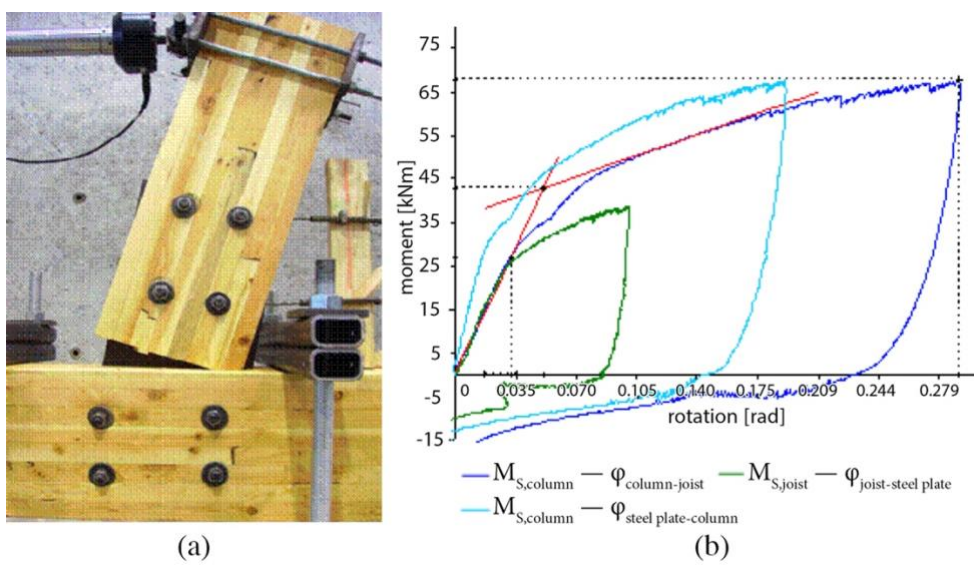

Figure 2.16 (a) Ductile connection failure and (b) moment-rotation graph of the same connection (Lam et al., 2008).

Some novel connections also showed higher ductility and stiffness. Figure 2.17 depicts moment-rotation graphs of four different connections presented earlier in this section. The smooth

curves with negligible load drops indicate good ductility. These joints, however, have some drawbacks. Joint configurations designed by Komatsu et al. (2008) and Araki et al. (2010) include exposed metal components, which is a detriment to their fire resistance and fire rating, especially when used in high-rise buildings. Embedding metal components within wood delays heat transfer to these components, which in turn slows down the loss of strength process due to melting (Barber, 2017). Similar issues can be observed in joints utilizing metal tubes in bolt holes, which He et al. (2016) capitalized upon. These tubes can potentially act as heat bridges that speed up heat transfer and the resulting steel-melting process. While the novel joints designed by Wakashima et al. (2010) showed desirable ductility through plastic deformation of the steel connectors, the issue is their compatibility with multi-bay moment frames. These joints are effective in portal frames, as some components need to be attached from the side of the column opposite to the beam interface. However, design revisions will be necessary if these connections are to be used in multi-bay structural frames.

A new connection is proposed in this research that addresses the three limitations discussed above:

- Brittle wood limit states that occur as the connection is subjected to increasing moment
- Exposed steel parts
- Assembly complications and incompatibility with multi-bay moment frames

The goal for the developed connection was to ensure that it would behave in a ductile manner as the moment increased, thus preventing the brittle wood limit states from governing the failure behavior. This connection would also provide more wood cover over the steel components, thereby improving fire resistance. The feasibility of using this connection in multi-bay moment frames was also considered.

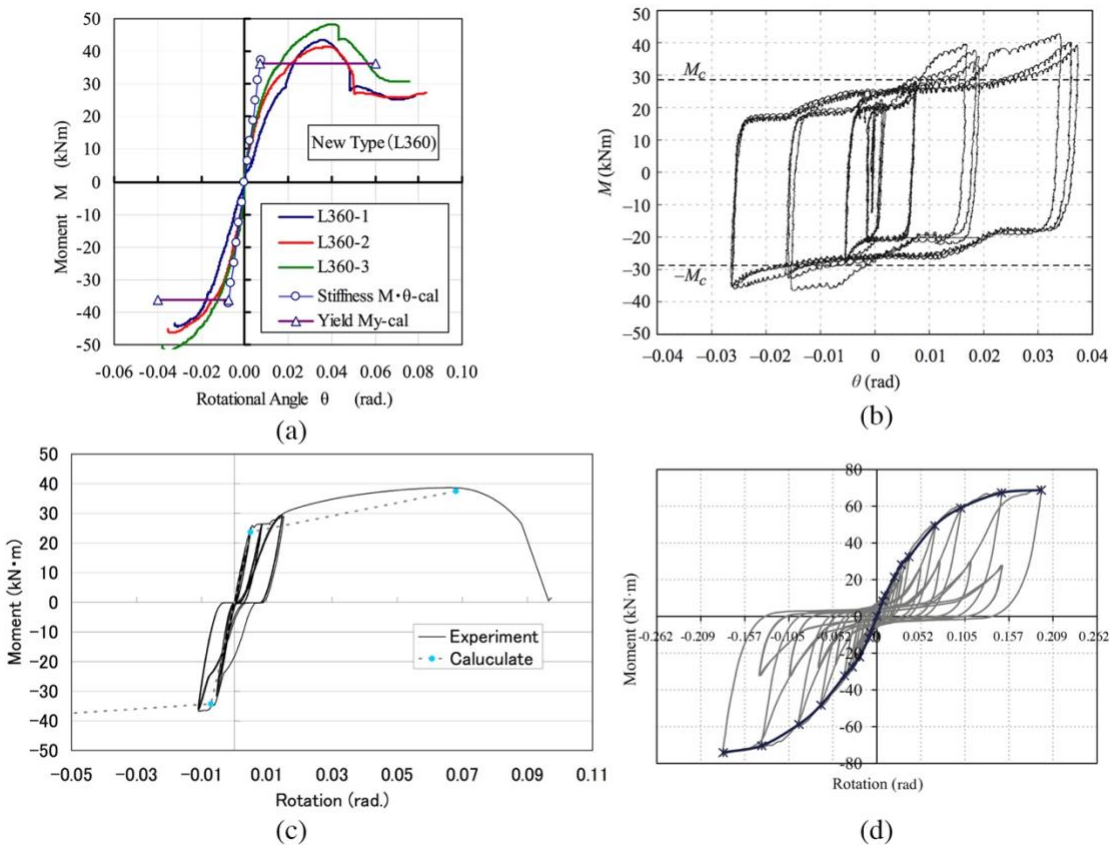

Figure 2.17 Moment-rotation graphs of connections developed by (a) Komatsu et al. (2008), (b) Araki et al. (2010), (c) Wakashima et al. (2010), and (d) He et al. (2016).

CHAPTER 3: DUCTILE YIELD LINK MOMENT CONNECTION

3.1 Introduction

The purpose of this research was to develop and test a new ductile glulam frame moment connection that could be feasibly incorporated into multi-bay moment frames. The goal of the proposed design was to yield a steel connector, thus preventing the non-ductile wood limit states from governing the failure behavior. The added wood cover over steel was intended to reduce heat transfer into the steel components and increase fire resistance (Barber, 2017).

3.2 Connection Design Approach

The proposed connection utilizes an embedded steel plate with a reduced section, as illustrated in Figure 3.1, which shows a generic configuration of this concept. This reduced section acts as a ductile link that limits the moment that is transferred through the connection. The goal for this configuration is to fail through the yielding of this ductile link, thus preventing non-ductile failure mechanisms due to wood limit states from occurring first.

The design process begins with sizing the reduced plate section. Using the moment demand and sizes of the glulam components, the dimensions of the reduced steel plate section can then be determined. These dimensions can subsequently be used to establish the moment demand on the bolt groups at the beam and column, separately. Afterwards, the number, size, and configuration of bolts at the beam and column are determined based on the moment demand and considering the various limit states specified by the Yield Limit Equations. The flexural strength of the column is then designed based on the total moment demand acting on the column. Finally, tension reinforcement can be determined based on tensile forces acting in the perpendicular-to-grain direction, to prevent splitting failure of wood.

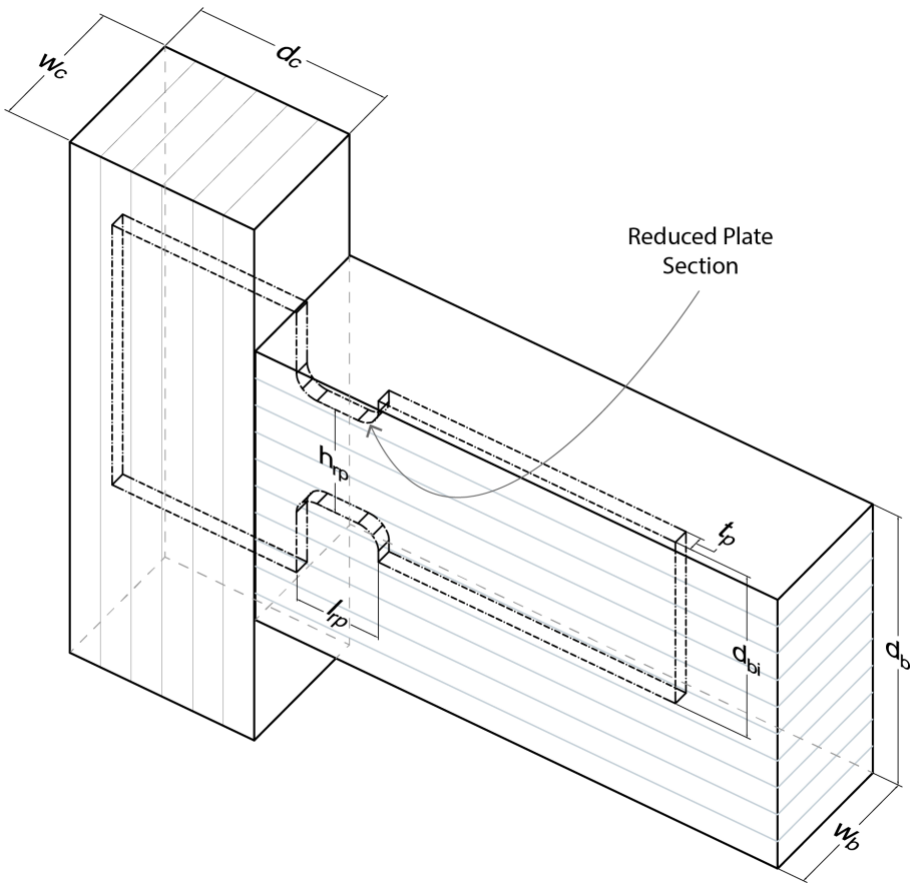

Figure 3.1 A generic connection configuration, showing the beam, column, and plate.

3.2.1 Target Moment Capacity of the Connection

In most cases, moment frames are drift-controlled, which means that the beam and column sizes are determined based on limiting the lateral drift of the frame. In seismic areas, the earthquake loads acting on a given structure can be determined using ASCE 7-16 *Minimum Design Loads and Associated Criteria for Buildings and Other Structures* (ASCE, 2017). These loads include a response modification factor, R, that varies based on the material and type of the moment frame. The moment demand on the connection, M_u, is then found using structural analysis as described by Equation (3-1).

Since there are no response modification factors for timber moment frames, a value for R would have to be assumed. However, to facilitate this preliminary study, the moment demand on the connection is assumed to be a fraction of the beam's moment strength. The moment demand on the connection, M_u, is thus calculated using Equation (3-2), where the moment demand is taken as 27% (γ=0.27) of the beam's moment strength for this project.

$$M_u = from\ structural\ analysis \tag{3-1}$$

$$M_u = \gamma F_b{}' S_{beam} \tag{3-2}$$

Where,

$\gamma =$ Ratio of connection moment demand to beam moment strength (taken as 0.27 for this project).

$F_b{}' =$ Adjusted bending strength of the beam.

$S_{beam} =$ Section modulus of the beam, $S_{beam} = \frac{w_b(d_b)^2}{6} - \frac{t_p(d_{bi})^3}{6d_b}$.

To design the connection, the Load and Resistance Factor Design (LRFD) method and the *National Design Specification for Wood Construction (NDS)* (American Wood Council, 2015) are utilized. The adjusted bending design value of the glulam, $F_b{}'$, is calculated according to Equation (3-3). Adjustment factors shall be applied to the reference design values to account for different environmental and use conditions. The adjustment factors in Equation (3-3) are determined according to Section 5.3 of the *NDS* (American Wood Council, 2015).

$$F_b{}' = F_b C_M C_t C_L C_V C_{fu} C_c C_I K_F \phi \lambda \tag{3-3}$$

Where,

$F_b =$ Reference Bending Strength.

$C_M =$ Wet Service Factor.

$C_t =$ Temperature Factor.

$C_L =$ Beam Stability Factor.

$C_V =$ Volume Factor.

$C_{fu} =$ Flat Use Factor.

$C_c =$ Curvature Factor.

$C_I =$ Stress Interaction Factor.

$K_F =$ Format Conversion Factor.

ϕ = Resistance Factor.

λ = Time Effect Factor.

3.2.2 Sizing of the Reduced Plate Section

The dimensions of the reduced plate section are determined based on several factors. One such factor is the moment demand on the connection, M_u. The plastic moment strength of the reduced section must be equal to or greater than M_u, as expressed in Equation (3-4). After calculating the required minimum value of the effective plastic section modulus, Z_e, using Equation (3-4), the required minimum dimensions of the reduced plate's cross-section can be determined. Given a plate thickness, the required minimum height of the reduced section, h_{rp}, can be determined using Equation (3-5).

$$M_u \leq \phi F_y Z_e \tag{3-4}$$

Where,

$M_u =$ Moment demand at the connection (as calculated in the previous section).

$\phi =$ Resistance factor (taken as 1.0 for this project).

$F_y =$ Specified minimum yield stress of the plate.

$Z_e =$ Effective plastic section modulus of the reduced plate section.

$$Z_e = \frac{t_p (h_{rp})^2}{4} \tag{3-5}$$

Where,

$t_p =$ Thickness of the steel plate.

$h_{rp} =$ Height of the reduced plate section.

Another factor that influences the dimensions of the reduced plate section is ductility. Based on a specified strain limit at the extreme fibers of the reduced section and a target rotation, the length of this reduced plate, l_{rp}, can be calculated using Equation (3-6).

$$\theta = \frac{\varepsilon}{0.5 h_{rp}} l_{rp} \tag{3-6}$$

Where,

$\theta =$ Rotation at the reduced plate section (an arbitrary value of 0.14 rad was used, to facilitate comparison with past research).

$\varepsilon =$ Strain limit at extreme fibers of the reduced plate section (taken as 0.1 in/in for this project).

$l_{rp} =$ Length of the reduced plate section.

Because the plate is assumed to be braced by the wood surrounding it, lateral torsional buckling is not expected to occur. It is also assumed that plate shear failure will not control, since the shear demand on the connection is typically smaller than moment demand.

3.2.3 Moment Demand on the Column Bolt Group

The moment demand on the column bolt group consists of two parts. The first part comes from the probable maximum moment demand at the plastic hinge of the reduced plate section, M_{pr}. This portion of moment can be found once the dimensions of the reduced plate section are determined. The value of M_{pr} shall be calculated according to the requirements of AISC 358-16 *Prequalified Connections for Special and Intermediate Steel Moment Frames for Seismic Applications* (AISC, 2016a), as described in Equation (3-7). The second part refers to the moment applied due to the eccentric shear force, v, at the plastic hinge of the reduced plate section. The shear force can be calculated according to Equation (3-8), and the total moment demand on the column bolt group can be calculated using the expression in Equation (3-9).

$$M_{pr} = C_{pr} R_y F_y Z_e \tag{3-7}$$

Where,

$M_{pr} =$ The probable maximum moment developed at the plastic hinge in the reduced plate section.

$C_{pr} =$ Factor to account for strain-hardening, $C_{pr} = \frac{F_y + F_u}{2F_y} \leq 1.2$ (AISC 358-16 Equation 2.4-2).

$R_y =$ Ratio of expected yield stress to specified minimum yield stress (AISC 341-16 Table A3.1).

$F_y =$ Specified minimum yield stress of the plate.

$$v = \frac{2M_{pr}}{\ell_{ph}} \tag{3-8}$$

Where,

$\ell_{ph} =$ the distance between the locations of the two plastic hinges.

$$M_{uc} = M_{pr} + ve \tag{3-9}$$

Where,

M_{uc} = Moment demand on the column bolt group.

v = Shear force at the plastic hinge assuming plastic hinging occurs at either end of the beam, calculated using Equation (3-8).

e = Eccentricity between the plastic hinge in the reduced section and the center of column bolt group.

3.2.4 Moment Resistance at Column Bolt Group

The strength of the column bolt group must be equal to or greater than the moment demand at that location; that is, $M_{rc} \geq M_{uc}$. The value of M_{rc} can be calculated using the simplified method in Equation (3-10). A diagram explaining the concept is shown in Figure 3.2.

$$M_{rc} = \sum_{i=1}^{n} z_b{}^{(i)} d^{(i)} \tag{3-10}$$

Where,

$z_b{}^{(i)}$ = Shear strength of bolt i.

$d^{(i)}$ = Distance from center of bolt i to center of bolt group.

n = Number of bolts at the column bolt group.

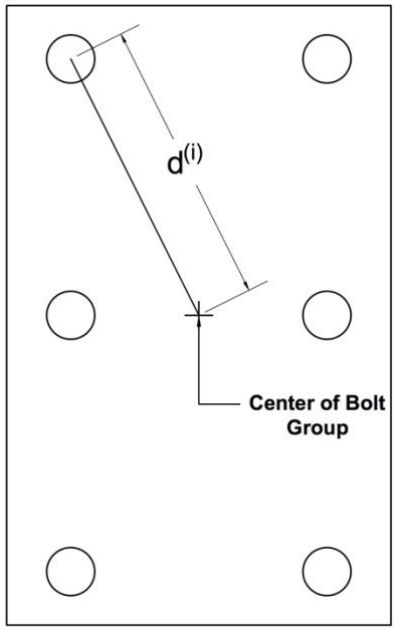

Figure 3.2 Diagram showing the concept of finding the moment strength of a bolt group.

While several combinations of bolt types, diameters, and configurations may provide sufficient moment strength, specific limit states must be checked. According to the requirements in Section 12.3 of the *NDS* (American Wood Council, 2015), the Yield Limit Equations—presented in Table 3.1—must be used to determine the maximum shear force, z, to be induced in a bolt. The shear force per bolt is governed by the lowest value allowed by the four failure modes represented by the Yield Limit Equations. That is, none of these failure modes is expected to occur before the governing value of shear is induced in a bolt. The smallest calculated value of z is then multiplied by 3.32*0.65 to convert it to LRFD.

Table 3.1 Yield Limit Equations for Double Shear (American Wood Council, 2015).

Yield Mode	Yield Limit Equation for Double Shear	Limit State
Mode I_m	$z = \frac{D\ell_m F_{em}}{R_d}$	Fastener bearing on main member (steel plate)
Mode I_s	$z = \frac{2D\ell_s F_{es}}{R_d}$	Fastener bearing on side member (wood)
Mode III_s	$z = \frac{2k_3 D\ell_s F_{em}}{(2+R_e)R_d}$	One plastic hinge in a fastener
Mode IV	$z = \frac{2D^2}{R_d}\sqrt{\frac{2F_{em}F_{yb}}{3(1+R_e)}}$	Two plastic hinges in a fastener

Where,

$$k_3 = -1 + \sqrt{\frac{2(1+R_e)}{R_e} + \frac{2F_{yb}(2+R_e)D^2}{3F_{em}{\ell_s}^2}}$$

D = Selected dowel diameter, in.

F_{yb} = Dowel bending yield strength, psi.

F_{em} = Main member dowel bearing strength, psi.

F_{es} = Side member dowel bearing strength, psi.

R_d = Reduction term.

$R_e = F_{em}/F_{es}$.

ℓ_m = Main member dowel bearing length, in.

ℓ_s = Side member dowel bearing length, in.

To determine the required shear force per bolt, z_{rc}, to resist the moment demand at the column bolt group, a simplified method shown in Equation (3-11) is employed. The specified shear strength of the bolt, z_b, must be equal to or greater than z_{rc}; this information can be used to select the bolt type and diameter. However, to prevent the failure modes of the Yield Limit Equations, the value of z_{rc} must not exceed z. That is, there are two conditions that need to be satisfied, namely $z_{rc} < z_b$ and $z_{rc} < z$. This process ensures that when the moment demand at the

connection reaches M_{uc}, the shear value in any bolt does not result in any of the failure modes expressed by the Yield Limit Equations. Selecting the type, diameter, number, and configuration of each bolt group is an iterative process.

$$z_{rc} \geq \frac{M_{uc}}{\sum_{i=1}^{n} d^{(i)}} \tag{3-11}$$

Where,

z_{rc} = Required shear strength at each column bolt to resist moment demand on the column.

$d^{(i)}$ = Distance between center of bolt i to center of bolt group.

n = Number of bolts at the column bolt group.

The actual strength of the connection at the column, M_{rc}, can be found using Equation (3-10). In this Equation, the value of z_b shall be equal to z, since this is the shear strength at which the corresponding Yield Limit Equation failure mode is expected to occur. The limit states related to the steel plate, including bolt shear, bolt bearing or tear out, and block shear, may need to be checked according to the procedures in AISC 360 *Specification for Structural Steel Buildings* (AISC, 2016c). These limit states are unlikely to control for this connection, but they may control in extreme cases.

3.2.5 Moment Demand and Resistance at Beam Bolt Group

The process for calculating the strength of the beam bolt group is similar to the one used at the column bolt group, with some variations. The moment demand on the beam bolt group, M_{ub}, is found using Equation (3-12) where it is equal to M_{pr}, and the moment resistance at bolt group, M_{rb}, can be found based on bolt strengths. The rest of the design process for the beam bolt group is the same as outlined in Section 3.2.4 for the column bolt group.

$$M_{ub} = M_{pr} \tag{3-12}$$

By ensuring that the yield strength of the reduced plate section is less than the resistance of the connection, the reduced plate section is expected to yield before wood failure or bolt yielding occurs at the connection.

3.2.6 Column Flexural Strength

In most cases, the flexural strength of the column is greater than the moment strength of the connection. However, in some cases where the column is not continuous through the connection—such as at the roof, or if the column is connected to beams on both sides—the total moment demand on the column may be greater than its flexural strength. The moment demand at the column is the sum of the contributions of M_{pr} from each of the connected beams, and the flexural strength of the column has to resist the cumulative demand. This issue is exemplified when the beams are relatively large compared to the column. This check, however, is not implemented here since it is assumed that it will not control.

3.2.7 Perpendicular-to-Grain Reinforcement

The connection design process presented thus far does not directly account for the perpendicular-to-grain splitting limit state. The *NDS* does not provide reference design values for tension perpendicular to grain. Spacing requirements and recommendations for staggering the bolts—both of which are provided in the *NDS*—help in reducing the tendency of wood to split (American Wood Council, 2015). Although these spacing requirements are not specifically provided for moment-resisting connections, it is assumed that following them reduces splitting tendency in such connections. Since the perpendicular-to-grain tensile strength property of wood is weak (as discussed in Chapter 2), perpendicular-to-grain reinforcement in wood members near moment-resisting connections may be necessary to prevent splitting from occurring.

One of the reinforcement methods that have recently been explored is the use of self-tapping screws (Lam et al., 2008). When driven into wood members prone to splitting in the perpendicular-to grain-direction, these screws help to prevent this limit state from occurring. The effectiveness of these screws is discussed in Chapter 2.

The required type, size, and number of self-tapping screws depend on the amount of force to be resisted. In bolted moment-resisting connections, this force is the accumulation of bolt shear

force contributions acting in the perpendicular-to-grain direction. At the beam, for instance, the shear force in each bolt i is comprised of two components. One component is due to direct shear at the connection and the other is from the moment applied due to eccentric loading. The direct shear component, ${V_{dy}}^{(i)}$, is calculated by dividing the total vertical shear at the connection, V, which can be found using statics, by the number of bolts, n, as in Equation (3-13).

The contribution of shear forces due to eccentric loading can be found using any method to calculate eccentric shear effects. In this study, the Traditional Elastic (Vector) Analysis presented in *Steel Structures Design and Behavior* (Salmon et al., 2009) is utilized. In this method, an assumed center of rotation for the connection is used to determine the vertical and horizontal components of shear force exerted in each bolt. Identifying this force assumes that its value is proportional to the distance between the center of bolt and center of rotation. The vertical shear component resulting from moment due to eccentric loading, ${V_{my}}^{(i)}$, is calculated using Equation (3-14); thus, the total shear force in each bolt can be found using Equation (3-15). The total vertical shear force acting on the connection, V_{Ty}, in the perpendicular-to-grain direction is then calculated by adding the force contributions from each bolt in that direction, as indicated in Equation (3-16). Figure 3.3 shows a schematic example of the shear force contributions due to moment resulting from eccentric loading, assuming that the center of rotation corresponds to the center of bolt group.

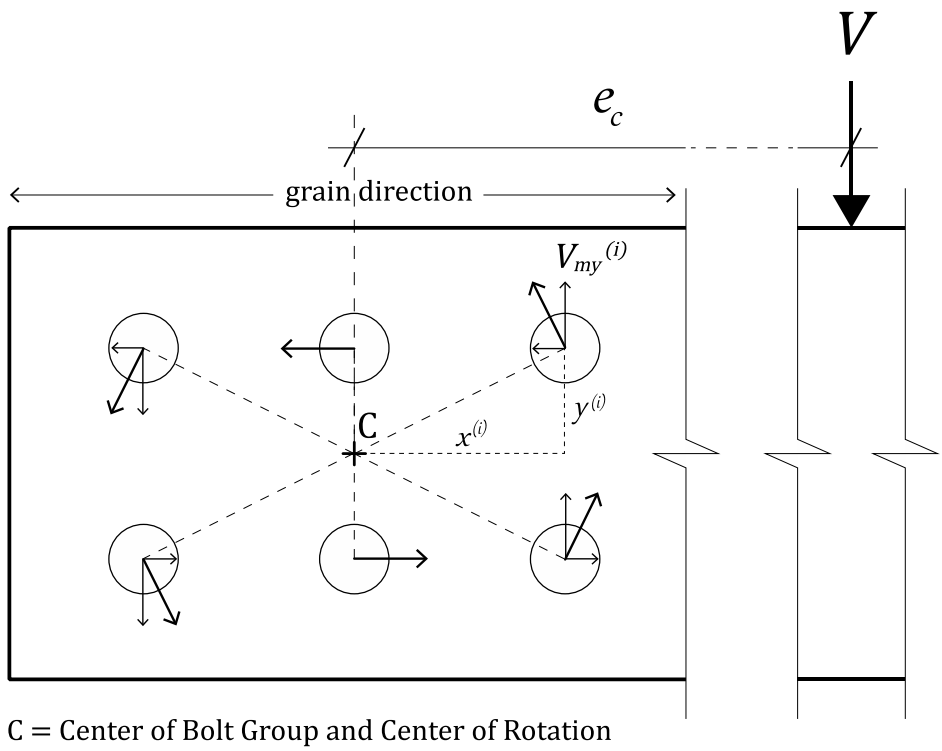

Figure 3.3 Schematic example of the shear force contributions due to moment resulting from eccentric loading.

$$V_{dy}{}^{(i)} = \frac{V}{n} \tag{3-13}$$

Where,

$V_{dy}{}^{(i)}$ = Direct vertical shear component of bolt i.

V = Total applied shear force at the connection.

n = Number of bolts at the beam bolt group.

$$V_{my}{}^{(i)} = \frac{V e_c x^{(i)}}{\sum_{i=1}^{n}(x^{(i)})^2 + \sum_{i=1}^{n}(y^{(i)})^2} \tag{3-14}$$

Where,

$V_{my}{}^{(i)}$ = Vertical shear component of bolt i due to applied moment.

V = Total applied shear force at the connection.

e_c = Moment arm (distance from applied force to center of rotation).

$x^{(i)}$ = Horizontal distance between center of bolt i to center of rotation.

$y^{(i)}$ = Vertical distance between center of bolt i to center of rotation.

$n =$ Number of bolts at the beam bolt group.

$$V_y{}^{(i)} = V_{dy}{}^{(i)} + V_{my}{}^{(i)} \tag{3-15}$$

Where,

$V_y{}^{(i)} =$ Total vertical shear component of bolt i.

$$V_{Ty} = \sum_{i=1}^{n} V_y{}^{(i)} \tag{3-16}$$

Where,

$V_{Ty} =$ Total vertical force at the beam in the perpendicular-to-grain direction.

The required tension reinforcement can be determined based on the total vertical force acting in the perpendicular-to-grain direction, V_{Ty}. When self-tapping screws are driven close to the connection, such that their axes are perpendicular to the wood grain, two design values must be checked. First, the total withdrawal strength of the screws, which is equal to the force per unit length multiplied by the thread length, shall be equal to or higher than the tension force. According to the *NDS*, the withdrawal strength per unit length is a function of the screw diameter and the specific gravity of wood, as in Equation (3-17) (American Wood Council, 2015). However, the manufacturer of the self-tapping screws may provide an alternative method to calculate the withdrawal strength that must be used. The second check pertains to the allowable tensile strength per fastener, which must not be exceeded. This value is provided by the manufacturer of the self-tapping screw. Locations of the self-tapping screws and their spacing requirements shall be determined according to the manufacturer's recommendations. The same design procedure can be utilized to determine required reinforcement at the column. However, the direct component of shear force at the column bolt group does not contribute to tension in the perpendicular-to-grain direction.

$$W = 2850G^2D \tag{3-17}$$

Where,

$W =$ Fastener withdrawal strength per unit length.

G = Specific gravity of wood.

D = Diameter of fastener.

3.3 Example Connection Design

This section presents a connection design example using the design approach outlined in the previous sections. The design of perpendicular-to-grain reinforcement, however, is not discussed in this section. The assumptions made for certain parameters are presented here. The connection developed in this section was then utilized to make the both of the test specimens. Note that the connection is assumed to be part of a 24-foot wide bay of a glulam moment frame. The beams and columns were manufactured from 24F-V8 glulam, which is composed of douglas fir-larch in the outer and inner laminations. This glulam type featured a balanced (symmetric) lamination layup, meaning that the design values for positive and negative bending are identical. The reference design values for this material are summarized in Table 3.2. The dimensions of the beam and column were 6-3/4 in. x 15 in. and 6-3/4 in. x 9 in., respectively, and the 3/4-in.-thick steel plate was made of ASTM A572 grade 50 steel.

Table 3.2 Reference design values for 24F-V8 glulam for bending about the element's shorter axis (x-axis) (American Wood Council, 2015).

Bending, F_b (psi)		2400
Compression Perpendicular to Grain, $F_{c\perp x}$ (psi)		650
Shear Parallel to Grain, F_v (psi)		265
Modulus of Elasticity, E (10^6 psi)	E_x	1.8
	$E_{x\ min}$	0.95
Specific Gravity, G		0.50

The moment demand on the connection, M_u, was determined using Equation (3-2). In real building design, however, the moment demand on the connection is typically obtained from structural analysis of the frame subjected to design loads. Because of the simplified approach explained in Section 3.2.1, this moment demand was determined to be 27% of the beam's moment strength. That is, the value of γ used in Equation (3-2) was 0.27.

The adjusted value of the bending strength of the beam, F'_b, was calculated by multiplying the reference design bending strength, F_b, by the appropriate factors shown in Equation (3-3). Testing was conducted under normal, dry conditions where moisture content was less than 16% and there was no sustained high temperatures around 150°F. Therefore, the wet service factor C_M and the temperature factor C_t were both equal to 1.0. The beam was then loaded so that bending about the shorter axis (x-axis) would occur; therefore, the flat use factor C_{fu} was also 1.0, and since there were no curves, the curvature factor C_c was 1.0. The stress interaction factor C_I does not apply since the glulam elements were not tapered, so it was also equal to 1.0. The shear reduction factor C_{vr} applied since testing was performed on glulam connections, and was equal to 0.72 (American Wood Council, 2015). The smaller of the beam stability factor, C_L, and volume factor, C_V, applied here, and these values were calculated as 0.81 and 0.91, respectively, using equations provided in Section 5.3 of the *NDS* (American Wood Council, 2015) . To use the LRFD method, the *NDS* requires that the specific factors K_F, ϕ, and λ be applied to the reference bending design value, F_b, and they are provided by the *NDS* for each reference design value. For bending, the format conversion factor, K_F, was 2.54 and the resistance factor, ϕ, was 0.85. The time effect factor λ is equal to 1.0 for earthquake loading. The resulting value of the adjusted bending stress, F'_b, was equal to 4660 psi. Using Equation (3-2), with a calculated value of 225 in^3 for the beam's section modulus, the moment demand on the connection, M_u, was equal to 283 kip-in.

To determine the dimensions of the reduced plate section, Equation (3-4) was used to find the minimum required value of the effective plastic section modulus, Z_e. Using the value of M_u from above, a yield stress of 50 ksi for the plate, and a value of 1.0 for ϕ, the calculated value for Z_e was 5.66 in.^{3} Given the thickness of the plate, t_p, which was selected earlier as 3/4 in., the required minimum height of the reduced plate was found using Equation (3-5). Accordingly, a value of 5.50 in. was selected for the height of the reduced plate section, h_{rp}, that exceeds the minimum value, and the effective section modulus, Z_e, was thus found to be equal to 5.67 in^3.

Equation (3-6) was used to identify the length of the reduced section, l_{rp}. A target of 10% strain limit at the extreme fibers of the reduced plate was specified, while the target rotation was 0.140 rad. This value of rotation was used to facilitate comparison with literature. The value of l_{rp} was found to be equal to 3.85 in., and later rounded to 4.00 in., which resulted in a rotation, θ, of 0.145 rad.

The moment demand on the column bolt group was determined using Equation (3-7). The value of R_y used was 1.1 from Table A3.1 in AISC 341-16 *Seismic Provisions for Structural Steel Buildings* (AISC, 2016b), since the actual yield stress of the plate is greater than the minimum specified value. The factor C_{pr}, which was equal to 1.15, was used to account for strain hardening at the plate's reduced section. The use of these two factors is required by AISC 358-16 (AISC, 2016a). Using the values of Z_e and F_y from above, the calculated value of M_{pr} was 359 kip-in. To calculate the contribution of shear force at the plastic hinge location to the moment demand, Equation (3-8) was used. The value of ℓ_{ph} in that equation was equal to 381 in. based on the assumption that the plastic hinge occurs at the center of the reduced plate section. The resulting moment demand on the connection, M_{uc}, was equal to 376 kip-in.

The moment resistance at the column bolt group must be greater than the moment demand calculated above. An iterative process to determine the value of bolt shear, z_b, such that $z_{rc} < z_b$ and $z_{rc} < z$, was utilized. The selected connection configuration, featuring 8 bolts, is shown in Figure 3.4. The same connection configuration with self-tapping screw reinforcement is shown in Figure 3.5. Using Equation (3-11), the required shear strength per column bolt, z_{rc}, was equal to 9.31 kips. The bolts were of type A307, each with a diameter of 1 in. and a shear strength of 31.9 kips, which was larger than z_{rc}. Using the Yield Limit Equations, the maximum allowed value of z was 13.5 kips, which was also larger than z_{rc}. The value of z, in this case, was controlled by the limit state of a single plastic hinge occurring in at least one bolt (Mode III_s). The moment strength of the connection at the column, M_{rc}, was found to be 545 kip-in, using Equation (3-10). These calculated parameters are summarized in Table 3.3. The design values of the beam bolt group were calculated similarly to the column bolt group and are also presented in the same table.

Table 3.3 Summary of calculated design values.

$F_b{}'$	4660 psi
M_u	283 kip-in.
M_{pr}	359 kip-in.
M_{uc}	376 kip-in.
v	2.61 kips
e	6.50 in.
z_{rc}	9.31 kips
z_{rb}	10.9 kips
z_b	31.9 kips
z	13.5 kips
M_{rc}	545 kip-in.
M_{rb}	443 kip-in.

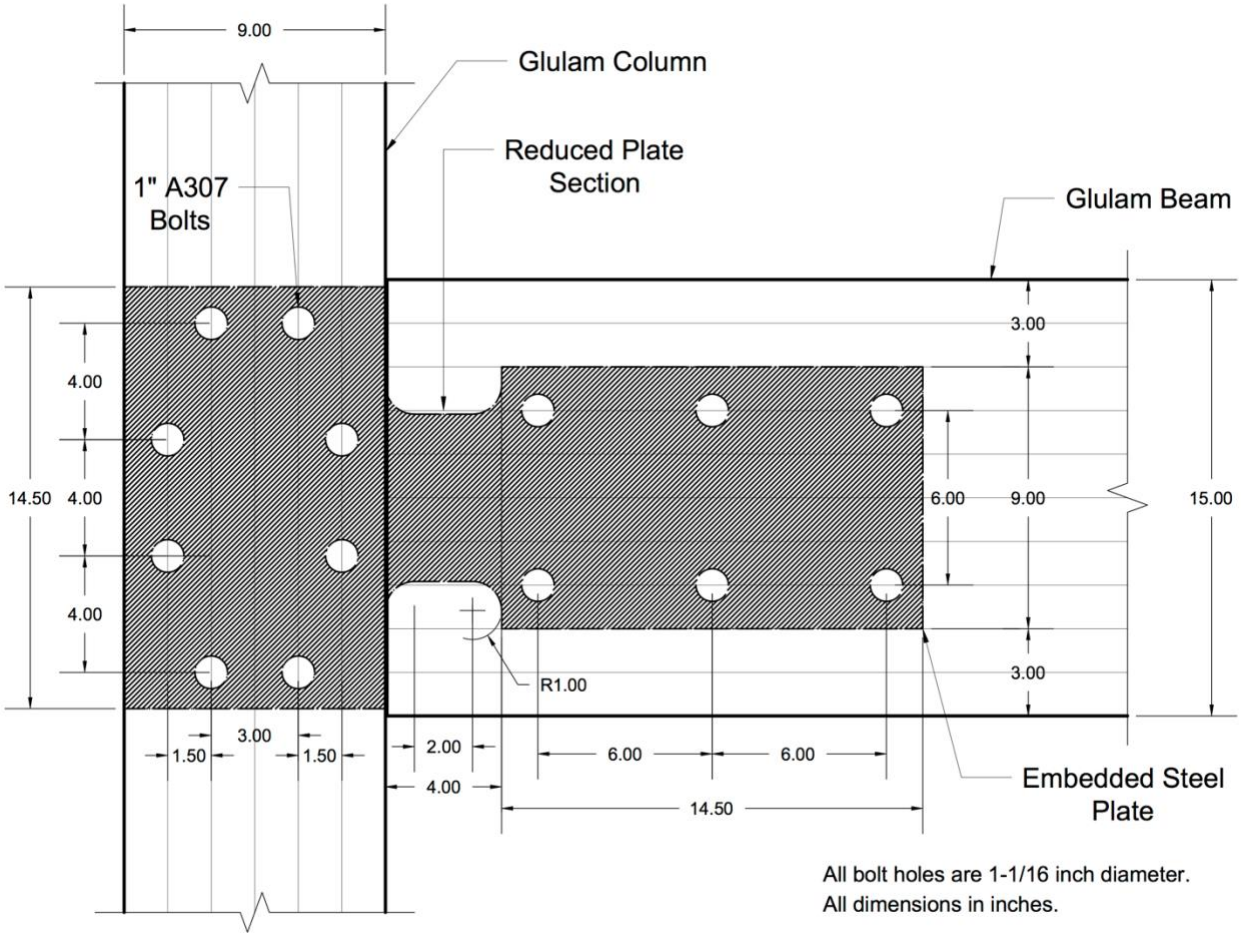

Figure 3.4 The example connection design developed in this section.

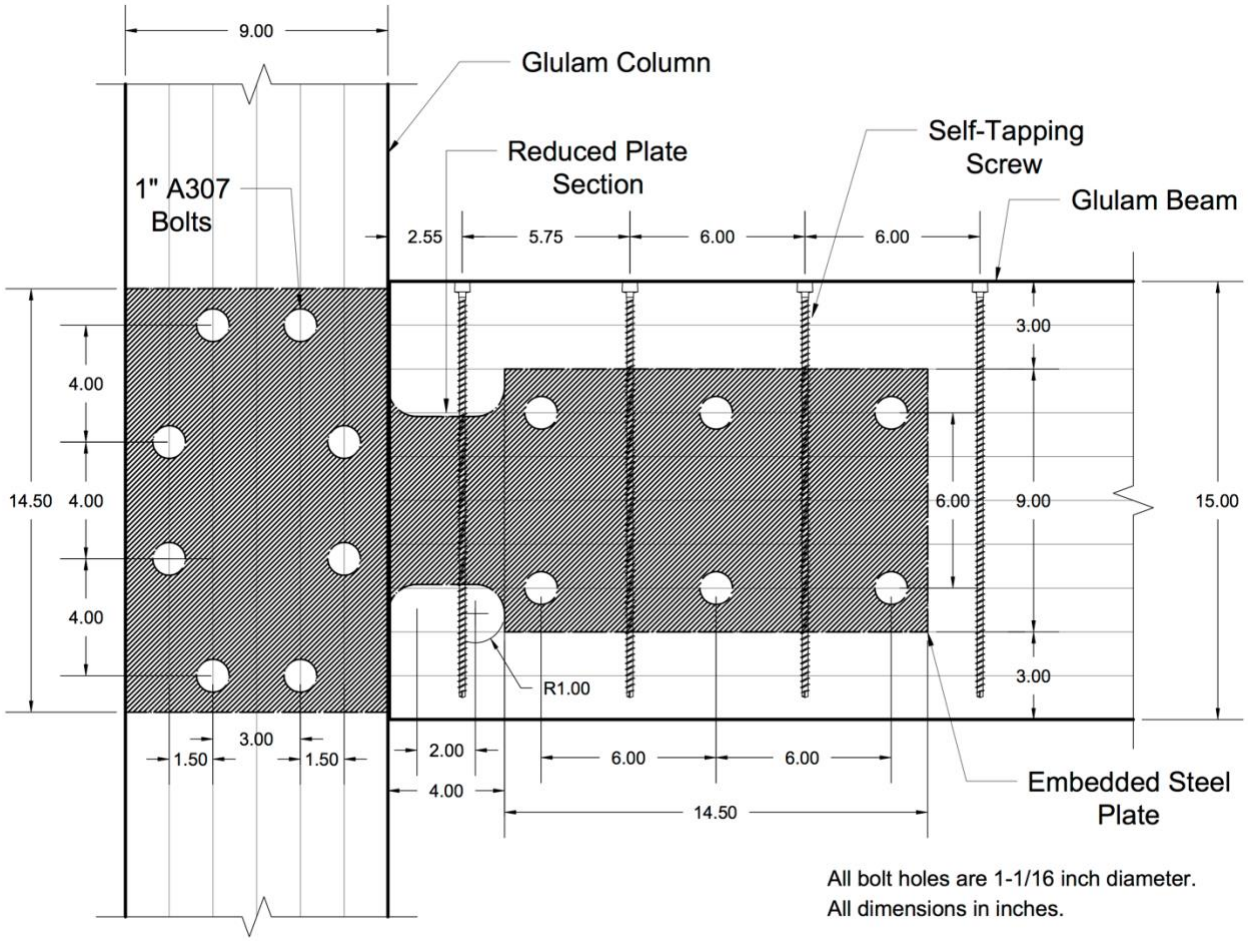

Figure 3.5 The example connection design developed in this section with self-tapping screws.

CHAPTER 4: EXPERIMENTAL WORK

This chapter presents the experimental work performed in this research study. The details pertaining to test specimens—including materials, dimensions, and fabrication procedures—are presented first. Then, the layout of the test setup and the instrumentation plan are discussed. Finally, details of the monotonic tests on the two specimens are explained.

4.1 Test Specimens

4.1.1 Materials and Dimensions

Loading tests were performed on two specimens, each of which was based on the example connection design presented in detail in Section 3.3. This connection design will henceforth be referred to as the Baseline Connection. Compared to the example connection design, the only modification made was in the height of the slits in which the steel plates fit. The slits in the glulam beams were cut from top to bottom of the cross-section. It is assumed that this modification had no effect on the performance of the connection specimens. Details of the material properties are specified in Chapter 3 and the design values of glulam are summarized in Table 3.2. The overall dimensions of the Baseline Connection and its various components are shown in Figure 3.4. Each of the specimens was assembled with a 12-ft.-long beam and a 8-ft.-long column. A summary of information related to test specimens is provided in Table 4.1.

Each of the two specimens was based on the example connection design. Specimen 2 was reinforced with 8 ASSY VG CYL self-tapping screws, which were driven perpendicular to the wood grain on the tension side of the connection, as illustrated in Figure 3.5. Each screw was 10 mm in diameter and 360 mm long. The allowable tension strength per screw was 2.55 kips. Four screws were located on either side of the embedded steel plate between the bolts, between the last line of bolts and beam end, and after the last line of bolts. The design procedure for perpendicular-to-grain reinforcement (discussed in Section 3.2.7) had not been developed until after the second test was performed. That is, the locations of self-tapping screws were based on spacing requirements provided by the manufacturer, coupled with information from prior research. Specifically, these screws were located at the midpoint between the bolts in a similar manner to the reinforced specimens tested by Lam et al. (2008).

Table 4.1 Summary information of the specimens to be tested.

Specimen Name	Reduced Section Dimensions		Loading Protocol	Comments
	h_{rp} (in.)	l_{rp} (in.)		
Sp. 1	5.50	4.00	Monotonic	Baseline Connection
Sp. 2	5.50	4.00	Monotonic	Baseline Connection with STS Reinforcement

4.1.2 Fabrication of Test Specimens

Most of the components comprising the test specimens were fabricated at the Thomas M. Murray Structures Lab at Virginia Tech. The fabrication procedures were similar for the two specimens. Specifically, slits in the glulam beams and columns were first cut using a small, mountable chain mortiser tool (Makita 7104L), which had an 8-in.-long bar (Figure 4.1). The thickness of each slit was 7/8 in. to fit the 3/4-in. plate. These slits were oversized to account for the expansion and contraction of wood, as well as the inaccuracy of the chain mortiser. Because the chain was shorter than the column's depth, the slit was extended through the column by cutting it from the other side (Figure 4.2). The slits at the beam ends were cut in a procedure similar to that used to cut the column, as shown in Figure 4.3.

Figure 4.1 The chain mortiser is mounted on the column to cut the slit.

Figure 4.2 A slit for a steel plate is cut in one of the columns.

Figure 4.3 A slit for a steel plate is cut at the end of one of the beams.

Bolt holes were drilled in the beams and columns of each specimen after the slits were cut. A total of eight and six bolt holes were drilled in the column and beam, respectively. The diameter of each bolt hole was oversized to 1-1/16 in. to fit the 1-in. diameter, 8-1/2-in. long A307 bolts. To drill the holes, the glulam component was secured to a drill press using clamps (Figure 4.4 (a)). A close-up picture of some of the bolt holes can be seen in Figure 4.4 (b). A 1-1/16-in. diameter, 7-1/2-in. long Auger drill bit was used to drill the holes. Due to the short travel distance of the drill press, the drill bit stopped approximately 1/8 in. short from the full depth of the glulam component's thickness. Therefore, each of the holes was drilled further using a hand-held drill press with the same bit to extend the hole all the way through the thickness. When the connection parts were assembled, washers were used on both sides of the glulam beams and columns. Each bolt nut was finger-tightened, marked with a straight line that extended to the washer, and then turned a quarter of a turn using a hand wrench or an impact wrench. The beam and column in both specimens were joined such that no gap was left between them.

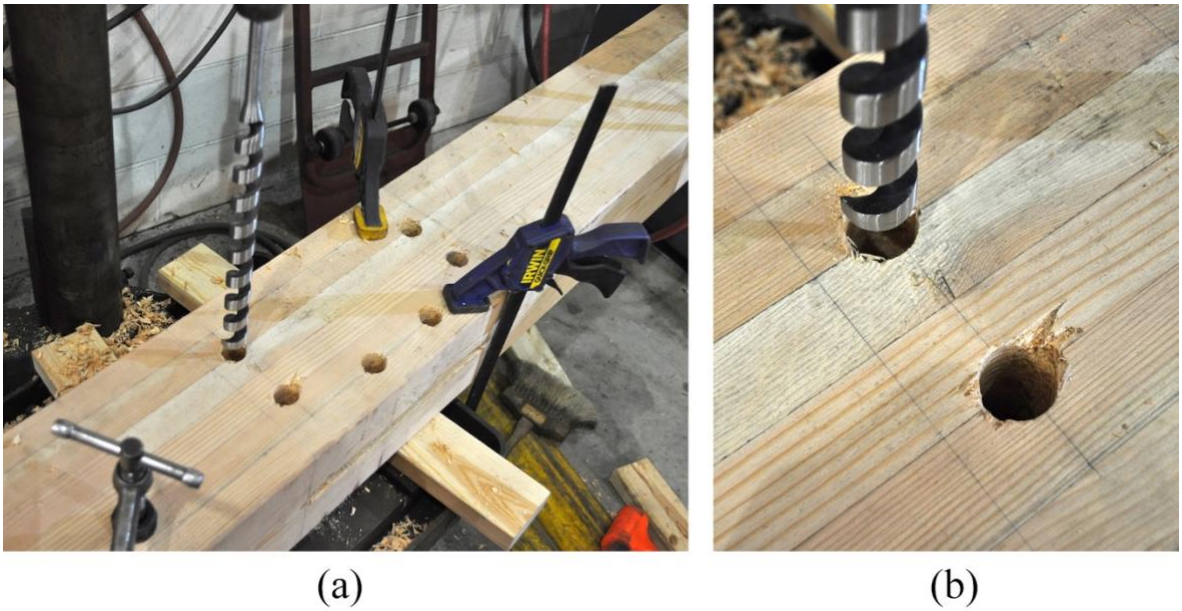

Figure 4.4 (a) A column is secured on the drill press to drill the holes, and (b) a close-up of two bolt holes.

Each of the 3/4-in.-thick embedded plates was cut from a 4 ft. x 4 ft. steel plate. The curved edges of the reduced section were cut using the highest quality waterjet cut, while the rest of the plate was cut using a low-quality waterjet cut. Each plate was fitted into the corresponding connection specimen to locate the bolt holes. The holes in the glulam beams and columns were used to match-mark the holes in the plate, which were drilled using a magnetic drill with a 1-1/16-in. annular cutter. Figure 4.5 shows a sample plate from one of the test specimens with a magnetic drill attached. The self-tapping screws were installed using a low-rpm, high-torque drill, per the recommendations of the manufacturer (Figure 4.6). Pilot holes to guide each screw were drilled using a 7-in. -long, 1/4-in. drill bit. The layout of these screws in Specimen 2 can be seen in Figure 4.7.

Figure 4.5 A magnetic drill is attached to a steel plate to drill a bolt hole.

Figure 4.6 A low-rpm, high-torque drill is used to drive a self-tapping screw into the glulam beam.

Figure 4.7 Specimen 2 with the self-tapping screw reinforcement installed.

4.2 Test Setup and Instrumentation

4.2.1 Layout and Assembly of Test Setup

The layout of the test, which was used for both specimens, was designed to induce an increasing moment at the beam-column connection. A schematic test layout is shown in Figure 4.8. The beam and column were laid horizontally so that the plane passing through them was parallel to the floor and was approximately 14 in. away from it (Figure 4.9). Bolted plates were used to compress the column ends against reaction blocks that were bolted to the reaction floor (Figure 4.10). One end of the beam was bolted to the column using the embedded steel plate, while the other end rested on a steel angle connected to a set of reaction blocks. An identical angle was secured above the beam and connected to the same reaction blocks in order to brace it against out-of-plane (upward or downward) movement. An MTS hydraulic actuator, which was bolted to another reaction block, was positioned perpendicular to the beam at the free end such that it produced a load at a point approximately 91.6 in. away from the face of the column. This actuator had 54- and 82-kip in tension and compression capacity, respectively, and featured static and dynamic stroke limits of 10 in. It was used to monotonically load each of the test specimens. Two 5x2-in. steel tubes were extended from the loading plate to transfer the load to the beam through

top and bottom steel angles (Figure 4.11). Blocks of wood were used as a shim material between the angles and the beam. This set of angles was connected with one threaded rod that allowed these angles to rotate as the load increased in order to reduce embedment on wood. To prevent the loading point of the actuator from moving as the beam was being loaded, two reaction blocks braced the load-carrying tubes against lateral movement. An angle above the upper tube was clamped to the reaction block to restrain upward movement (Figure 4.12). To reduce friction between test setup components and certain parts of the specimen, two 1/32-in.-thick PTFE Teflon layers were placed at the interface of sliding elements such that each layer was attached to one element using double-sided tape. Reducing friction was of particular importance at the interface between the beam and the bracing angles to allow the connection to resist the applied moment with minimal contribution from friction forces.

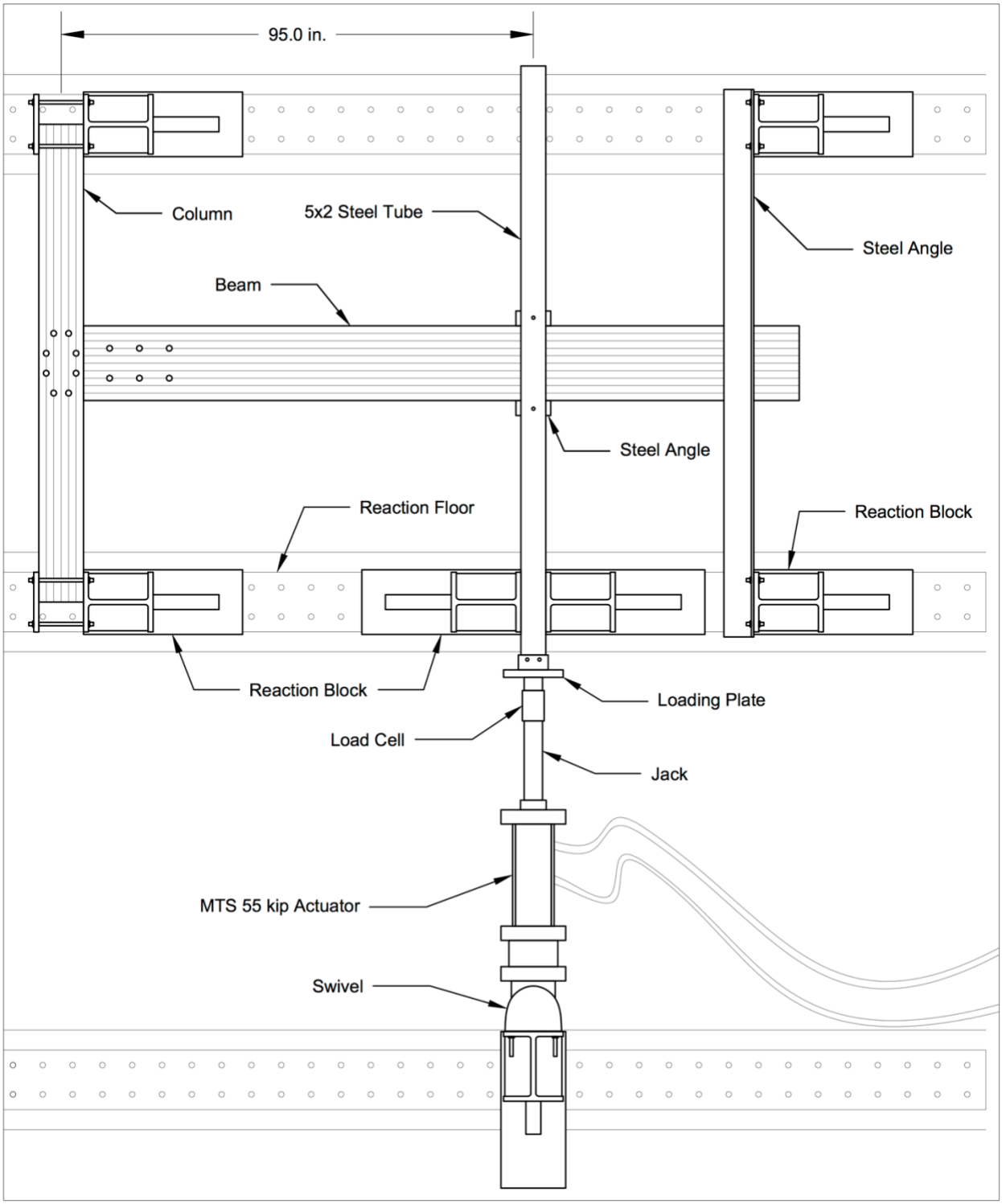

Figure 4.8 Schematic layout of the test setup.

Figure 4.9 Test setup of specimen 1.

Figure 4.10 One end of a column is secured with a steel plate and threaded rods to create a fixed-end condition.

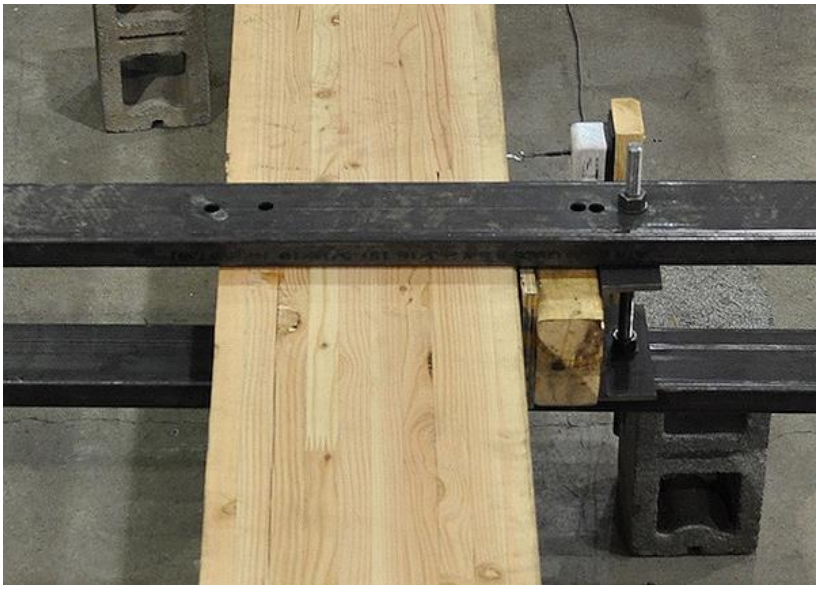

Figure 4.11 Two tubes transfer load from the actuator to the beam through angles.

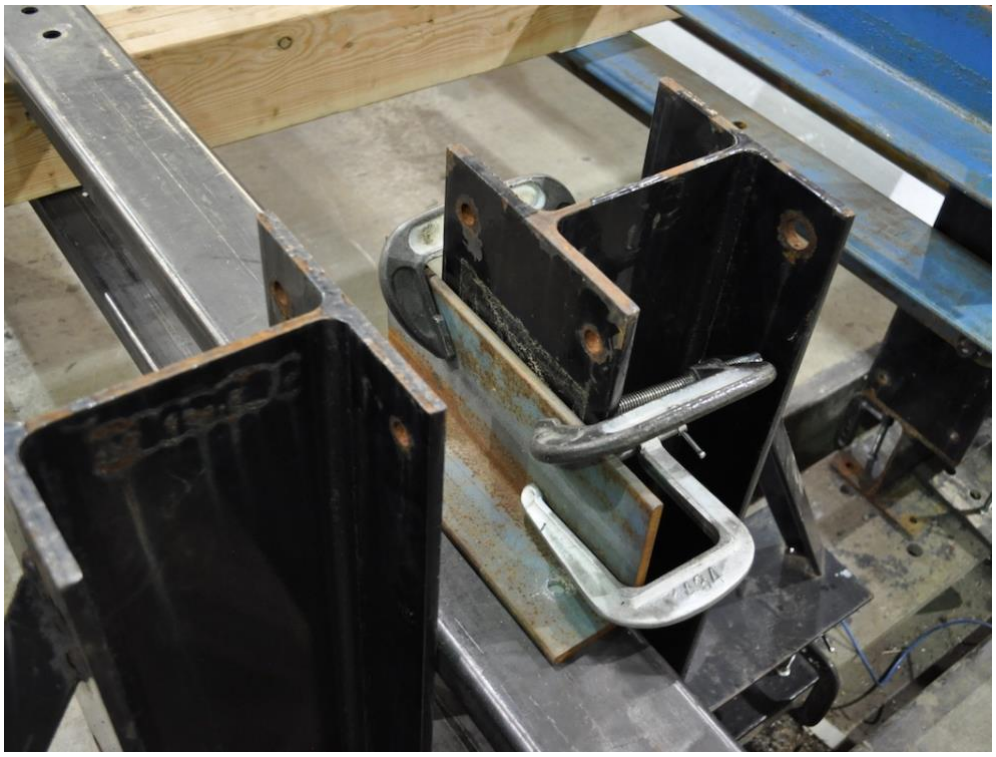

Figure 4.12 An angle clamped to the reaction block prevents upward movement of the load-transferring tube.

4.2.2 Instrumentation

The instrumentation plan was devised to measure displacements at specific locations in each test specimen. These displacement changes were then utilized to produce plots that were essential for analyzing the behavior of the connection. A total of nine string potentiometers were used at each test specimen, and their locations are shown in Figure 4.13 and Figure 4.14. Note that, due to a mistake in measuring, the centerline of the beam at Specimen 1 coincides with a point that is approximately 9 in. away from the midpoint between the two column supports. It is assumed that this mistake does not affect the performance of the specimen. To measure the rotation angle of the beam, the difference between the displacement values at string potentiometers SP07 and SP05 was divided by the distance between SP07 and the centerline of the column (distance 1). Similarly, the rotation angle of the column was calculated by subtracting the displacement value of SP06 from that of SP01 and dividing the result by the distance between them (distance 2). The story drift angle could then be calculated as the difference between the rotation angles of the beam and column, which eliminates rigid-body movement of the specimen. The difference between string potentiometers SP08 and SP09, divided by the distance between their locations (distance 3), gives the rotation angle of the connection—that is, the rotation of the beam relative to the column at the connection. The column slip was measured using string potentiometer SP05, while the slip of the beam relative to the column was measured using SP04. The distances at both specimens are summarized in Table 4.2.

Table 4.2 Distances used to calculate rotational angles at both specimens.

	Distance 1	Distance 2	Distance 3
Specimen 1 & Specimen 2	84 in.	96 in.	18 in.

Appendix A presents plots showing the corrected and uncorrected change of displacement values with time for each of the string potentiometers used at each specimen. To correct the data of each string potentiometer, the displacement values at the beginning of the next loading phase were first shifted such that their values continued from the displacement values at the end of the current loading phase. This correction eliminated the displacement values that were recorded when the string potentiometers were relocated between the loading phases. Afterwards, the data was shifted such that displacement values began at zero.

Two cameras were used during testing to take pictures at regular time intervals. One of the cameras was placed above the test setup to capture the overall view of the test (Figure 4.15), while the other camera was located closer to the connection (Figure 4.16). The time interval between pictures was approximately 3 seconds. These pictures were compiled into time-lapse videos to visually inspect and analyze the behavior of each connection specimen throughout the different stages of the experiment.

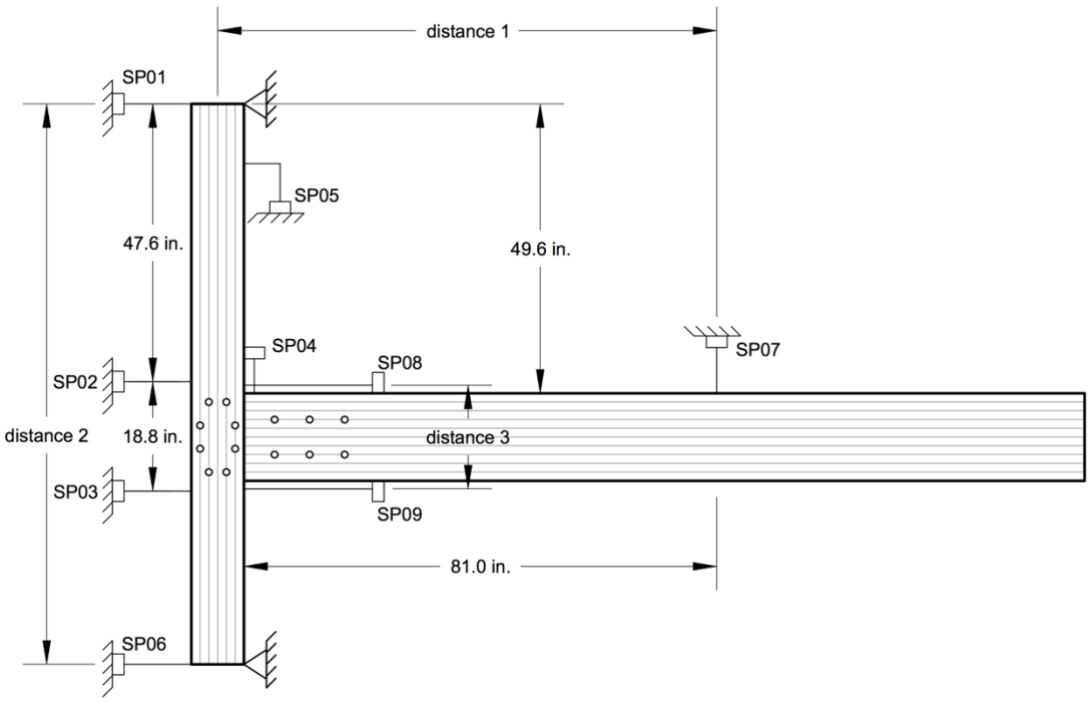

Figure 4.13 A diagram of the locations of the nine string potentiometers at Specimen 1.

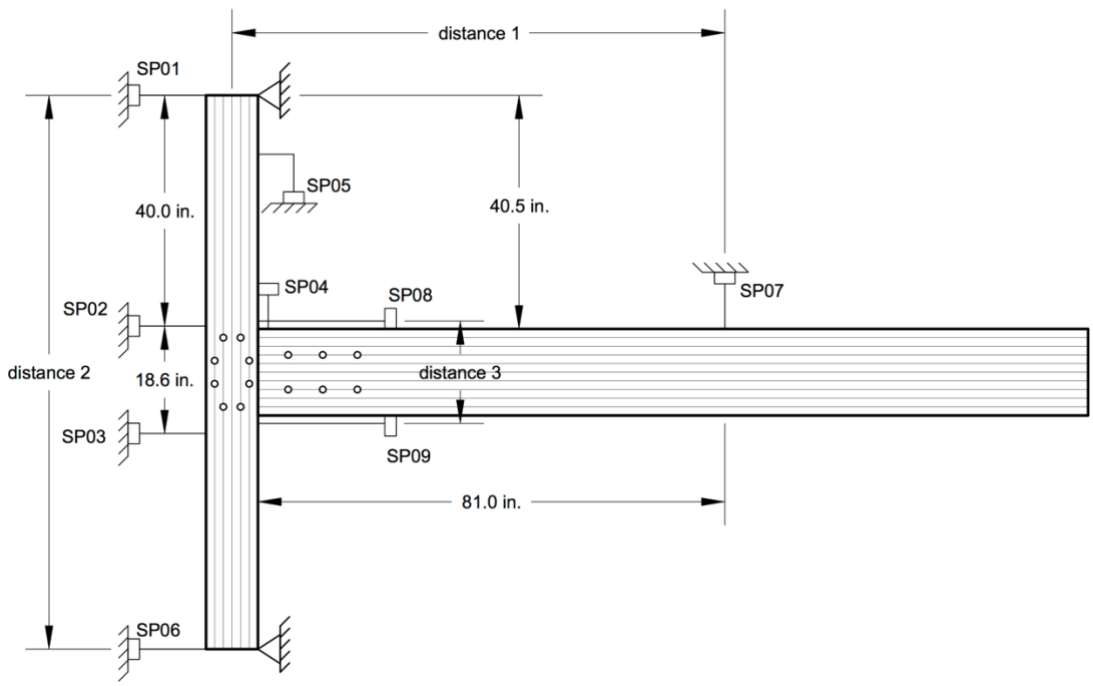

Figure 4.14 A diagram of the locations of the nine string potentiometers at Specimen 2.

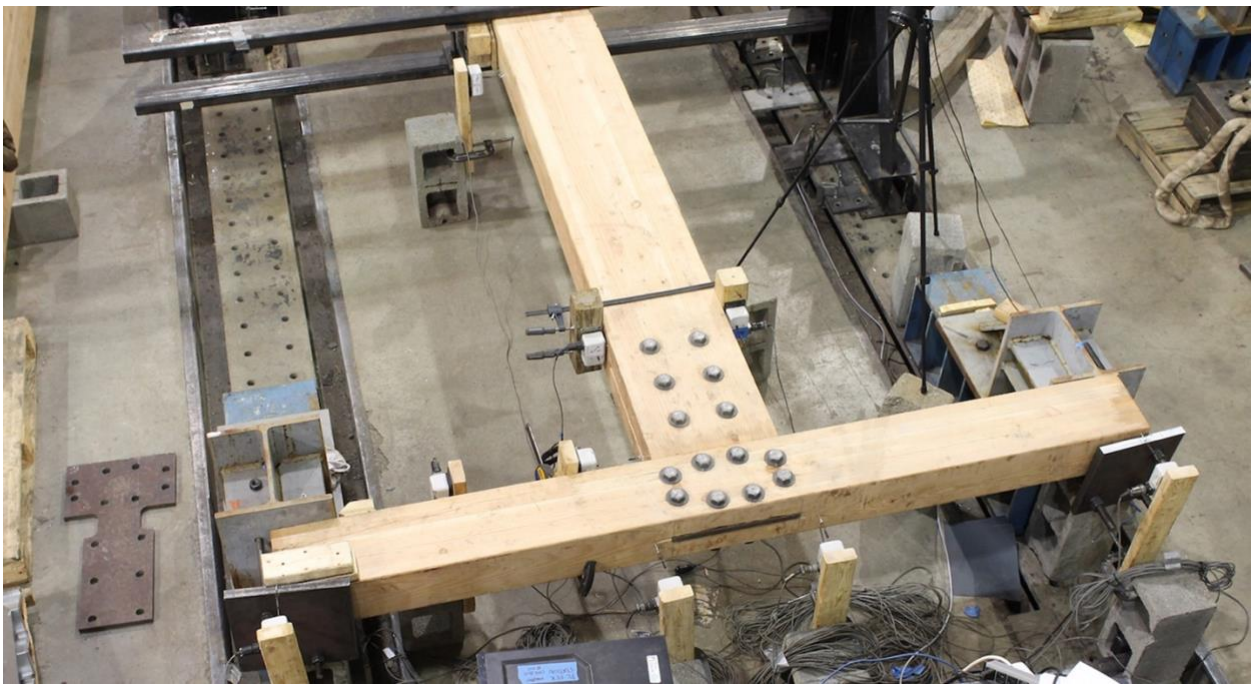

Figure 4.15 Overall view of the test setup from the upper camera (specimen 2 is shown).

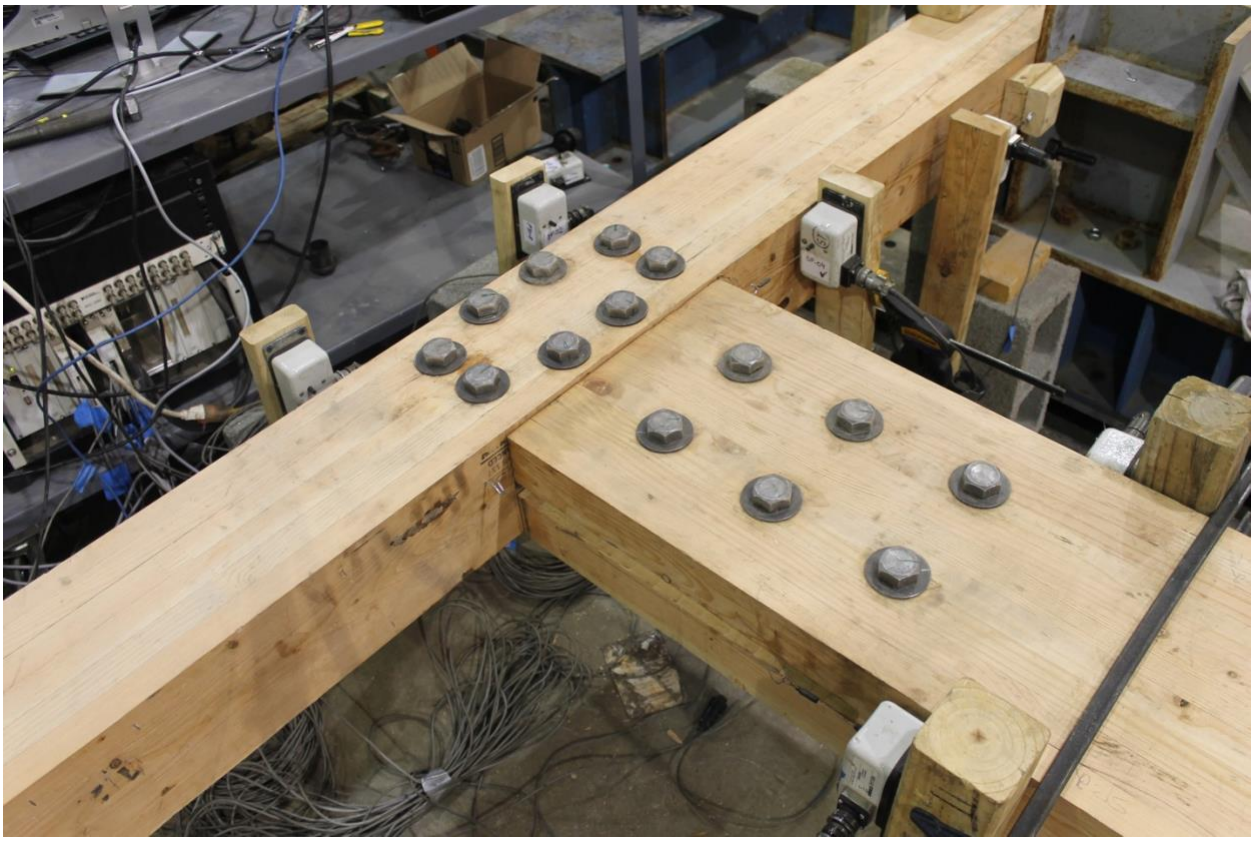

Figure 4.16 A close-up view of the test setup from the lower camera (specimen 2 is shown).

4.3 Methods

4.3.1 First Test: Specimen 1

This test was conducted in two phases. In the first phase, the load was applied such that the actuator was pushing the beam at a displacement rate of 0.33 in. per minute. Additional steel angles were attached on the side of the beam opposite to where the first set of angles were placed in order to push the beam (Figure 4.18). However, due to concerns related to the stability of the test specimen under loading, the force direction was reversed such that the actuator was pulling the beam (second phase). Only the set of angles necessary to pull the beam were attached, and wood blocks were used as shim material between the beam and the remaining set of angles (Figure 4.19). Loading was then resumed, but at a rate of 0.5 in. per minute, and the beam was loaded all the way until failure.

Figure 4.17 Specimen 1 before testing.

Figure 4.18 Angles on both sides of the beam were used to either push or pull the beam.

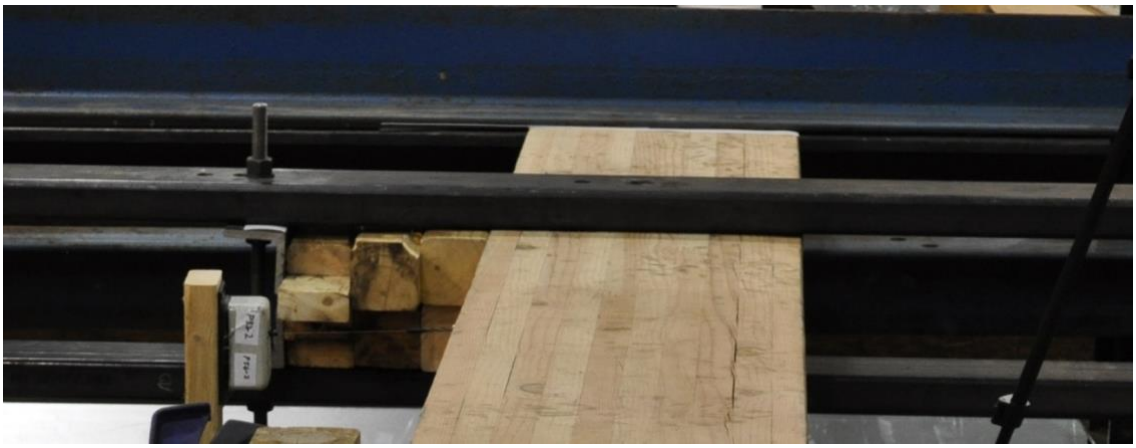

Figure 4.19 Wood blocks were used as shim material between the beam and steel angles.

4.3.2 Second Test: Specimen 2

In this test, the beam was being pulled toward the actuator throughout the experiment. This test was conducted in three phases of loading and unloading because of the limitations of the actuator stroke. When the stroke limit was reached, the specimen was unloaded, the string potentiometers were relocated accordingly, and the actuator was adjusted for maximum stroke. Blocks of wood were used as shim material between the load-transferring angles and the beam. The loading rate used in the first phase was 0.5 in. per minute, while in the second and third phases the rate was 2 in. per minute.

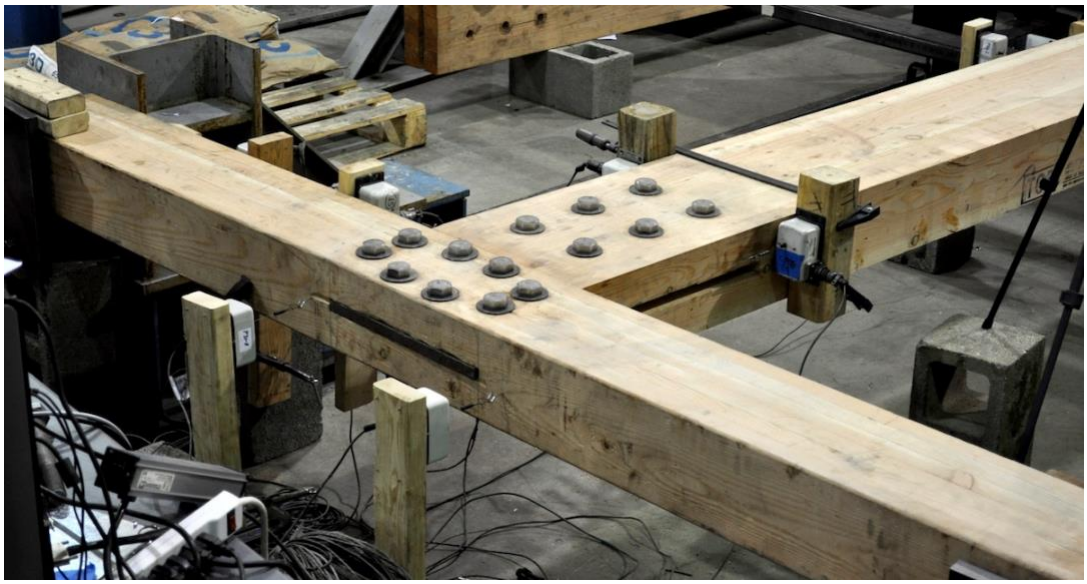

Figure 4.20 Specimen 2 before testing.

CHAPTER 5: RESULTS AND DISCUSSION

In this section, the results of each test will be presented and analyzed in detail. The behavior of the specimens throughout the experiment and observations will be discussed through plots and pictures. The stiffness, ductility, and strength of each connection specimen will be evaluated. Failure modes of each specimen will be examined and hypothesized reasons for these failures will be presented and discussed.

5.1 Specimen 1 Results

5.1.1 Behavior of the Specimen Under Loading

Specimen 1 was subjected to monotonic loading during the first test until failure. A plot of story drift angle versus moment is presented in Figure 5.1. After adjusting the data to remove rigid-body movement effects, the moment was calculated by multiplying the applied load from the actuator by the moment arm—approximately 91.6 in.—which is the distance from the point where the load was applied to the face of the column. A plot of connection moment versus rotation angle is presented in Figure 5.2.

In the first loading phase (when the actuator was pushing the beam), no cracks were observed as the beam was loaded for less than 2 in. of displacement (less than 0.022 rad of rotation). However, cracks in the beam started to appear early in the second loading phase. Specifically, the beam started to split at the top horizontal row of bolts after a crack developed between the beam's edge and the last bolt in this row (Figure 5.3). This crack started to enlarge as soon as the bottom-left corner of the beam started to bear on the column, as can be seen in Figure 5.4. Two more cracks immediately initiated as the first one got wider, which can also be observed in the same figure. One crack occurred between the two lower-right beam bolts, while the third one developed between the two middle bolts in the vertical column bolt row closer to the beam. At failure, both cracks at the beam extended beyond the respective bolt rows. Additionally, wood crushing occurred between the top and bottom rows of bolt at the beam away from its end (Figure 5.5).

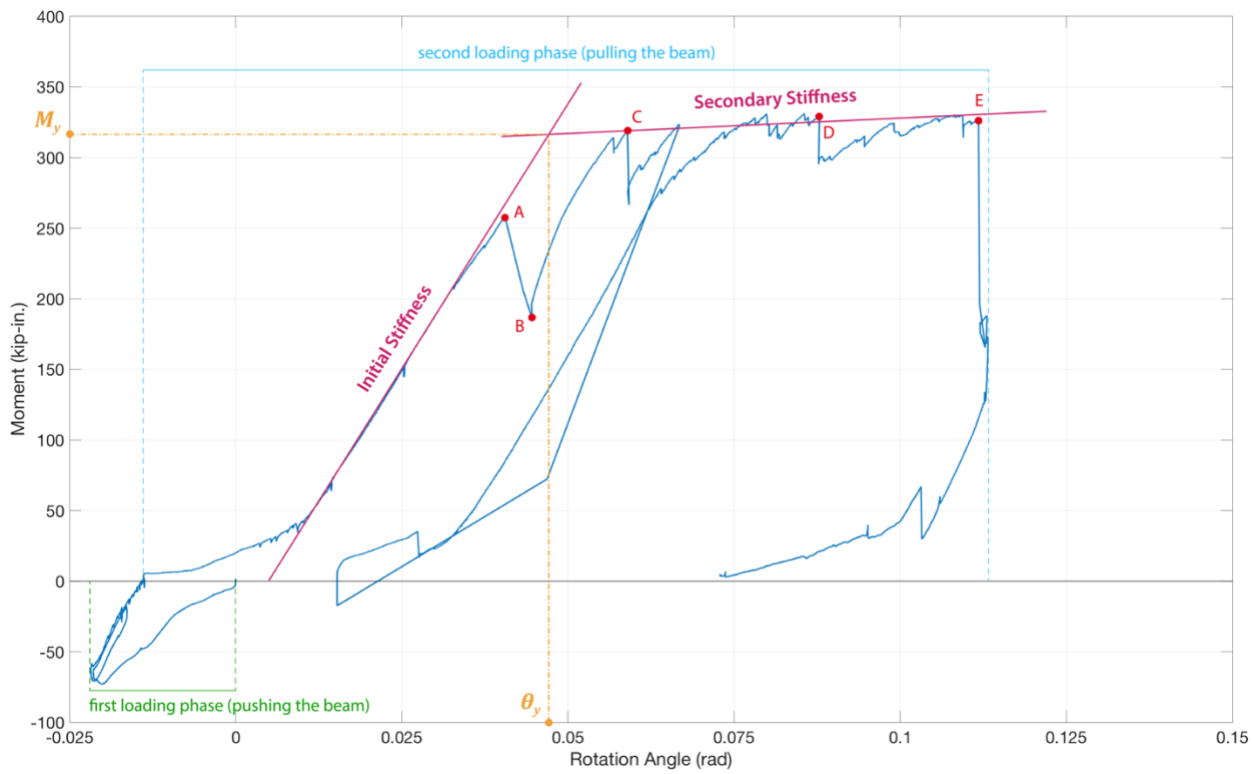

Figure 5.1 Moment-story drift angle plot for Specimen 1.

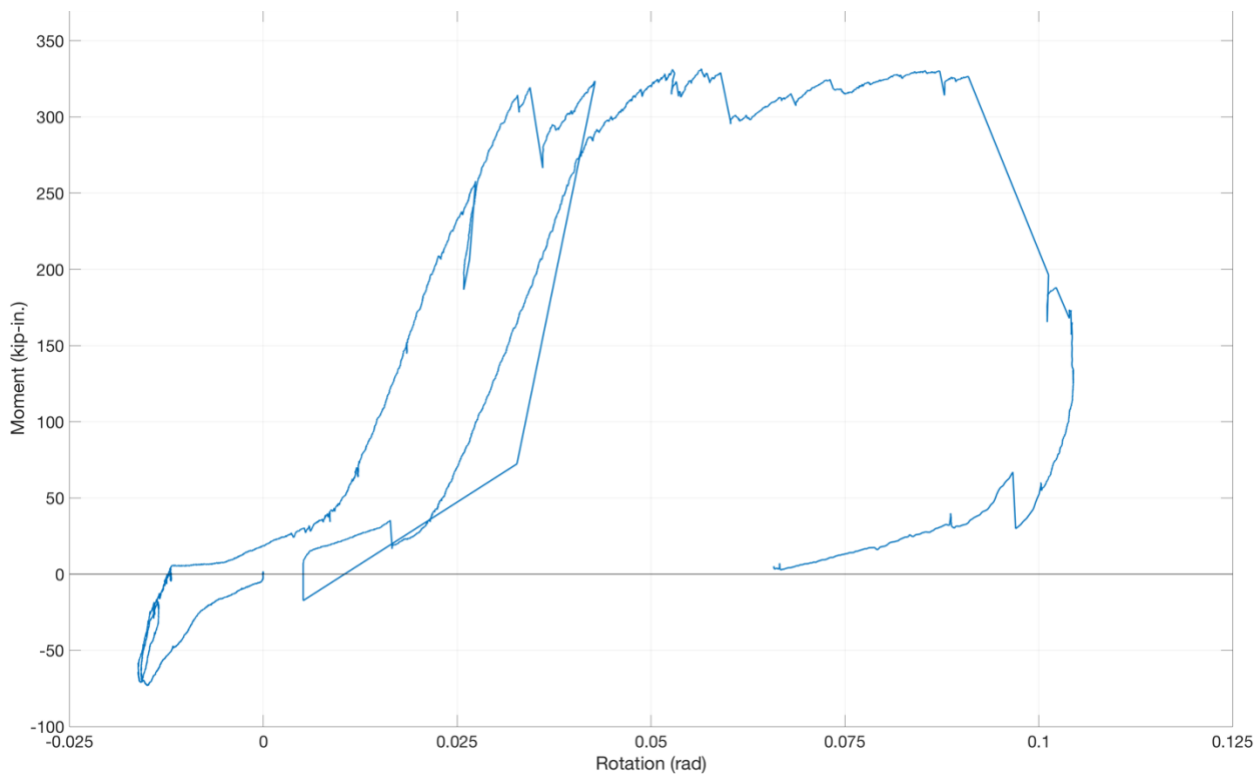

Figure 5.2 Connection moment-rotation angle plot for Specimen 1.

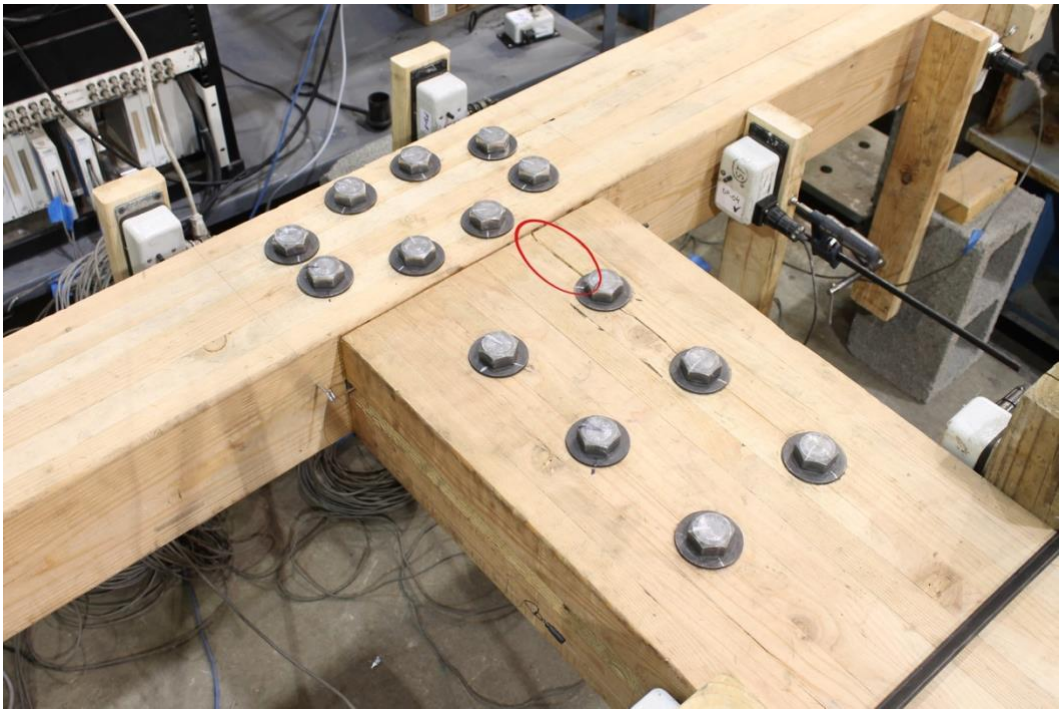

Figure 5.3 A crack initiated between the last bolt in the top bolt rows at the beam, resulting in splitting along this bolt row.

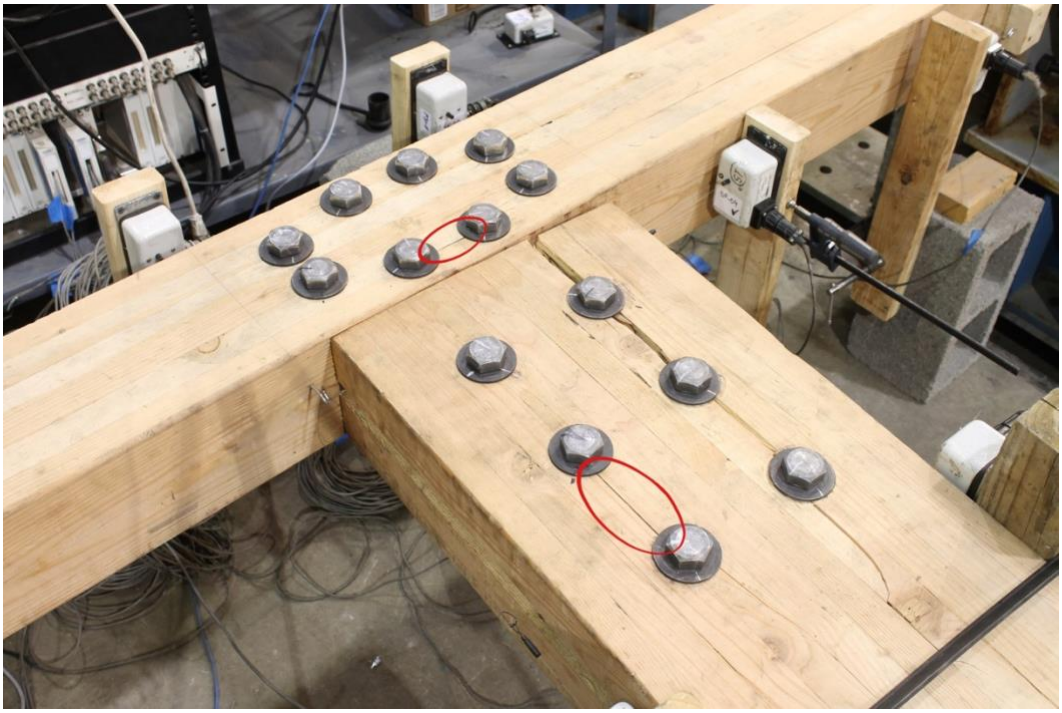

Figure 5.4 Two more cracks developed at the beam and column while the first crack started to get wider.

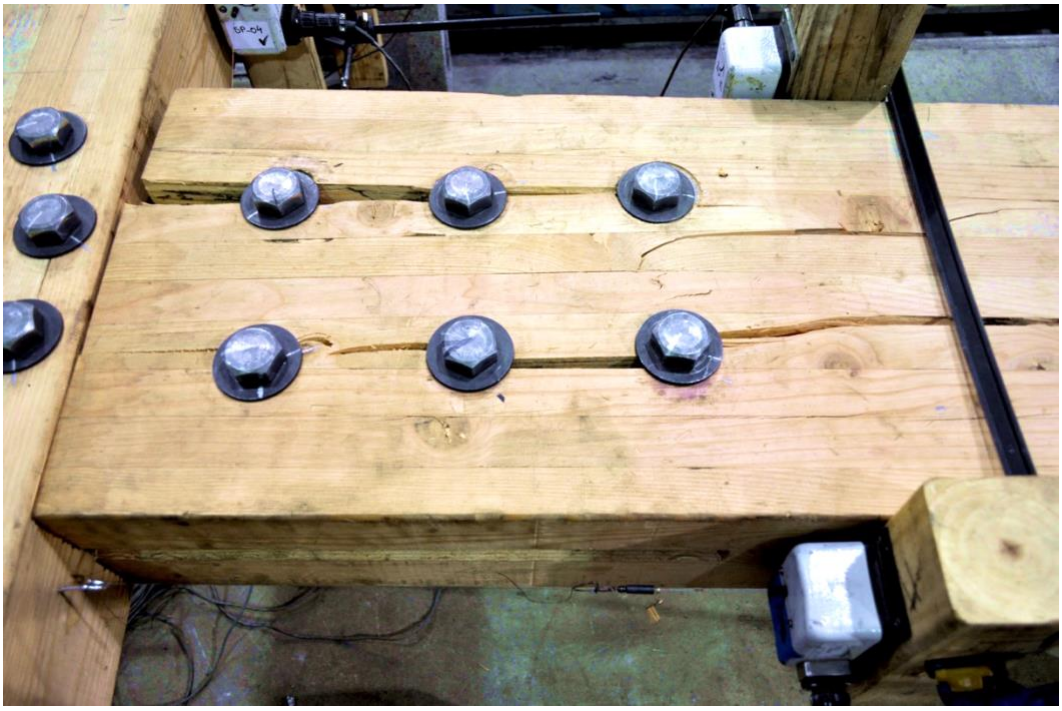

Figure 5.5 At failure, wood crushing occurred between the last top and bottom bolts away from the beam's end (right side), while the original beam cracks extended beyond the two bolt rows.

It can be observed from the moment-story drift angle plot that, at different stages of the test, there were reductions in moment. These reductions correspond to either slippage in the test setup or cracking at the glulam specimen. In the second loading phase, a steady decrease in moment from 258 kip-in. to 187 kip-in. started at a rotation of 0.0406 rad (point A) and ended at a rotation of 0.0446 rad (point B), corresponding to slippage in a test setup component. As the specimen started to pick up load again, another, more abrupt reduction in moment was observed. Specifically, it decreased from 319 kip-in. (point C) to 266 kip-in. at a rotation of 0.0589 rad, corresponding to the crack that developed at the beam's top bolt row (on the tension side). Afterwards, the test was paused as major slippage in a test component occurred. When the test was resumed, a drop from 328 kip-in. (point D) to 298 kip-in. of moment was observed at a rotation of 0.0878 rad, at a time when cracks at the top and bottom bolt rows of the beam enlarged. No further moment reductions were observed until failure occurred (point E).

At the beginning of the second loading phase, the stiffness of the connection was low compared to the initial and secondary stiffnesses. The oversized holes may have been the major contributor to low stiffness; as the load on the connection increased, the gaps between the bolts

and oversized holes closed, marking the start of the initial stiffness stage. The stiffness was calculated as the slope of the line tangent to the curve at that stage. This line passes through a point of 0.0121 rad of rotation and moment of 53.4 kip-in. and another point of 0.0327 rad of rotation and moment of 208 kip-in. The resulting initial stiffness was 7500 kip-in./rad. The secondary stiffness was defined by a point with a rotation of 0.0590 rad and 319 kip-in. of moment and an another point with 0.109 rad of rotation and 330 kip-in. of moment. The specimen had a secondary stiffness of 2180 kip-in./rad. The yielding point was taken as the intersection of the two lines defining the initial and secondary stiffnesses. The yielding moment, M_y, was equal to 316 kip-in. at a yielding rotation, θ_y, of 0.0471 rad. The specimen resisted an ultimate moment, M_u, of 332 kip-in. at a rotation, θ_u, of 0.0856 rad. The value of moment at specimen failure, M_f, equaled 327 kip-in. which occurred at a failure rotation, θ_f, of 0.112 rad. The ductility of the connection can be calculated using Equation (5-1). For this specimen, the ductility ratio was equal to 1.82.

$$\mu = \frac{\theta_u}{\theta_y} \tag{5-1}$$

5.1.2 Failure Modes

This specimen failed primarily at the beam in the form of splitting. The cracks that formed at the top and bottom bolt group at the beam propagated beyond the last bolt, especially at the lower row where the crack extended close to the beam's midpoint (Figure 5.6). The initiation of these cracks at the beam occurred due to the tension forces acting in the perpendicular-to-grain direction. The center of rotation of the connection may have shifted to the lower-left corner of the beam as bearing on the column occurred at the same location, which also resulted in embedment at the column (Figure 5.7). Accordingly, per the design process presented in Section 3.2.7, the shear force at each bolt, which results from applied moment, increased due to a longer moment arm at each bolt, resulting in perpendicular-to-grain splitting failure.

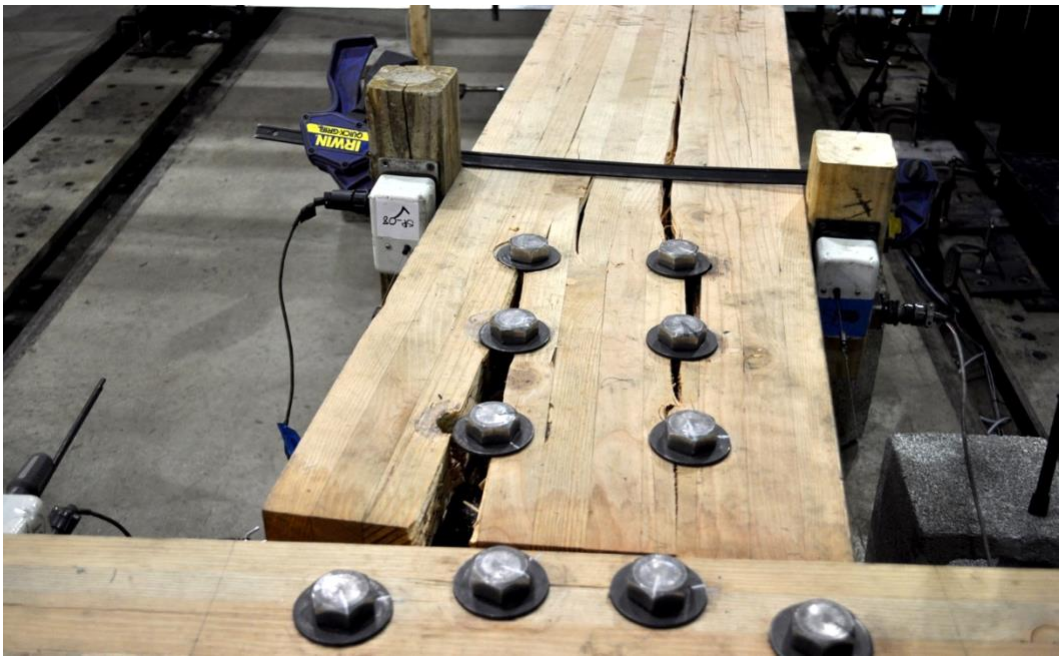

Figure 5.6 Cracks extended beyond the last bolt in either bolt row.

Figure 5.7 Beam bearing on column occurred at the beams end's lower-left corner.

After the test was concluded, the specimen was disassembled to inspect its various components and analyze the failure modes. At the beam, the cracks at the top and bottom bolt rows resulted in splitting failure in the perpendicular-to-grain direction. As can be seen in Figure 5.8, no deformation at bolt holes were perceivable, suggesting that splitting failure occurred before bolt

bearing could ensue. The steel plate did not yield, evidenced by the fact that no permanent deformation could be observed (Figure 5.9). Similarly, none of the bolts was deformed.

Figure 5.8 Only splitting failure in the perpendicular-to-grain direction occurred at the beam.

Figure 5.9 No permanent deformation occurred at the steel plate.

5.2 Specimen 2 Results

5.2.1 Behavior of the Specimen Under Loading

In the second test, Specimen 2 was monotonically loaded until failure. Figure 5.10 shows a plot of story drift angle versus moment for this specimen. The applied force was multiplied by the moment arm (91.6 in.), resulting in the applied moment on the connection. Figure 5.11 shows a plot of moment versus rotation angle at the connection.

Cracks at the glulam column appeared as the load on the connection started to increase. At first, a vertical crack appeared between the top-right bolt and the one below it, eventually extending to the third bolt in this vertical row (Figure 5.12). This crack was wider between the middle two bolts compared to the top two bolts in that row (Figure 5.13). The same figure shows beam bearing on the column, resulting in column bending. Another semi-vertical crack on the top-left bolt group immediately followed the first one, moving toward the left edge of the column (Figure 5.14). At the beginning of the second loading phase, this second crack started to widen at a higher rate than the first one, eventually splitting a diagonal layer of wood on the column's edge (Figure 5.15). In the third and final phase, the same crack developed further until column failure occurred. This crack propagated along the length of the column and progressed near one of its supports, resulting a combined splitting and bending failure in the column (Figure 5.16).

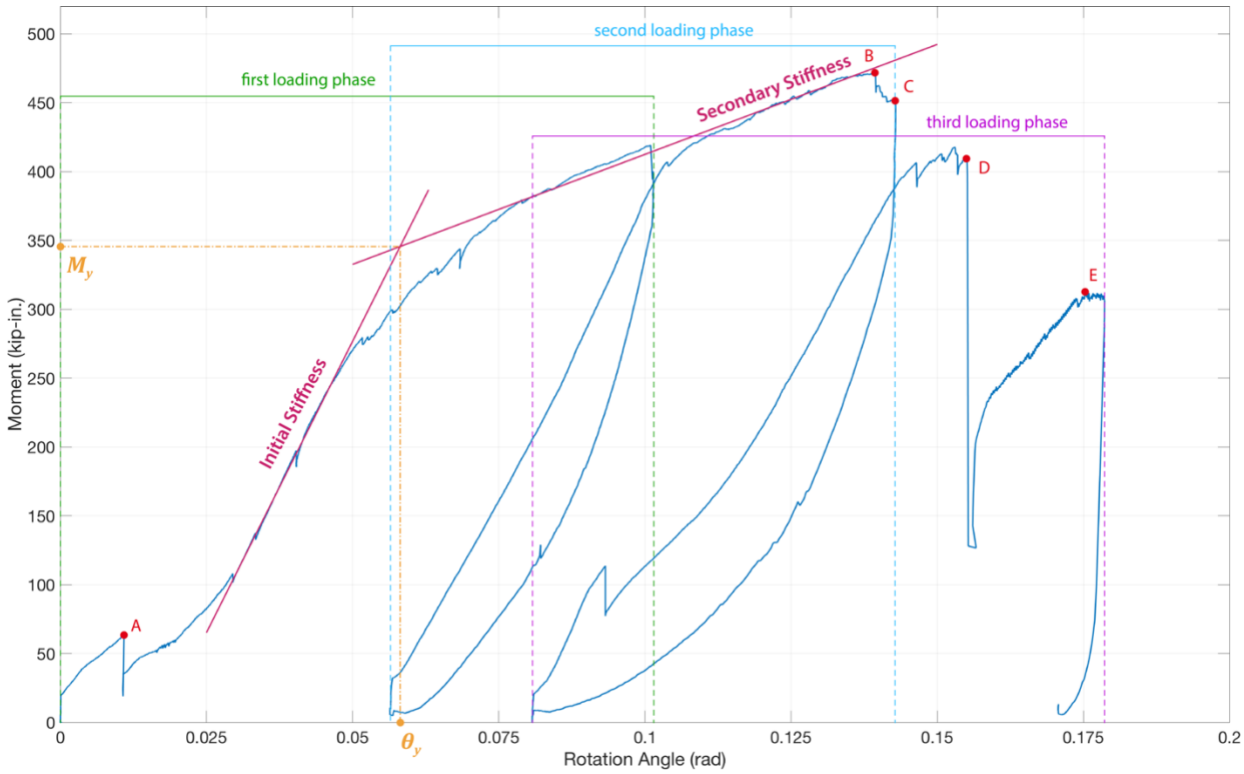

Figure 5.10 Moment-story drift angle plot for Specimen 2.

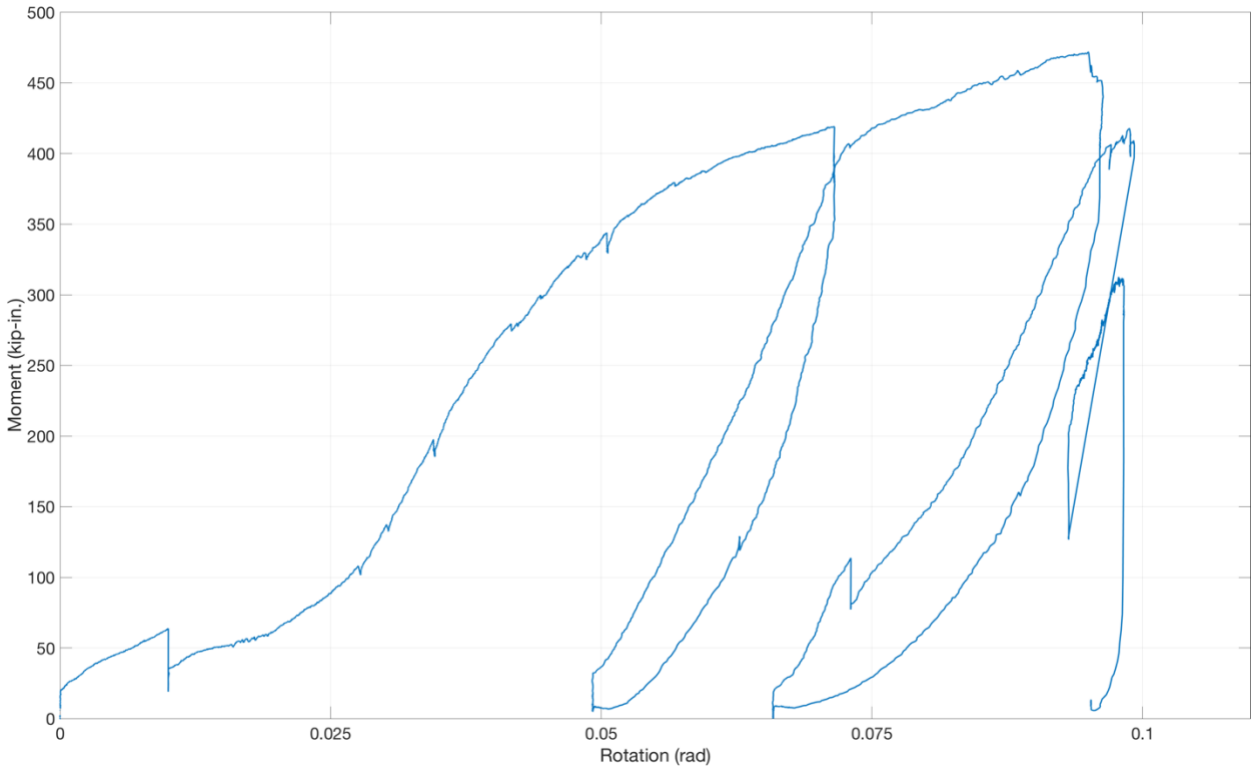

Figure 5.11 Connection moment-rotation angle plot for Specimen 2.

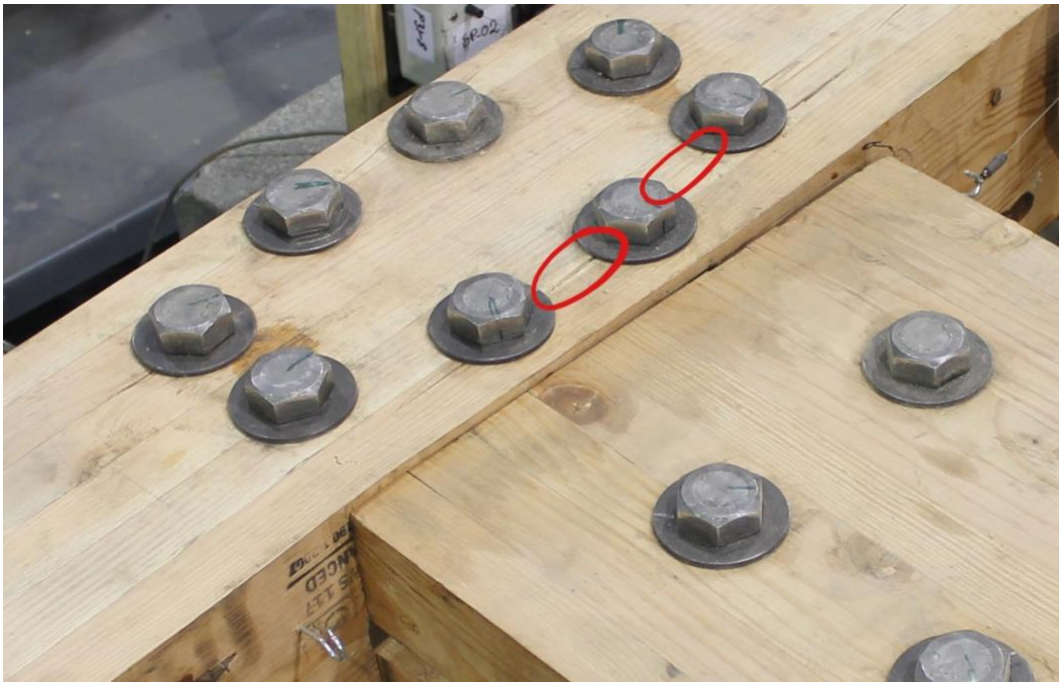

Figure 5.12 A crack initiated at the top-right column bolt group toward the end of loading phase 1.

Figure 5.13 A crack through the top-right column bolts was wider between the two middle bolts.

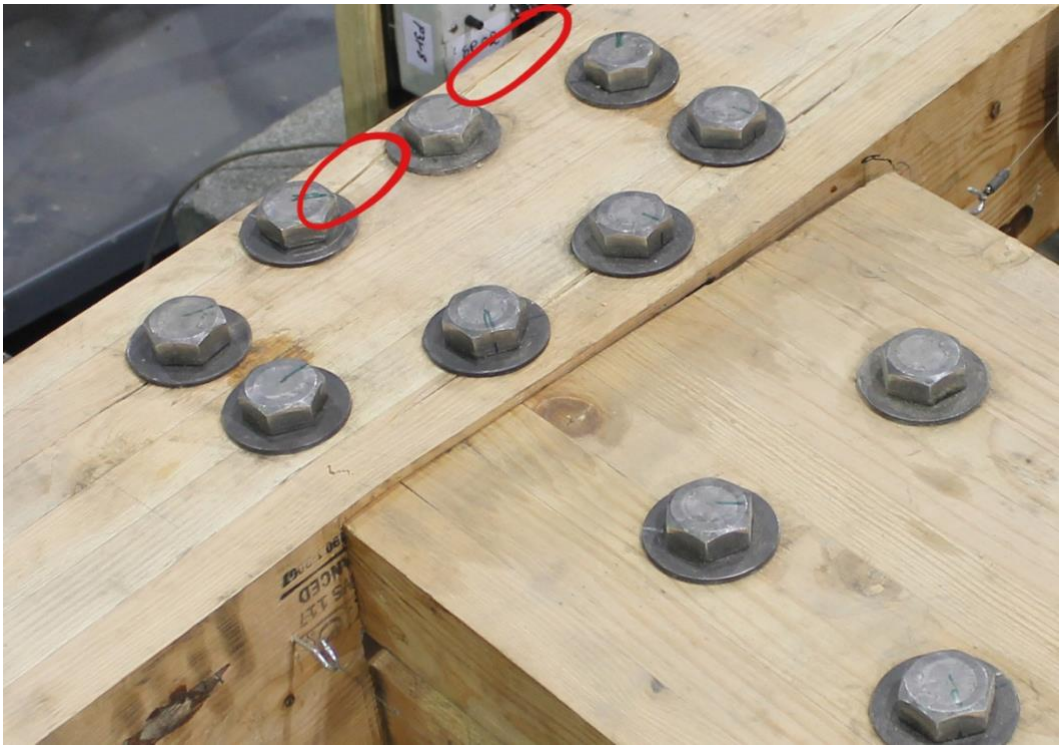

Figure 5.14 A second crack initiated on the left edge of the column as the first crack started to widen.

Figure 5.15 The crack at the column edge split a layer of wood at the end of the second loading phase.

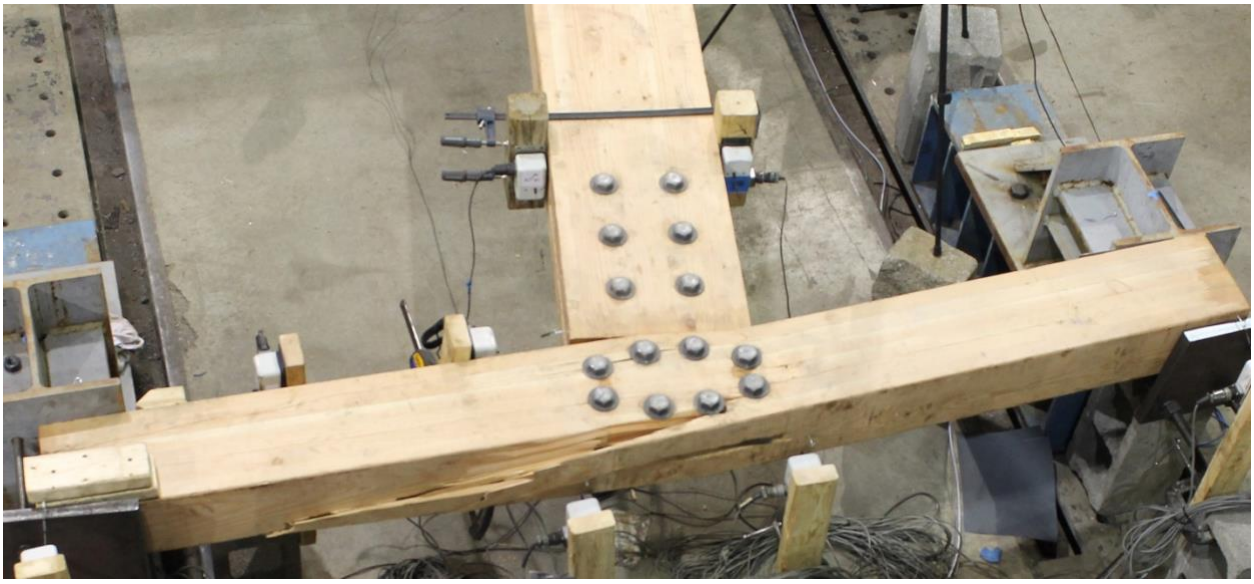

Figure 5.16 Combined splitting and bending failure occurred at the column.

A number of noticeable reductions in moment—possibly due to crack development—could be observed in the moment-story drift angle plot. At approximately 0.0109 rad of rotation, the moment dropped from 63.7 kip-in. (point A) to 19.0 kip-in. However, no slippage in the specimen was observed when this moment reduction occurred, which was confirmed by the lack of abrupt change in string potentiometer readings. Additionally, no cracks in the specimen were visible, suggesting that this moment drop may have corresponded to internal cracking in either of the glulam beam or column. Smaller moment reductions—consistent with the cracks that occurred during the first loading phase—can also be observed as the moment increased. At the end of the second loading phase, specifically at 0.139 rad of rotation, another reduction from the ultimate moment of 472 kip-in. (point B) to 452 kip-in. (point C) was observed, which was coincident with the crack that occurred at the column face opposite to where the beam was connected. In the final loading stage, the largest moment drop occurred shortly after the connection picked up the highest moment in this stage of 418 kip-in., falling from 409 kip-in. (point D) to 127 kip-in. at a rotation of 0.155 rad. This drop corresponded to connection failure in the form of column bending failure and splitting, as will be discussed later. Immediately after failure, the connection resisted up to 313 kip-in. of moment (point E) immediately before it was unloaded.

At the beginning stages of loading, the stiffness of the connection was low compared to initial and secondary stiffnesses at later stages. Similar to the first test, the gaps between the

oversized holes and the bolts are believed to have contributed to this low stiffness. The initial stiffness stage started around 0.0295 rad of rotation, which corresponded to 102 kip-in. of moment. At around 0.0464 rad of rotation and a moment of 246 kip-in., the initial stiffness stage ended, resulting in an initial stiffness of 8520 kip-in./rad (calculated as the slope of the line tangent to the moment-rotation curve). The line defining the secondary stiffness was approximated between 0.0803 rad and 0.135 rad of rotation, corresponding to 381 kip-in. and 469 kip-in. of moment, respectively. The resulting calculated secondary stiffness was 1600 kip-in./rad. The initial stiffness of the second loading phase was similar to that of the first phase, while the third phase exhibited a lower stiffness. The yielding moment, M_y, equaled 346 kip-in. at a yielding rotation, θ_y, of 0.0581 rad. The ultimate moment, M_u, equaled 472 kip-in. at a rotation, θ_u, of 0.139 rad. When the specimen failed, the recorded failure moment, M_f, was equal to 409 kip-in. at a failure rotation, θ_f, of 0.155 rad. To measure the ductility of the connection, Equation (5-1) was utilized, resulting in a ductility ratio of 2.39. The highest value of moment in the third loading phase, during which the specimen exhibited lower strength compared to the first two phases, was 418 kip-in. That is, the strength of the specimen dropped to around 88.6% after column splitting occurred at the end of the second loading phase.

5.2.2 Failure Modes

The connection failure primarily occurred at the column. As mentioned in the previous section, the column failed through a crack that initiated from the connection area and extended toward one column support. Figure 5.17 and Figure 5.18 show the extent of this crack along with the smaller crack developed at the top right vertical bolt row. Because the beam was reinforced with self-tapping screws, no splitting occurred at either of the bolt rows. Instead, the beam embedded on the column, resulting in column bending, which was more prominent than splitting, as shown in Figure 5.18 and Figure 5.19. It can be concluded that these two failure modes—crack propagation and bending—occurred simultaneously. That is, as bending of the column continued to increase due to beam bearing, the column crack on the side opposite to the beam connection widened. This splitting failure was caused by the increased tension forces acting in the perpendicular-to-grain direction at the column due to rotation of the bolt group.

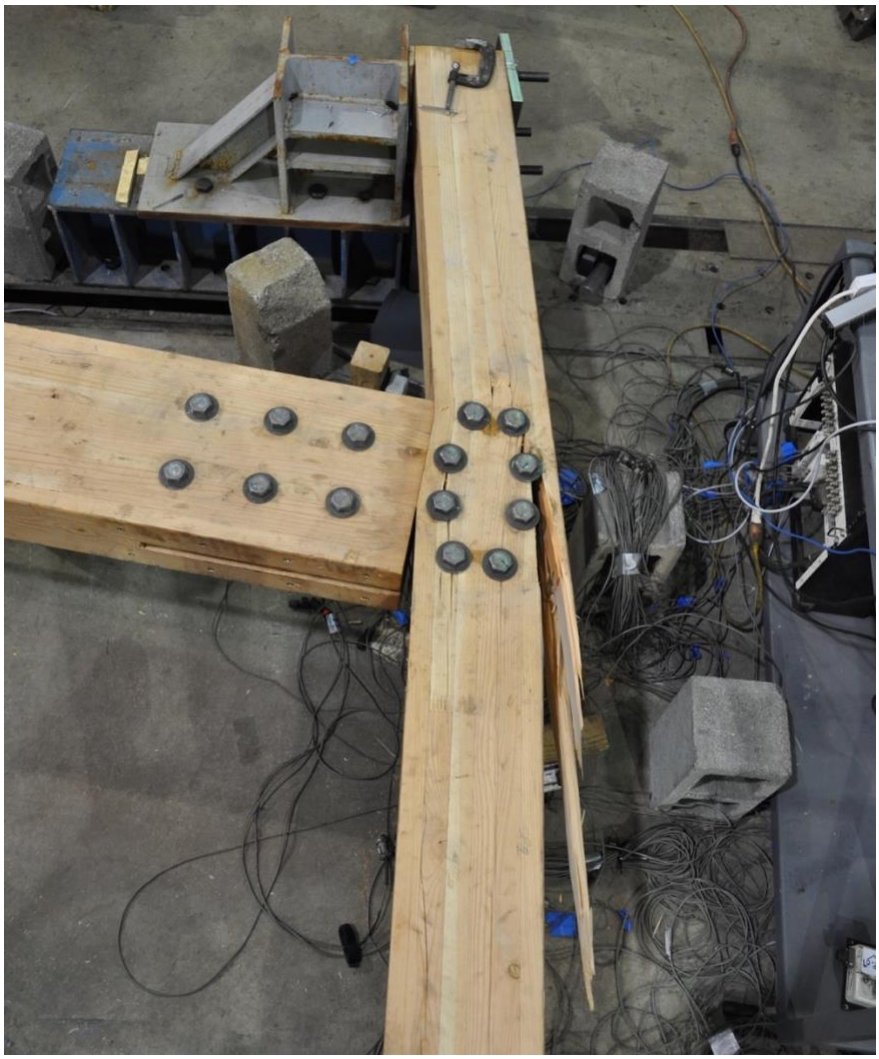

Figure 5.17 A crack extending form the column bolt group toward its support defines one of the failure modes observed.

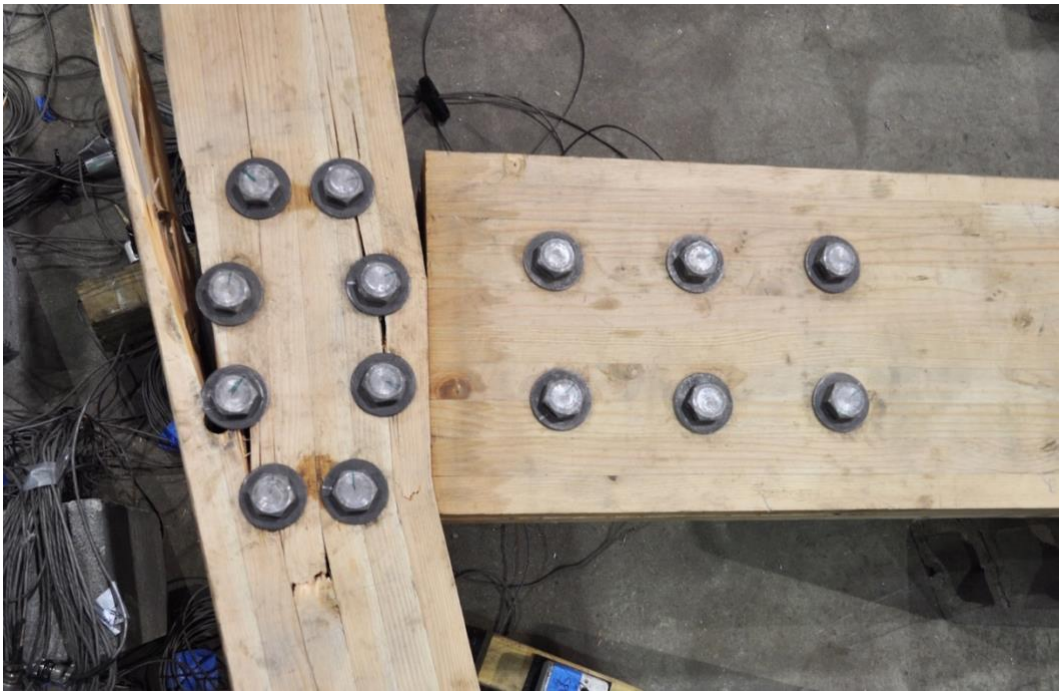

Figure 5.18 The cracks at the left and right vertical column bolt rows widened at failure as the beam embedded on the column.

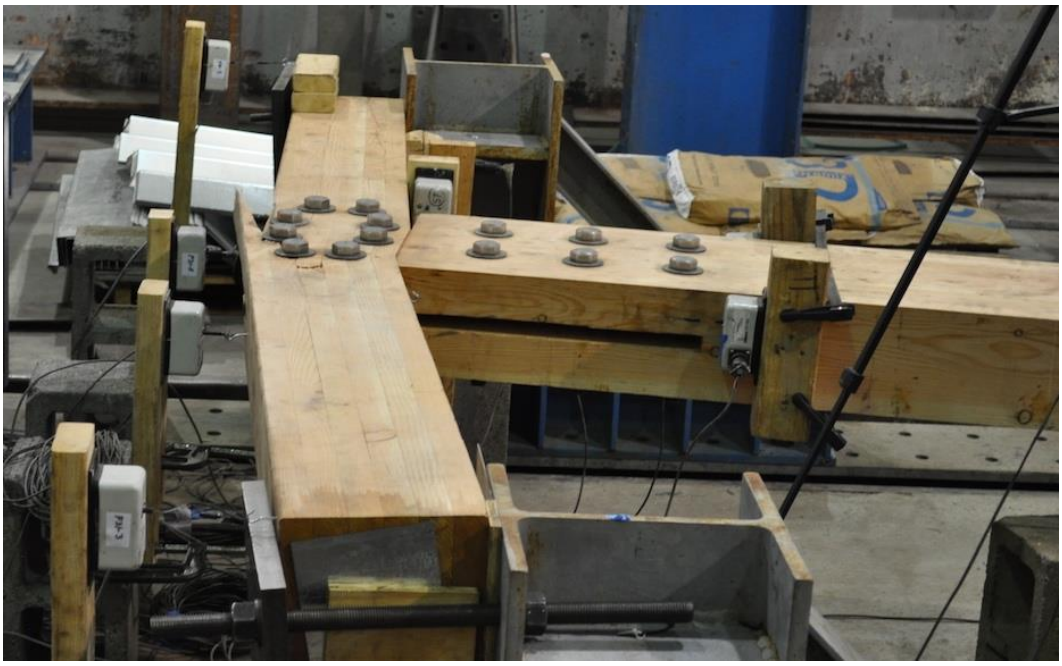

Figure 5.19 A combination of beam bending and splitting define the failure of the column.

To further analyze the test specimen post-failure and examine modes of failure, the connection was disassembled after completion of the test. The beam did not show signs of failure

as there were no cracks or bolt embedment on the holes (Figure 5.20). In addition to the cracking and bending explained earlier, some bolt holes at the column showed signs of deformation attributed to bolt bearing (Figure 5.21). The reduced section of the steel plate endured permanent, plastic deformation, suggesting that it yielded. The angle of deformation of the reduced plate section was approximately 0.04 rad (Figure 5.22). Four of the bolts—shown in Figure 5.23—deformed in bending. The first bolt (number 1) was the top-left bolt at the column, while the other three comprised the top bolt row at the beam, as shown in Figure 5.24.

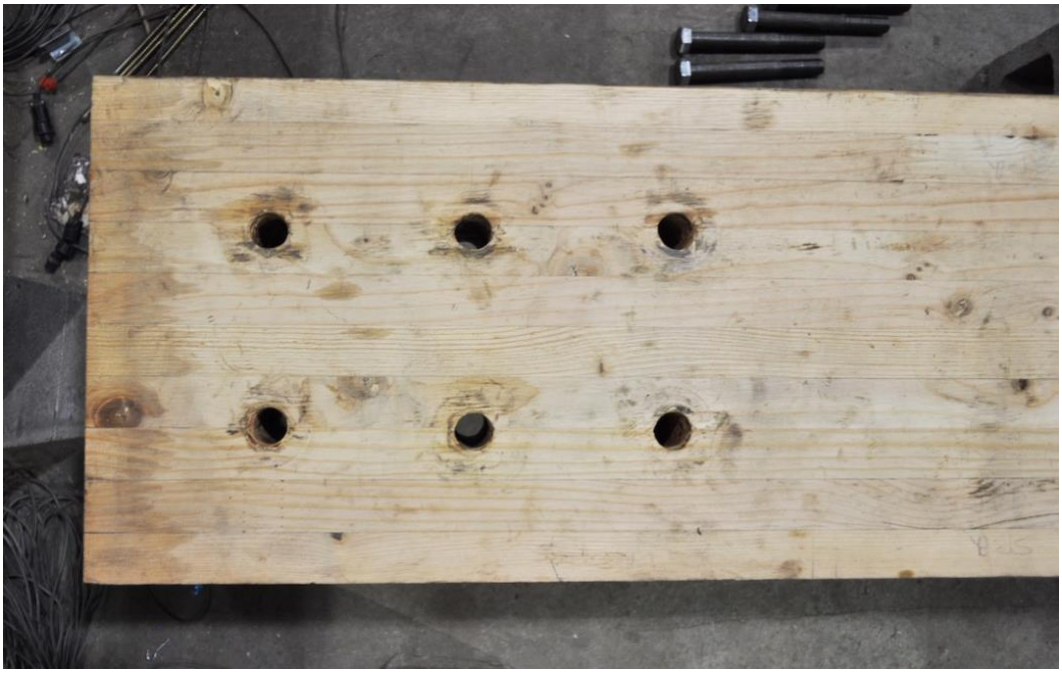

Figure 5.20 No cracks or bolt embedment can be observed at the beam.

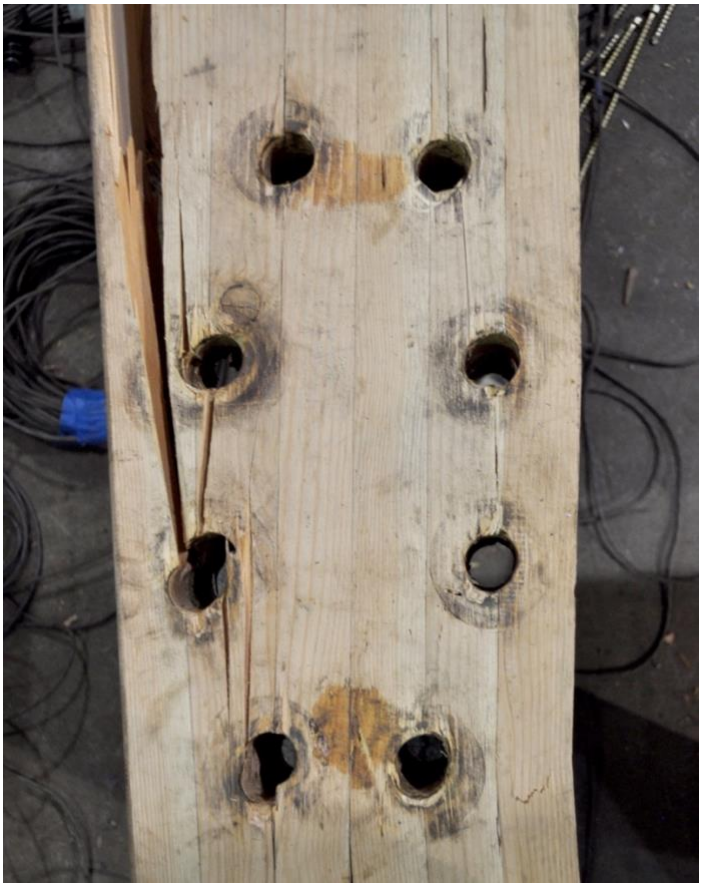

Figure 5.21 Deformation of glulam can be observed at some bolt holes due to bolt bearing.

Figure 5.22 The reduced section of the steel plate is deformed (the white, dashed lines are parallel to one another).

Figure 5.23 Four of the bolts in Specimen 2 were deformed.

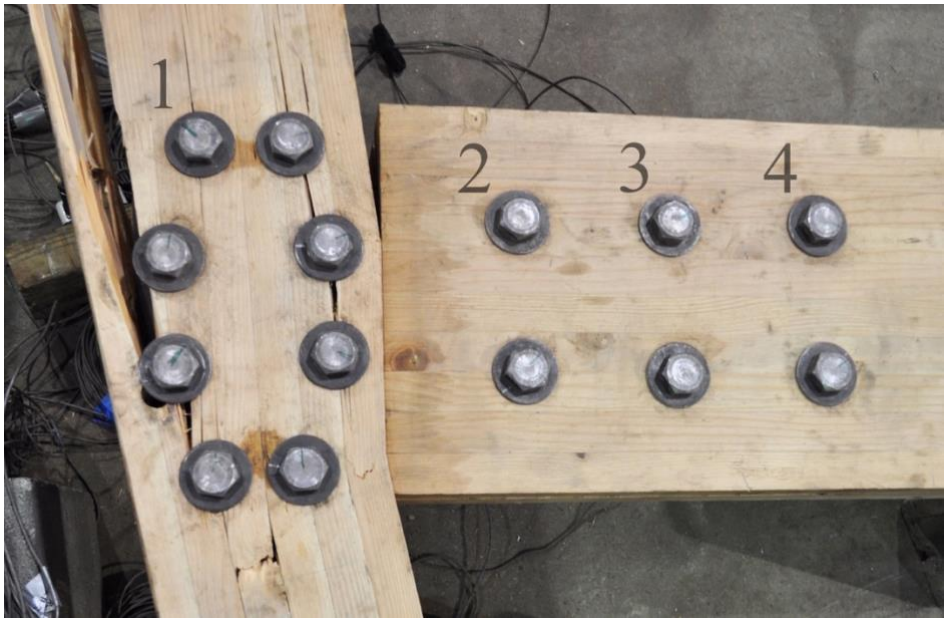

Figure 5.24 Locations of the four deformed bolts in Specimen 2.

5.3 Discussion

5.3.1 Strength, Stiffness, and Ductility

In general, Specimen 2 showed improved performance over the unreinforced Specimen 1. A summary of results obtained from the two tests is provided in Table 5.1. The initial stiffness of Specimen 2 was 13.6% higher than that of Specimen 1. However, the secondary stiffness decreased by 26.6%. The ultimate moment of Specimen 2 showed 42.2% improvement compared to Specimen 1, while the yielding moment increased by 9.49%. Additionally, a 25.1% enhancement in failure moment was obtained in the second specimen.

Specimen 2 exhibited larger rotational angles than Specimen 1. The rotation at yielding and ultimate moment increased by 23.4% and 62.4%, respectively, from Specimen 1 to Specimen 2. At failure, the second specimen showed 38.4% more rotation than the first one. Ductility of Specimen 2 was 31.3% higher than that of Specimen 1.

Table 5.1 Values obtained from results of the two tests are compared.

Parameter		**Specimen 1**	**Specimen 2**	**% Difference**
Yield	M_y (kip-in.)	316	346	9.49%
	θ_y (rad)	0.0471	0.0581	23.4%
Ultimate	M_u (kip-in.)	332	472	42.2%
	θ_u (rad)	0.0856	0.139	62.4%
Failure	M_f (kip-in.)	327	409	25.1%
	θ_f (rad)	0.112	0.155	38.4%
Ductility Ratio	μ	1.82	2.39	31.3%
Initial Stiffness	K_i (kip-in./rad)	7500	8520	13.6%
Secondary Stiffness	K_s (kip-in./rad)	2180	1600	-26.6%
Connection-to-Beam Strength (M_y/M_{beam})		30.1%	33.0%	9.63%

5.3.2 Failure Mechanisms

In the first specimen, the reduced section of the steel plate did not yield, which was attributed to the fact that the strength of the connection did not develop to the point where the plate

could yield. Because splitting failure at wood occurred prematurely, the highest value of moment that the connection resisted was 332 kip-in. Per design calculations for the Baseline Specimen presented in Section 3.3, which was the design used for Specimen 1, the steel plate would yield at 359 kip-in. of applied moment. The failure of specimen 1 was primarily brittle, as the cracks that initiated at the earlier stages of loading continued to widen until sudden failure occurred. Minor wood crushing at the column due to beam bearing was also observed.

In the second test, the steel plate did yield. It is unclear at which value of applied moment did plastic deformation occur at the plate's reduced section. Using the measured location of the yielding point (the intersection of the lines defining initial and secondary stiffnesses), yielding at the connection ensued at 346 kip-in. of applied moment, which is less than the calculated yielding moment of 359 kip-in. The inclusion of self-tapping screws as perpendicular-to-grain reinforcement improved the strength of the beam and prevented splitting failure. That, in turn, allowed the forces at the beam to develop and transfer to the reduced plate section, causing it to yield. While the failure mechanism of Specimen 2 was brittle, it exhibited some ductility when plate yielding occurred.

The design procedure described in Section 3.2.7 was used to investigate the failure of both specimens. Because bearing of the beam's lower-left corner on the column occurred at the earlier loading stages, the center of rotation of the connection shifted to the contact point. Figure 5.25 shows shear force distributions around the shifted center of rotation resulting from applied moment. Due to the relocation of center of rotation, the average moment arm was 13.9 in. compared to 5.47 in., which is the average moment arm if the center of rotation coincides with the center of bolt group, as illustrated in Figure 3.3. Therefore, the resulting total shear force acting in the perpendicular-to-grain direction at the beam, V_{Ty}, was 29.4 kips. Since the *NDS* does not provide design values for perpendicular-to-grain tension, this procedure only helps in determining the required perpendicular-to-grain reinforcement. The eight self-tapping screws used to reinforce the second specimen were able to resist a total of 20.4 kips of tension force, which was governed by the maximum tensile force of 2.55 kips per fastener. This total force resistance is lower than the calculated tensile forces, V_{Ty}, which suggests that the design procedures detailed in Section 3.2.7 may be conservative, since no splitting was observed at the beam. If only the force contributions from the top row of bolts at the beam were considered in the analysis, the total force acting in the perpendicular-to-grain direction, V_{Ty}, would be equal to 17.2 kips, which is lower

than the strength of the self-tapping screws. That is, when designing a perpendicular-to-grain reinforcement, it may be sufficient to only account for the force contributions from the row of bolts at which splitting failure is expected to occur. For example, if wood splitting is expected to occur at the bottom row of beam bolts, another set of specifically-designed self-tapping screws can be implemented at that location to prevent this limit state. However, this procedure requires further validation. Similarly, the reinforcement at the column can be designed such that splitting failure is prevented.

To develop the full strength of the moment connection, it is necessary to strengthen the glulam components against splitting in the perpendicular-to-grain direction. Reinforcement methods, such as the use of self-tapping screws, result in connections with higher strengths and ductility as well as greater predictability.

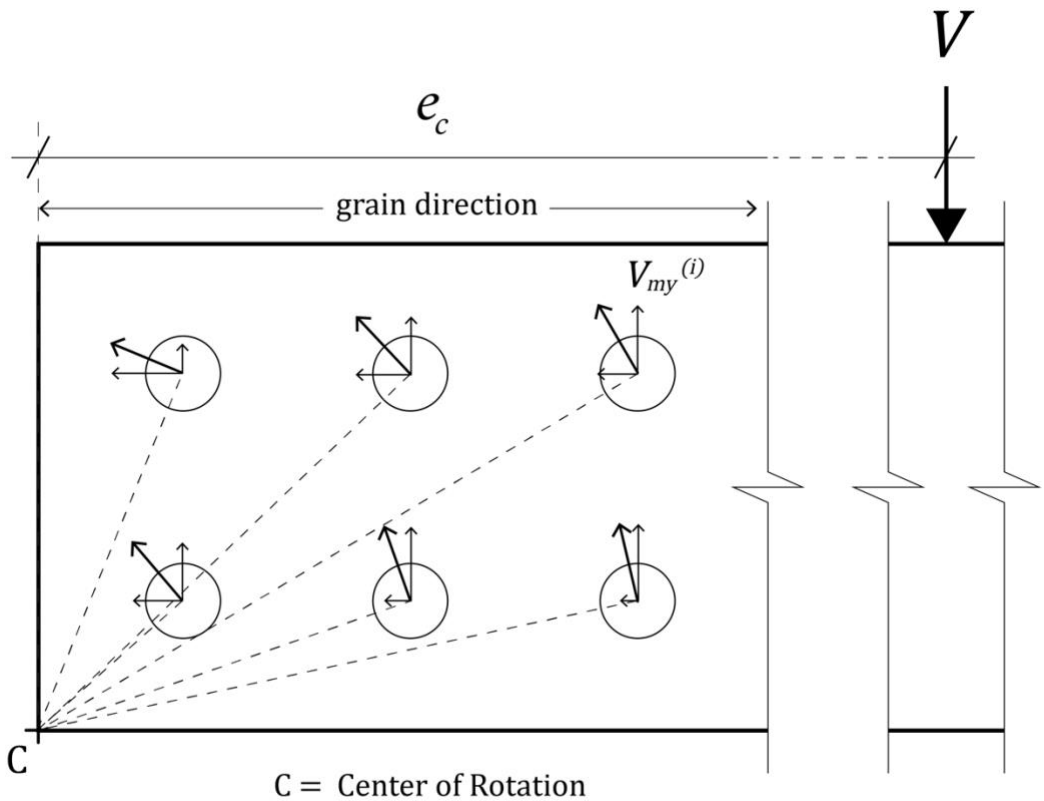

Figure 5.25 Shear force contributions due to moment resulting from eccentric loading at specimens 1 and 2.

CHAPTER 6: SUMMARY, CONCLUSIONS, AND RECOMMENDATIONS FOR FUTURE WORK

6.1 Summary

A design procedure for a glulam moment-resisting connection was presented and used to develop a Baseline connection design. This procedure utilizes an embedded steel plate with a reduced section that yields as the applied moment on the connection increases, preventing wood limit states from occurring prematurely. While researchers have developed high-strength and ductile glulam moment connections, this research addressed limitations related to incompatibility with multi-bay moment frames and low fire rating.

Two test specimens based on the Baseline connection were then designed, fabricated, and subjected to monotonic loading. To analyze the results of the tests, plots of moment-versus-story drift angle for each test specimen were produced. Comparisons between the performance of the two test specimens were presented and discussed.

6.2 Conclusions

Test results indicated that self-tapping screw reinforcement enhanced the performance of the connection in comparison to the unreinforced specimen. Improvements of 42.2% in ultimate moment, 13.6% in initial stiffness, and 31.3% in ductility were achieved. Additionally, the connection-to-beam strength ratio for the first and second specimens were 30.1% and 33.0%, respectively.

The performance of the connection specimens developed in this research is comparable to connections described in the literature. In terms of strength, the second specimen exhibited moment-resistance performance similar to high-strength connections. The stiffness, however, was comparable to middle- to low-stiffness connections. For example, some traditional connections have been characterized by initial stiffnesses in the range of 2000 to 3000 kip-in/rad, while some novel connections have achieved initial stiffnesses as high as 20000 kip-in/rad. In terms of ductility, the connection specimens were also on the lower side. Some novel connections achieved ductility ratios above 9, compared to the 2.39 ratio that characterized the second specimen.

In conclusion, while the connections developed in this study exhibited high strength, they did not perform as well as expected in terms of stiffness and ductility. However, the potential for

future refinements to the design process can result in improved ductility and stiffness. Compared to the connections presented in past research, the design approach presented here can be modified to allow for the development of connections that are compatible with multi-bay moment frames. Additionally, higher fire ratings can be achieved since this design approach provides more wood cover over the steel plate in comparison to existing connections.

6.3 Recommendations for Future Work

While the connections developed in this study did not perform as intended in terms of stiffness and ductility, the results described herein suggest a range of opportunities for future development. A number of recommendations for future work aimed at improving the performance of the connections developed in this study are provided below:

1. To prevent the beam from bearing on the column, a gap may be incorporated at the intersection of the two members. Additionally, the corners of the beam can be rounded to allow it to rotate without bearing on the column at the earlier loading stages.
2. Self-tapping screws can be used to reinforce the column to prevent wood splitting. This may help improve ductility. Also, the column may need to be designed for higher flexural capacity.
3. Staggering the bolts at the beam may help reduce the tendency of splitting failure to occur.
4. Comprehensive fire testing may be required to validate and quantify the fire resistance of the connections.
5. An improvement to the initial stiffness of the connections is necessary. Oversized holes, which result in low initial stiffness due to clearance, are necessary in wood structures to allow wood to expand and shrink without incurring internal stresses. Some proposed stiffness improvement methods in the literature include fiberglass reinforcement (Windorski et al., 1997) and epoxy resin filler at bolt holes (Buchanan & Moss, 1999).

REFERENCES

AISC. (2016a). *Prequalified Connections for Special and Intermediate Steel Moment Frames for Seismic Applications (ANSI/AISC 358-16)* (ANSI/AISC). American Institute of Steel Construction. https://doi.org/10.1061/40889(201)5

AISC. (2016b). *Seismic Provisions for Structural Steel Buildings (AISC 341)*. American Society of Civil Engineers.

AISC. (2016c). *Specification for Structural Steel Buildings (AISC 360)*. American Society of Civil Engineers.

American Wood Council. (2015). *National Design Specification for Wood Construction*.

Andreolli, M., Piazza, M., Tomasi, R., & Zandonini, R. (2011). Ductile moment-resistant steel–timber connections. *Proceedings of the Institution of Civil Engineers - Structures and Buildings*, *164*(2), 65–78. https://doi.org/10.1680/stbu.9.00098

Araki, Y., Endo, T., & Iwata, M. (2010). Feasibility of improved slotted bolted connection for timber moment frames. *Journal of Wood Science*, *57*(3), 247–253. https://doi.org/10.1007/s10086-010-1165-7

ASCE. (2017). *Minimum Design Loads and Associated Criteria for Buildings and Other Structures* (ASCE/SEI 7). American Society of Civil Engineers. https://doi.org/10.1061/9780784414248

Barber, D. (2017). Determination of fire resistance ratings for glulam connectors within US high rise timber buildings. *Fire Safety Journal*, *91*(xxxx), 579–585. https://doi.org/10.1016/j.firesaf.2017.04.028

Buchanan, A., & Moss, P. (1999). Design of Epoxied Steel Rods in Glulam Timber. *Forest Research Bulletin*.

Canadian Wood Council. (2002). Wood-Frame Housing – A North American Marvel, (4).

He, M., Zhao, Y., & Ma, R. (2016). Experimental investigation on lateral performance of pre-stressed tube bolted connection with high initial stiffness. *Advances in Structural Engineering*, *19*(5), 762–776. https://doi.org/10.1177/1369433215622863

Karagiannis, V., Málaga-Chuquitaype, C., & Elghazouli, A. Y. (2016). Behaviour of hybrid timber beam-to-tubular steel column moment connections. *Engineering Structures*, *131*, 243–263. https://doi.org/10.1016/j.engstruct.2016.11.006

Komatsu, K., Akagi, M., Kawai, C., Mori, T., Hattori, S., & Hosokawa, K. (2008). Improved column-beam joint in glulam semi-rigid portal frame. *10th World Conference on Timber Engineering 2008*, *2*, 1010–1017. Retrieved from https://www.scopus.com/inward/record.uri?eid=2-s2.0-84865796372&partnerID=40&md5=11006ff61d8fce1779481472d84a4cd1

Lam, F., Schulte-Wrede, M., Yao, C. C., & Gu, J. J. (2008). Moment resistance of bolted timber connections with perpendicular to grain reinforcements. *World Conference on Timber Engineering*, 3–10.

Milner, H. R. (2009). Sustainability of engineered wood products in construction. *Sustainability of Construction Materials*, 184–212. https://doi.org/10.1533/9781845695842.184

Organschi, A., Ruff, A., Oliver, C., Carbone, C., & Herrmann, E. (2016). Timber City : Growing an Urban Carbon Sink With Glue , Screws , and Cellulose Fiber. *Proceedings of the WCTE 2016 World Conference on Timber Engineering, Vienna / Austria, August 22-25, 2016*.

Salem, S. (2016). Experimental Testing of Steel-Wood-Steel Glulam Frame Bolted Connections. *Proceedings of the WCTE 2016 World Conference on Timber Engineering, Vienna / Austria, August 22-25, 2016*.

Salem, S., & Petrycki, A. (2016). Experimental testing of wood-steel-wood moment-resisting bolted connections. *World Conference on Timber Engineering*.

Salmon, C. G., Johnson, J. E., & Malhas, F. A. (2009). *Steel Structures Design and Behavior* (Fifth Edit). Pearson Prentice Hall.

Takač, S., Varevac, D., & Markulak, D. (2008). Analysis of the Stress Distribution in the Semispace of the Steel Pinned Joint. *World Conference on Timber Engineering*, 619–626.

Wakashima, Y., Okura, K., & Kyotani, K. (2010). Development of ductile semi-rigid joints with lagscrewbolts and glued-in rods. *11th World Conference on Timber Engineering 2010, WCTE 2010, June 20, 2010 - June 24, 2010*, *4*, 3221–3228.

Windorski, D. F., Soltis, D. F., & Ross, J. R. (1997). Feasibility of Fiberglass-Reinforced Bolted Wood Connections. *Most*, 12.

Yeh, M.-C., Wu, K.-C., & Lin, Y.-L. (2008). Moment-resisting capacity of bolt connections in japanese cedar structural glulam members. *Taiwan Journal of Forest Science*, *23*(4), 365–375.

APPENDIX A: DISPLACEMENT-TIME PLOTS

Corrected displacement data for each string potentiometer used in Specimen 1.

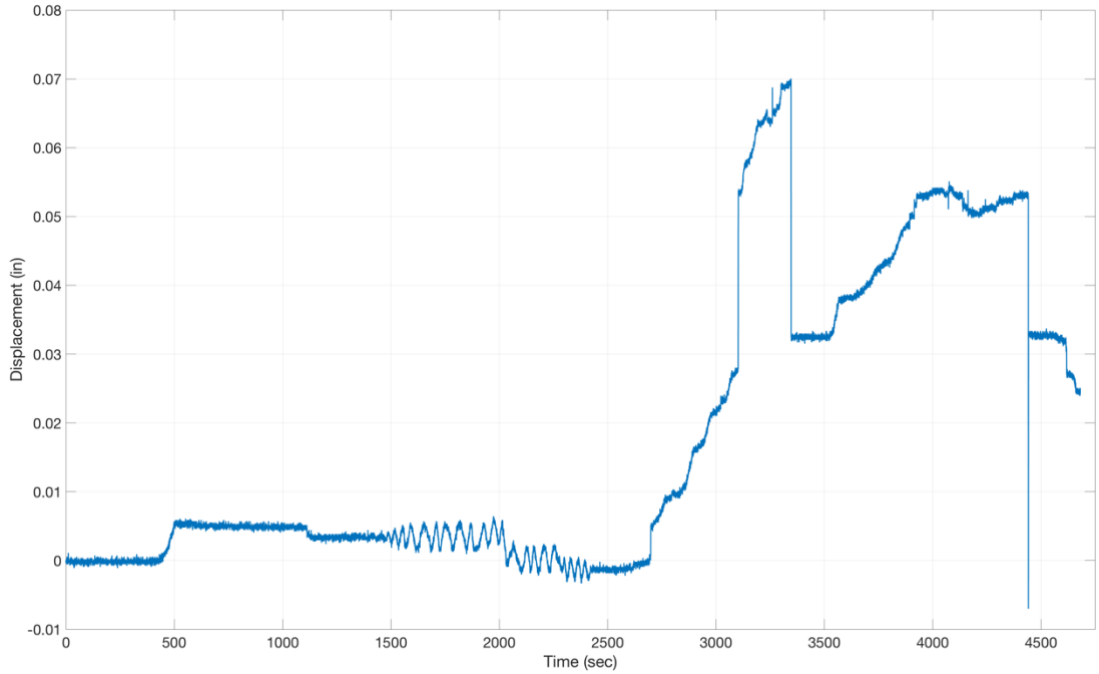

Figure A.1 Corrected displacement-time relationship for string potentiometer SP01 at Specimen 1.

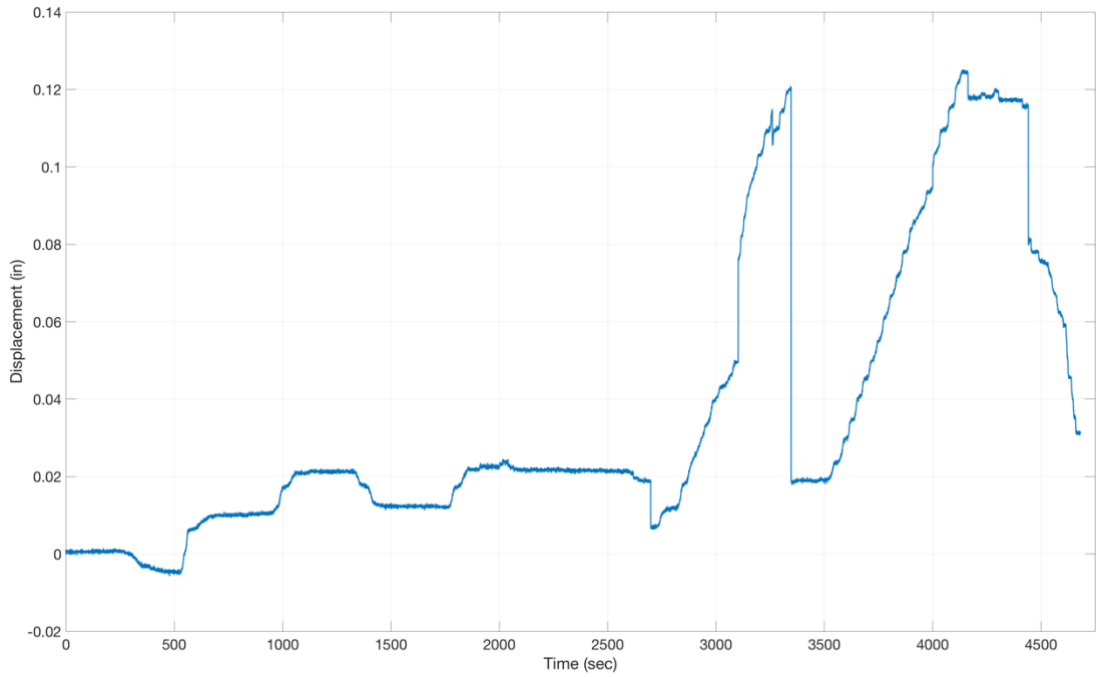

Figure A.2 Corrected displacement-time relationship for string potentiometer SP02 at Specimen 1.

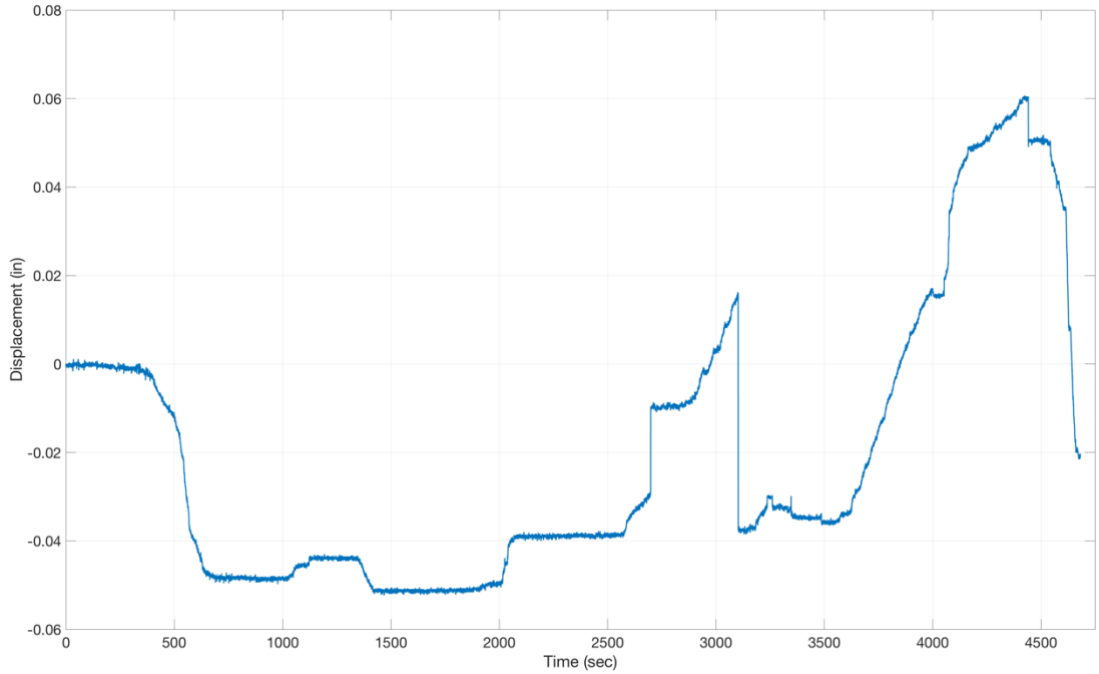

Figure A.3 Corrected displacement-time relationship for string potentiometer SP03 at Specimen 1.

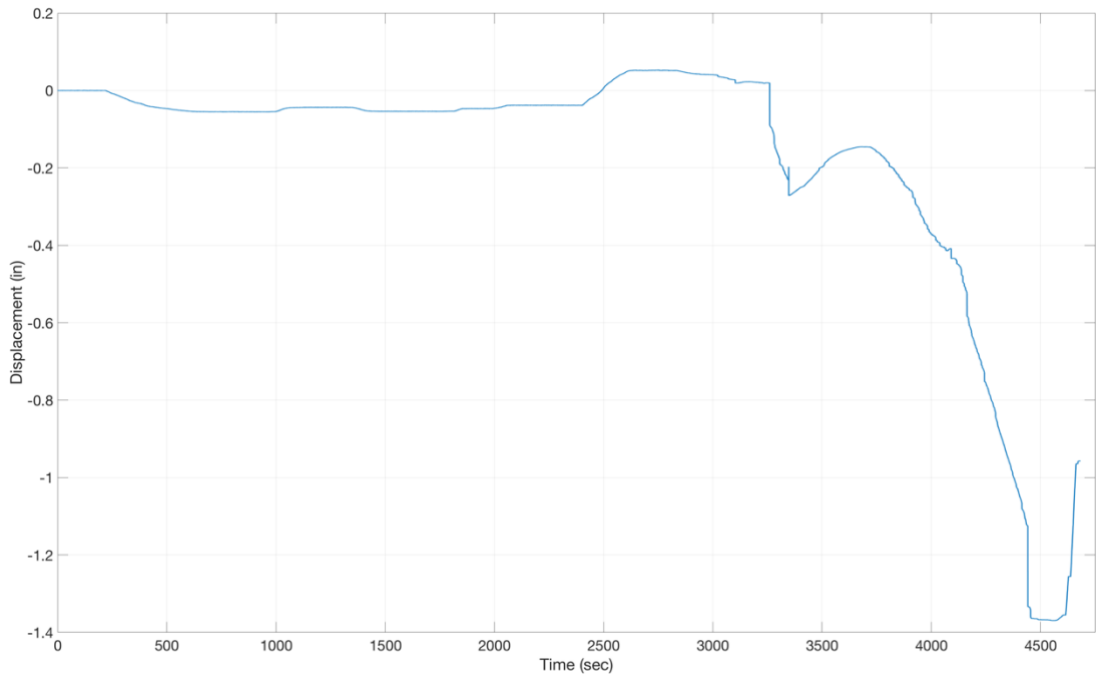

Figure A.4 Corrected displacement-time relationship for string potentiometer SP04 at Specimen 1.

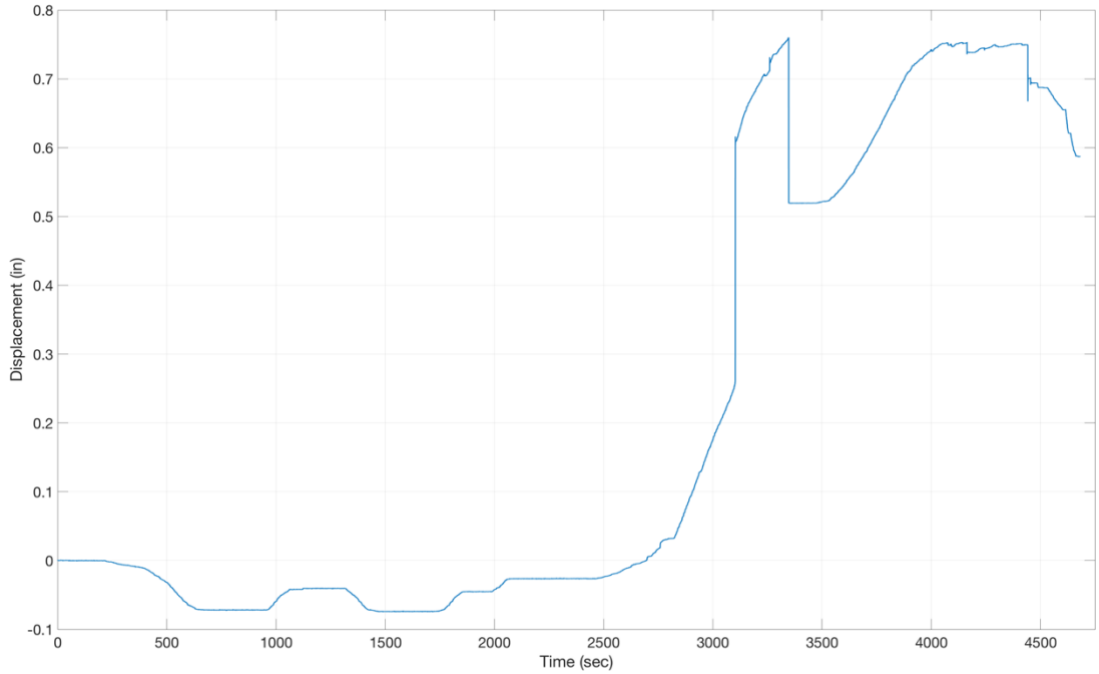

Figure A.5 Corrected displacement-time relationship for string potentiometer SP05 at Specimen 1.

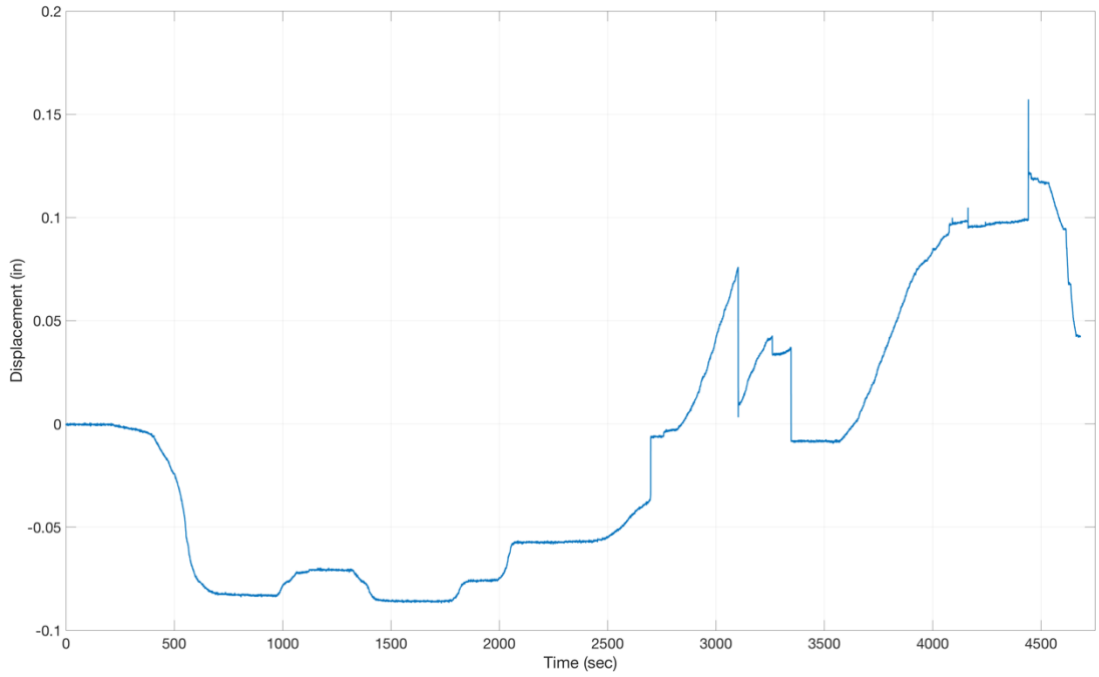

Figure A.6 Corrected displacement-time relationship for string potentiometer SP06 at Specimen 1.

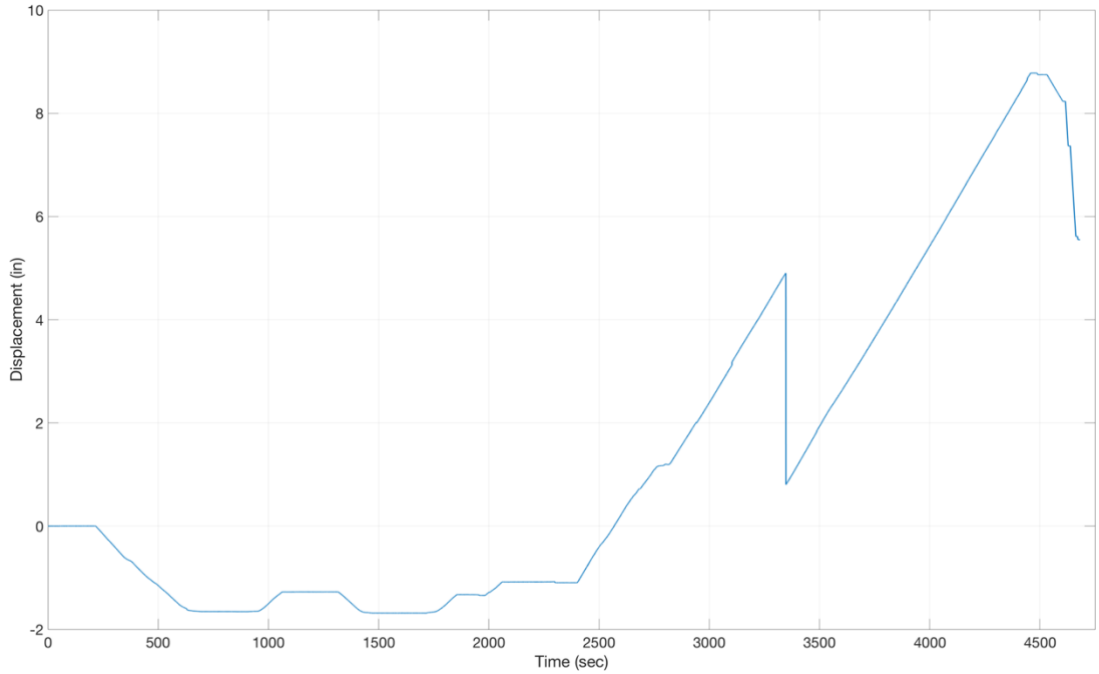

Figure A.7 Corrected displacement-time relationship for string potentiometer SP07 at Specimen 1.

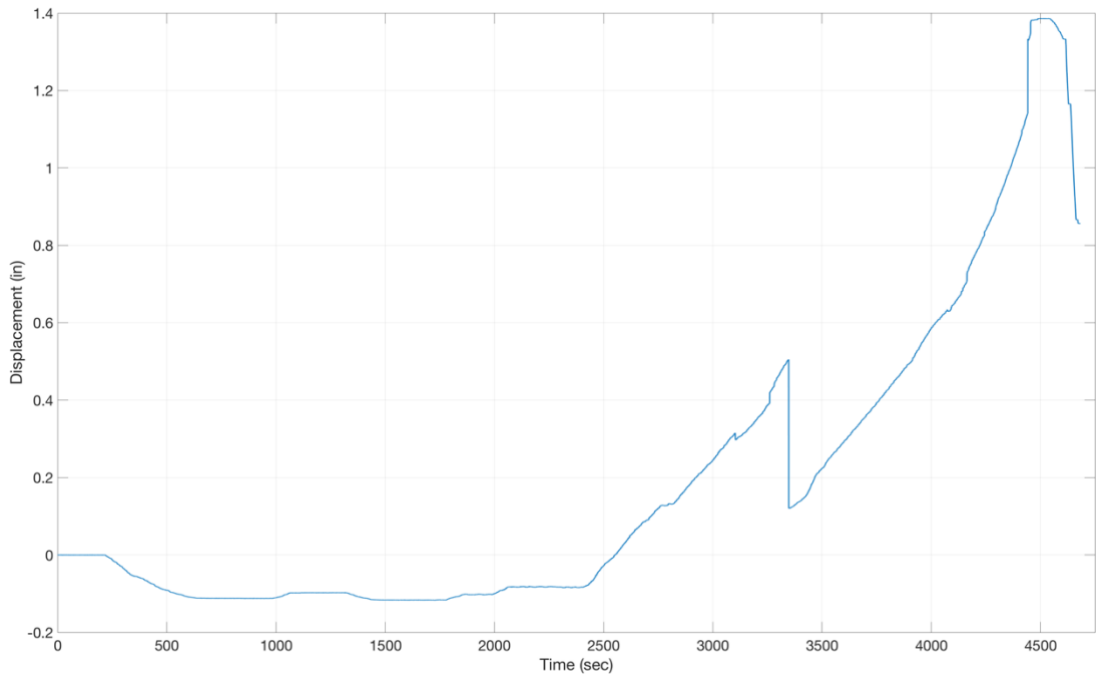

Figure A.8 Corrected displacement-time relationship for string potentiometer SP08 at Specimen 1.

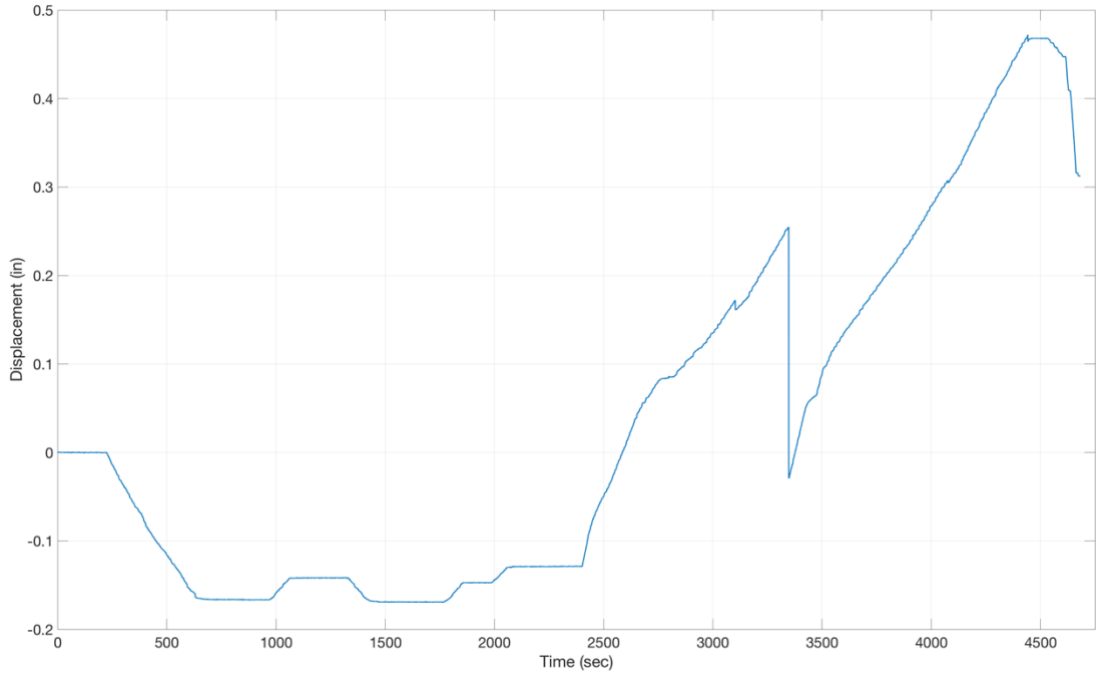

Figure A.9 Corrected displacement-time relationship for string potentiometer SP09 at Specimen 1.

Original (uncorrected) displacement data for each string potentiometer used in Specimen 1.

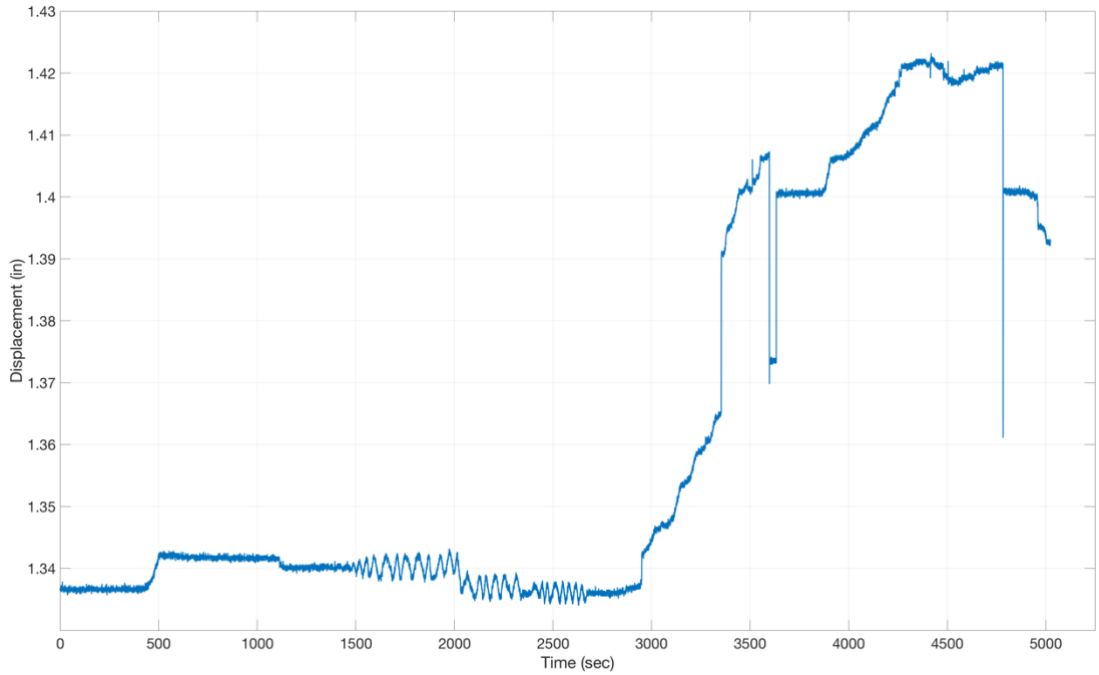

Figure A.10 Uncorrected displacement-time relationship for string potentiometer SP01 at Specimen 1.

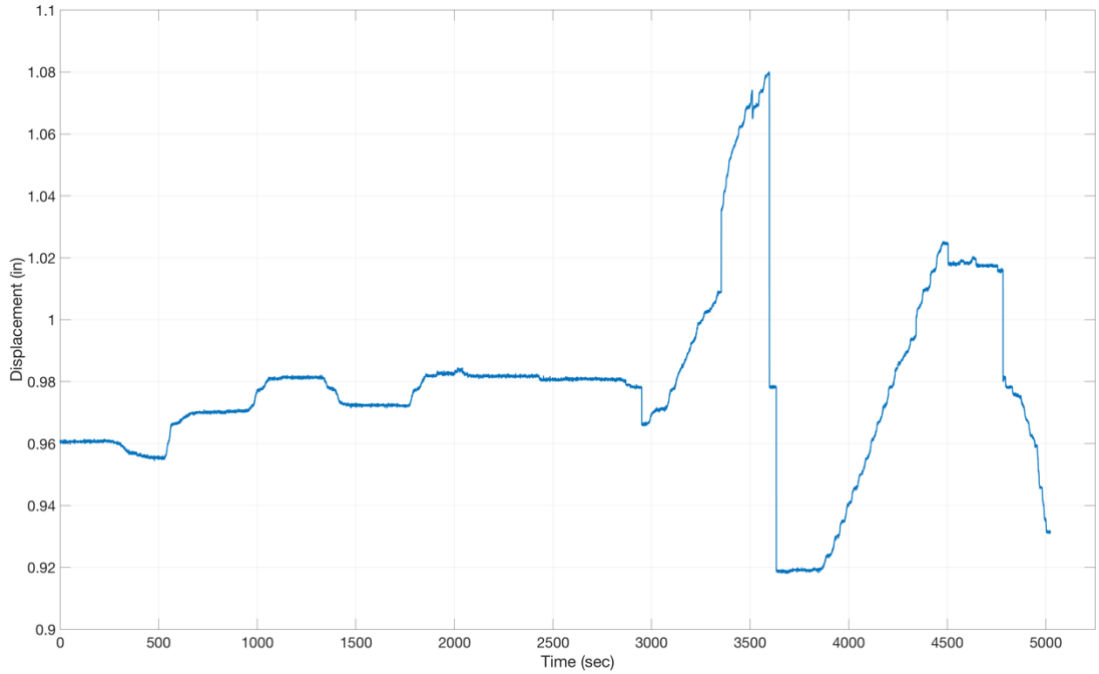

Figure A.11 Uncorrected displacement-time relationship for string potentiometer SP02 at Specimen 1.

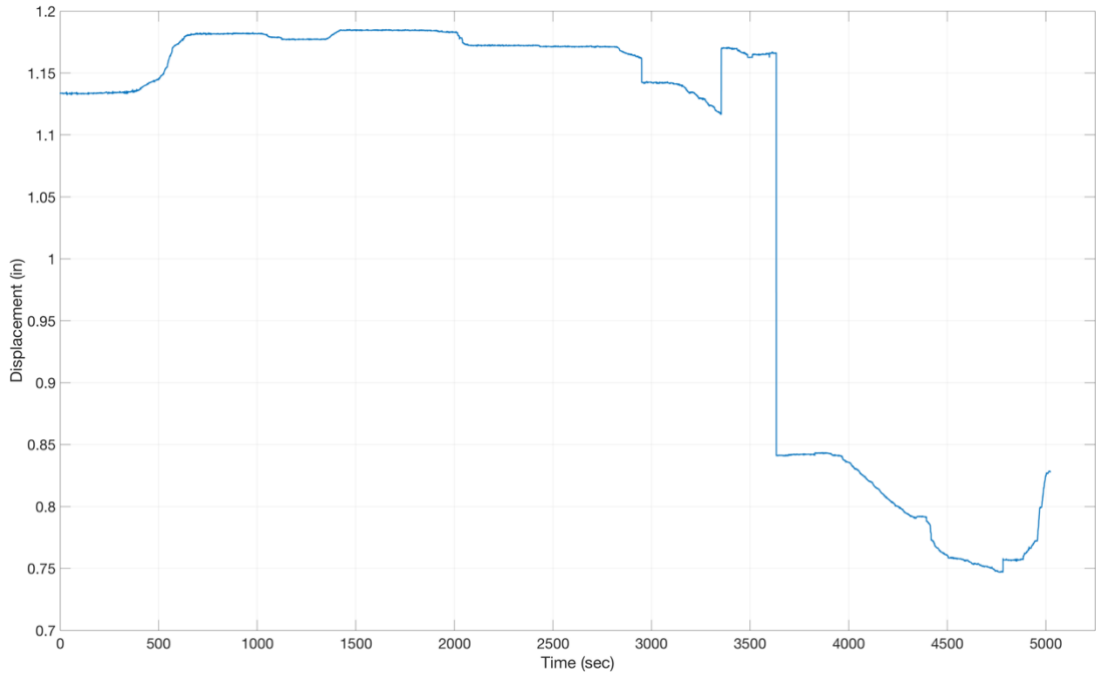

Figure A.12 Uncorrected displacement-time relationship for string potentiometer SP03 at Specimen 1.

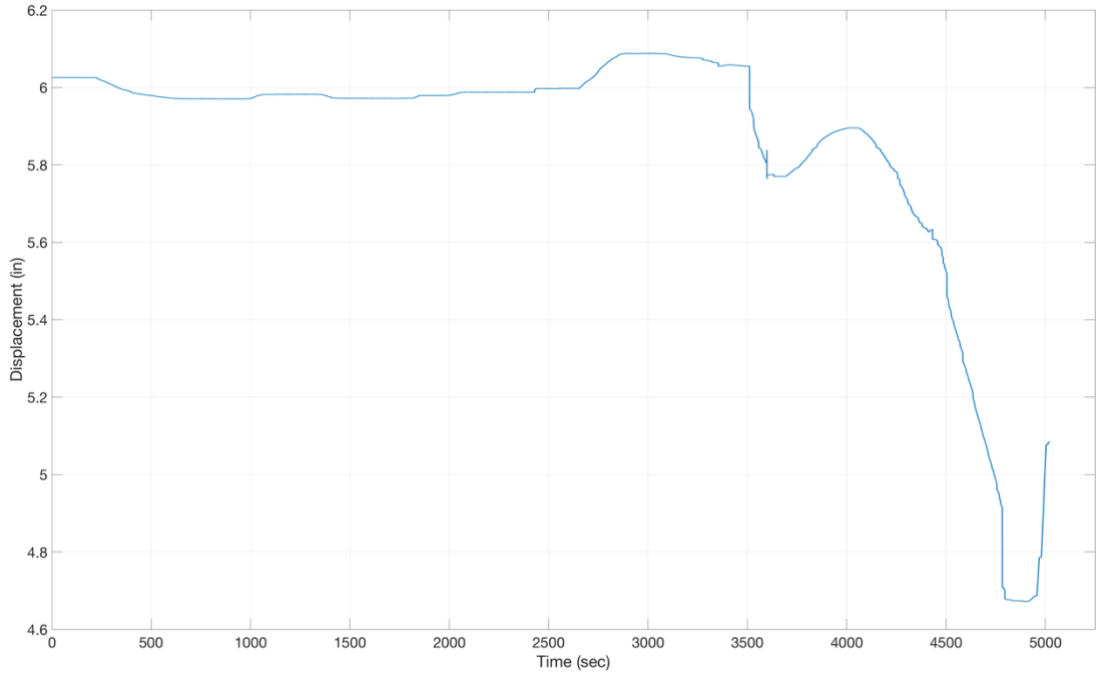

Figure A.13 Uncorrected displacement-time relationship for string potentiometer SP04 at Specimen 1.

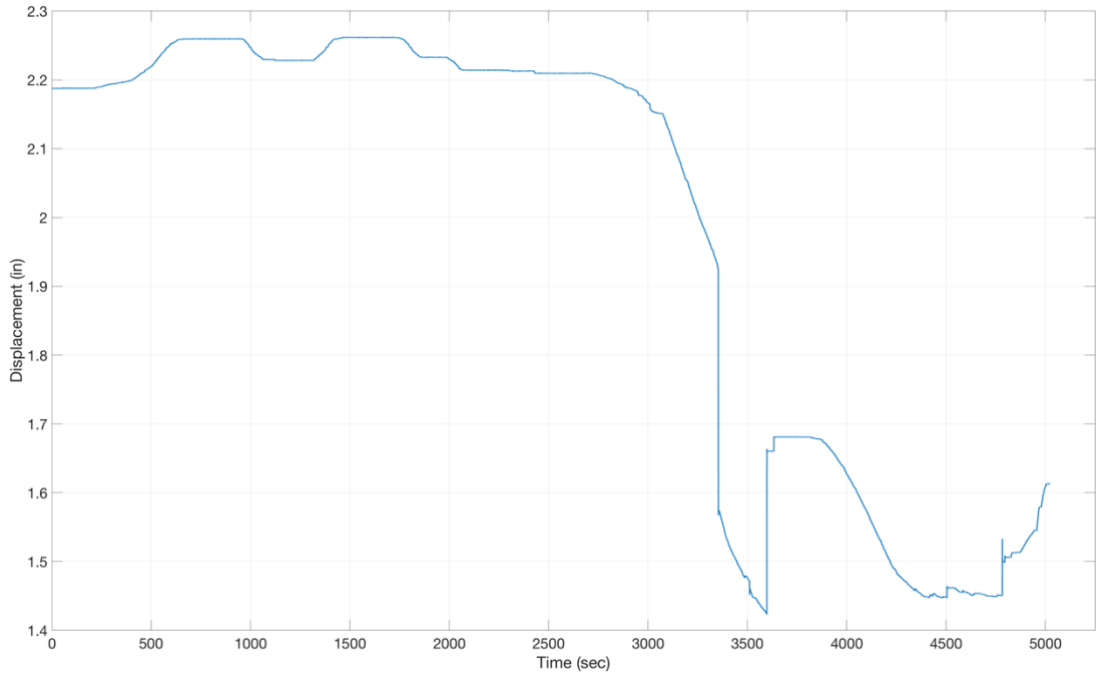

Figure A.14 Uncorrected displacement-time relationship for string potentiometer SP05 at Specimen 1.

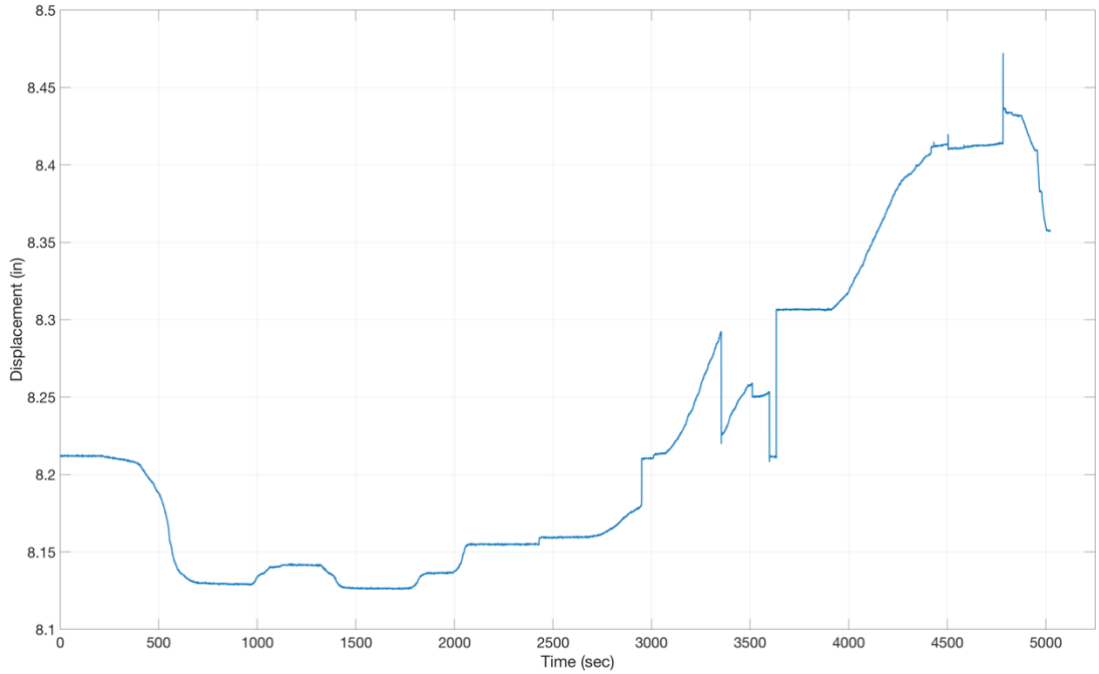

Figure A.15 Uncorrected displacement-time relationship for string potentiometer SP06 at Specimen 1.

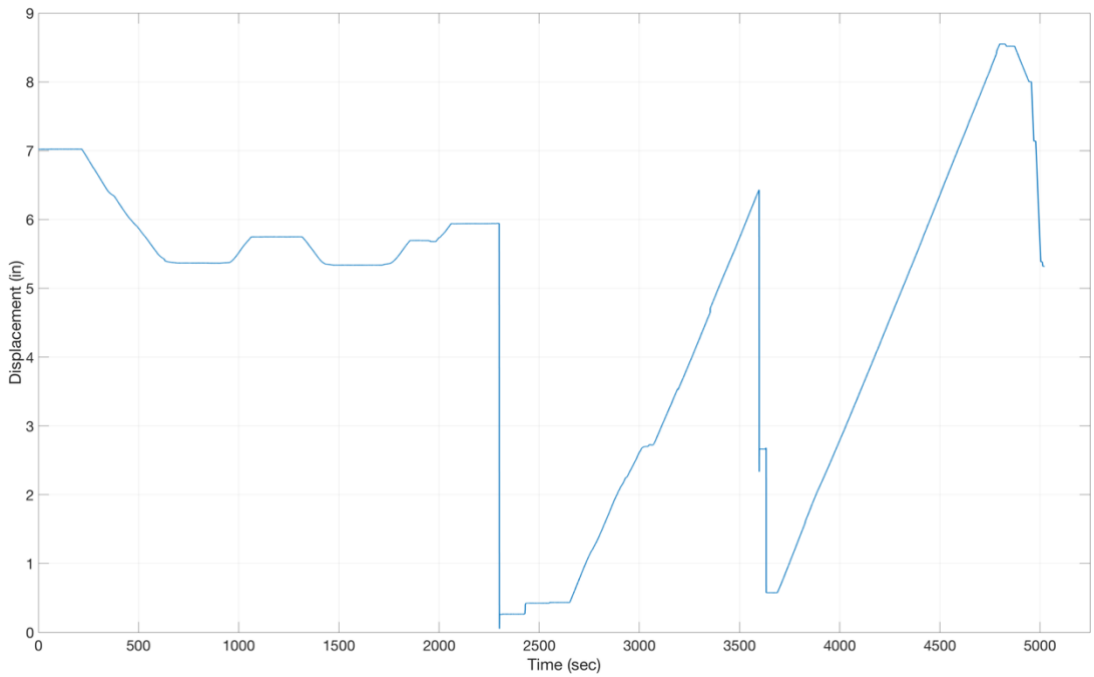

Figure A.16 Uncorrected displacement-time relationship for string potentiometer SP07 at Specimen 1.

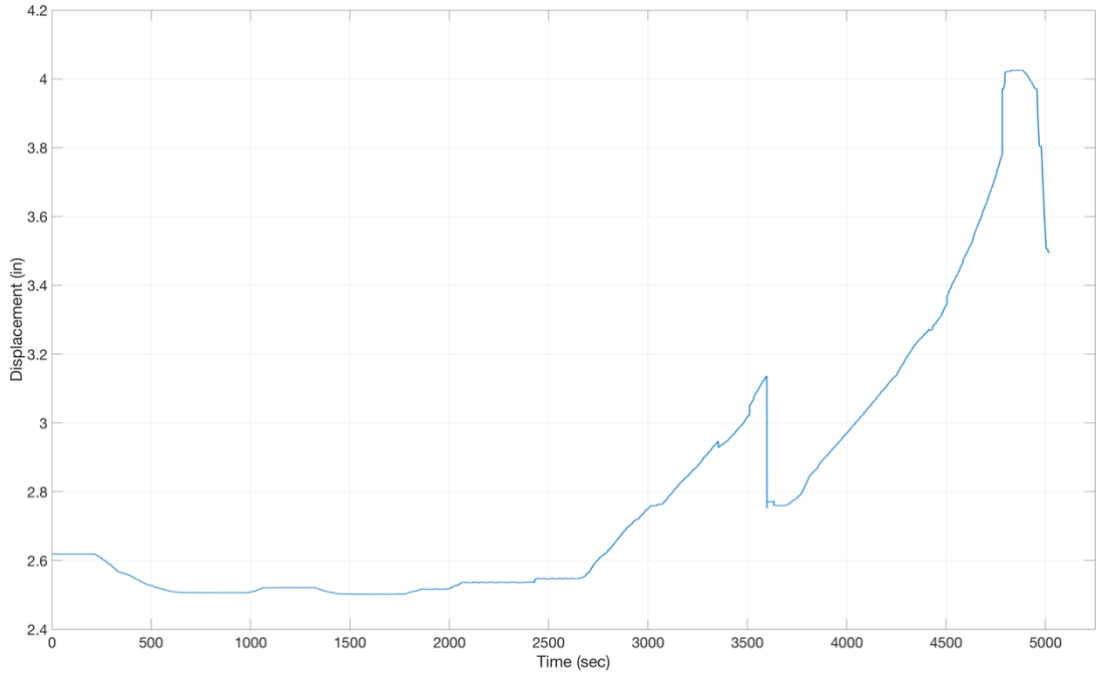

Figure A.17 Uncorrected displacement-time relationship for string potentiometer SP08 at Specimen 1.

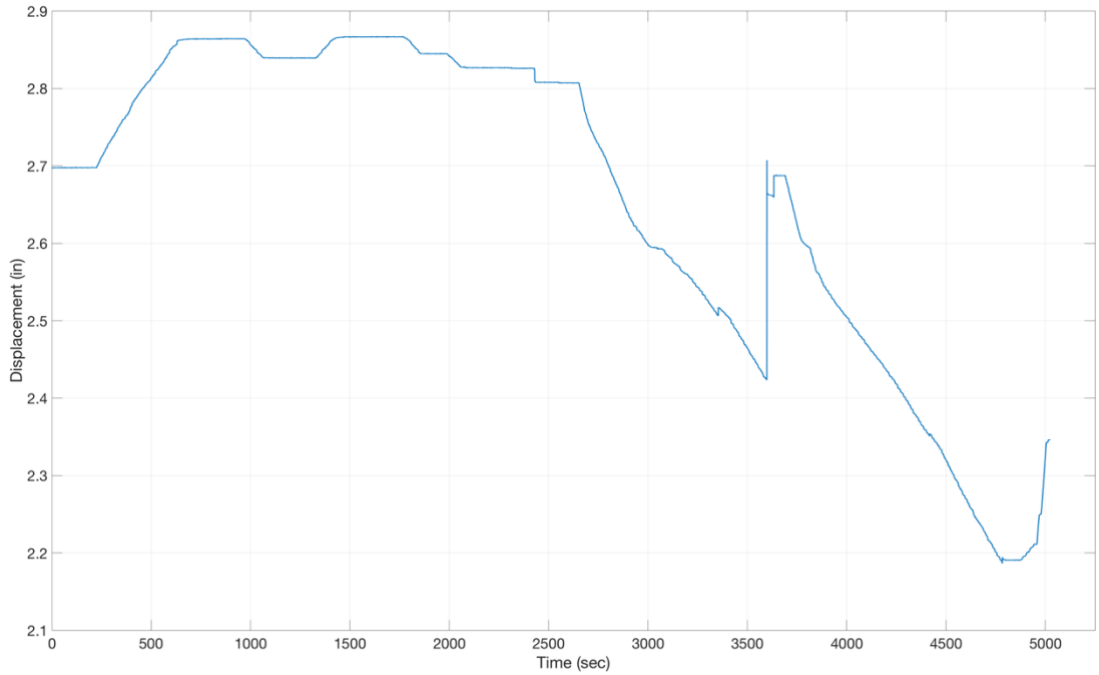

Figure A.18 Uncorrected displacement-time relationship for string potentiometer SP09 at Specimen 1.

Corrected displacement data for each string potentiometer used in Specimen 2.

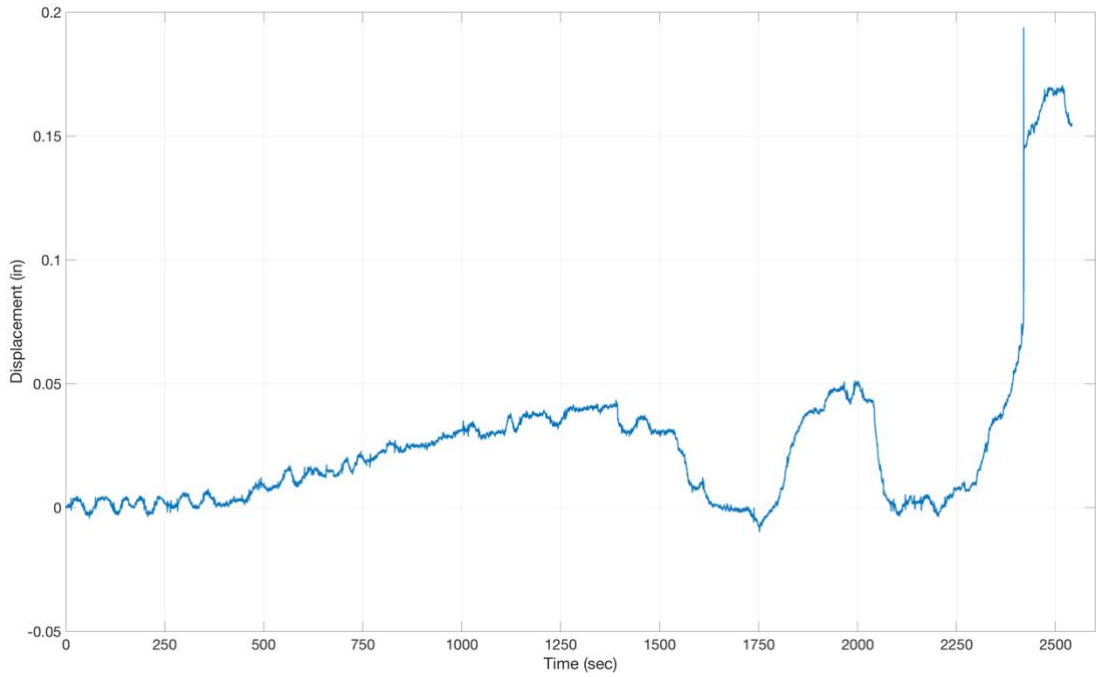

Figure A.19 Corrected displacement-time relationship for string potentiometer SP01 at Specimen 2.

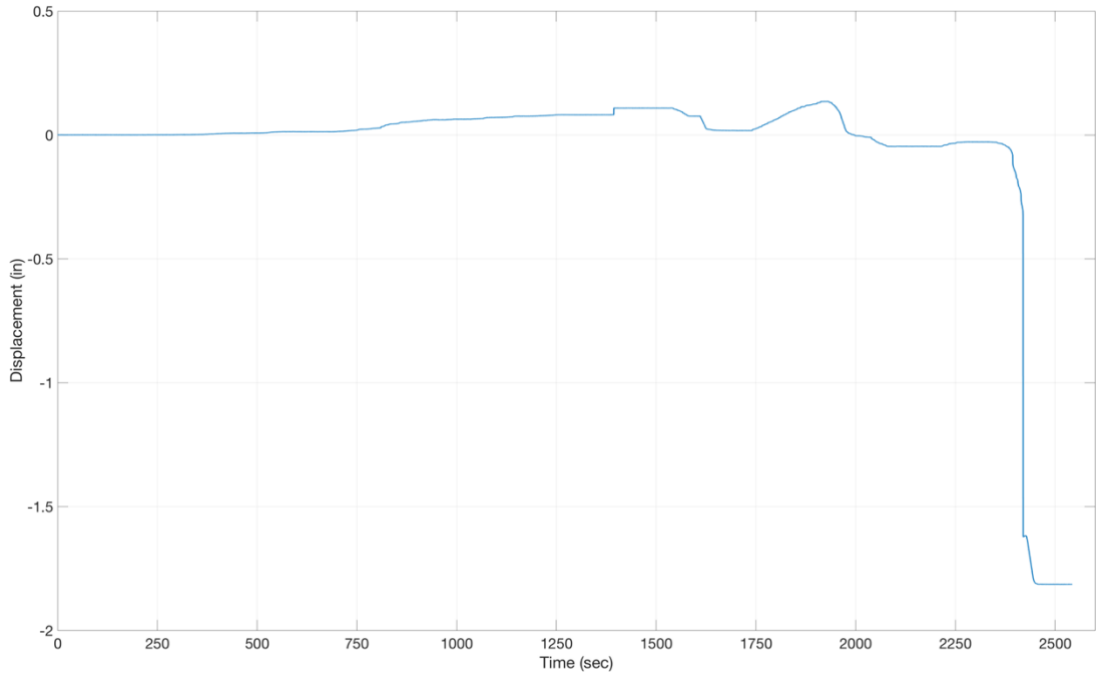

Figure A.20 Corrected displacement-time relationship for string potentiometer SP02 at Specimen 2.

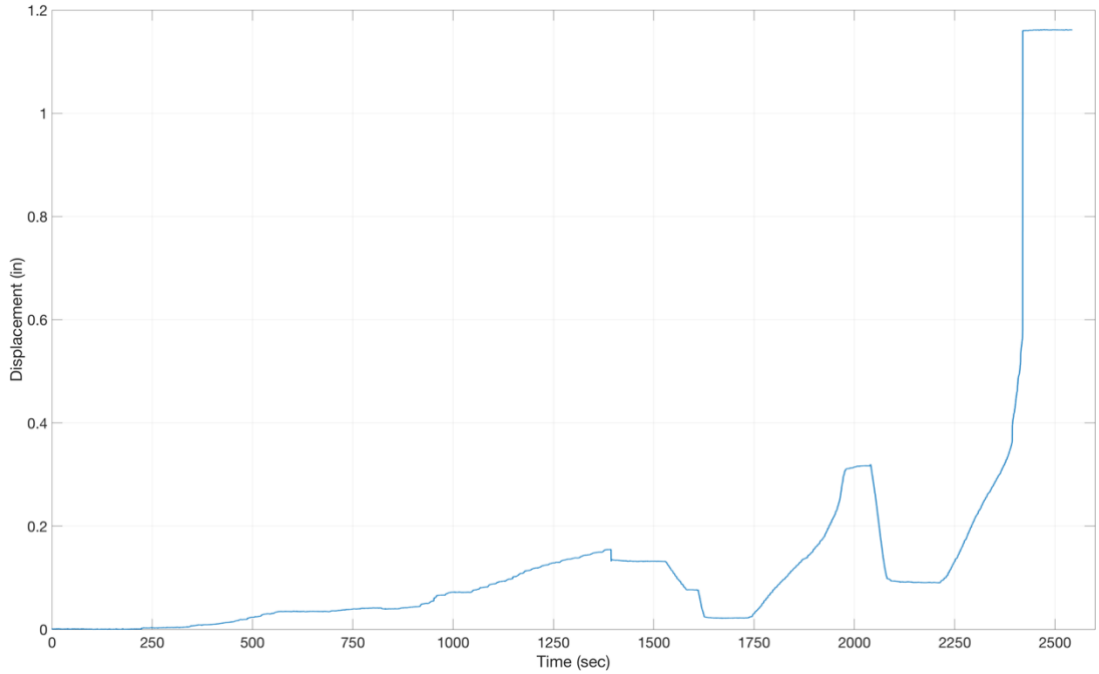

Figure A.21 Corrected displacement-time relationship for string potentiometer SP03 at Specimen 2.

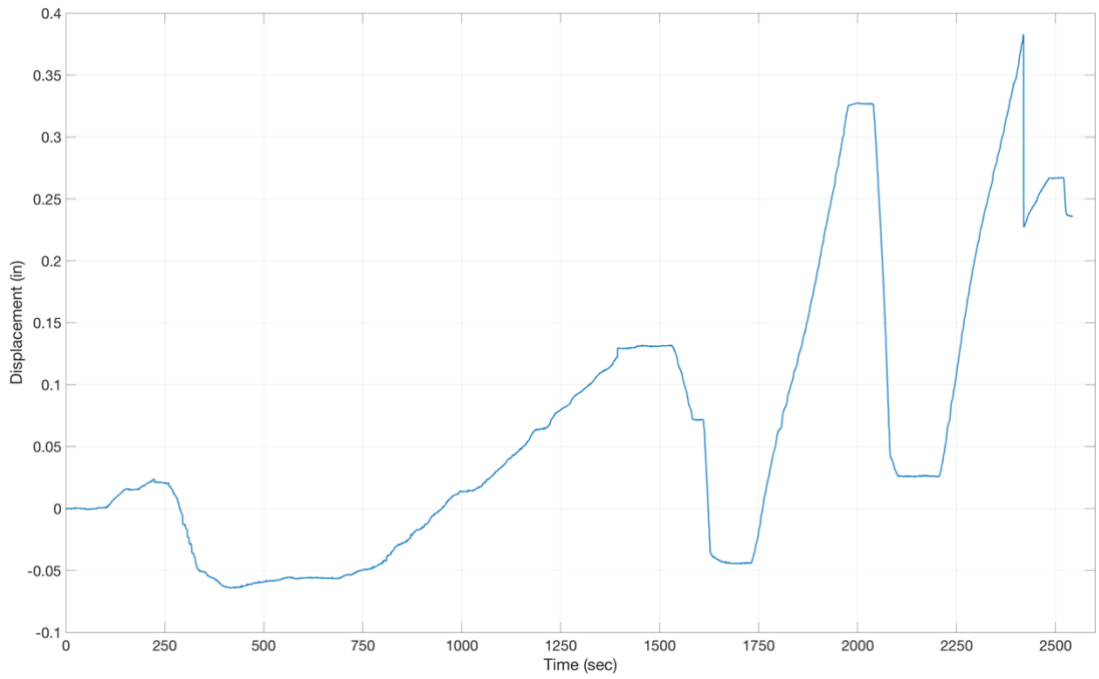

Figure A.22 Corrected displacement-time relationship for string potentiometer SP04 at Specimen 2.

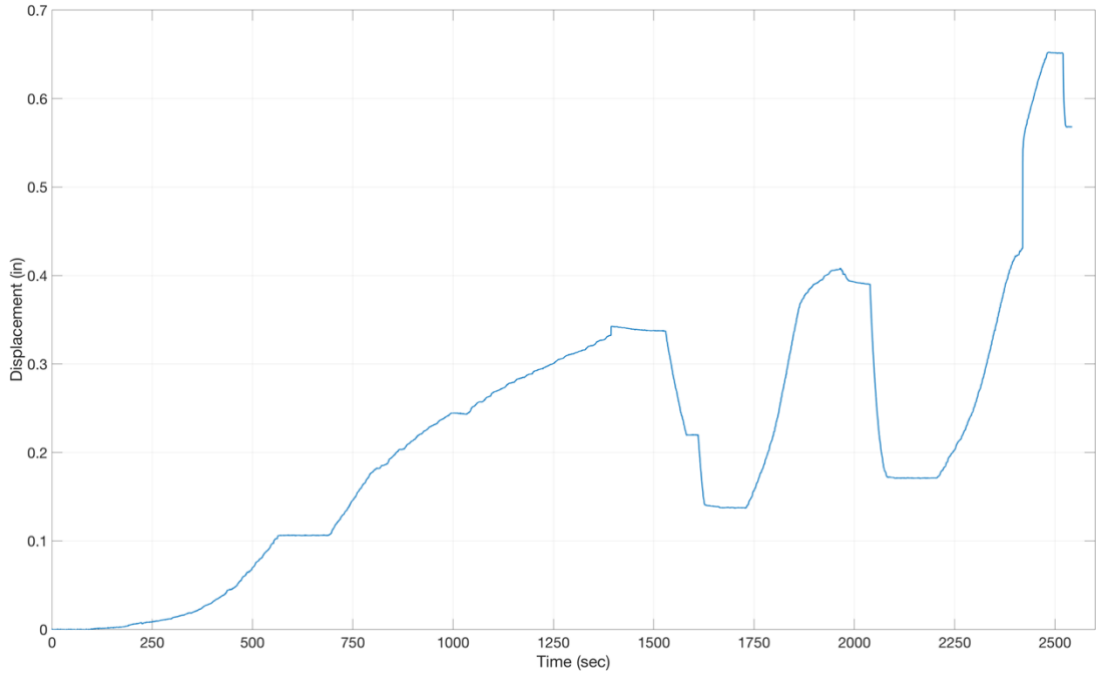

Figure A.23 Corrected displacement-time relationship for string potentiometer SP05 at Specimen 2.

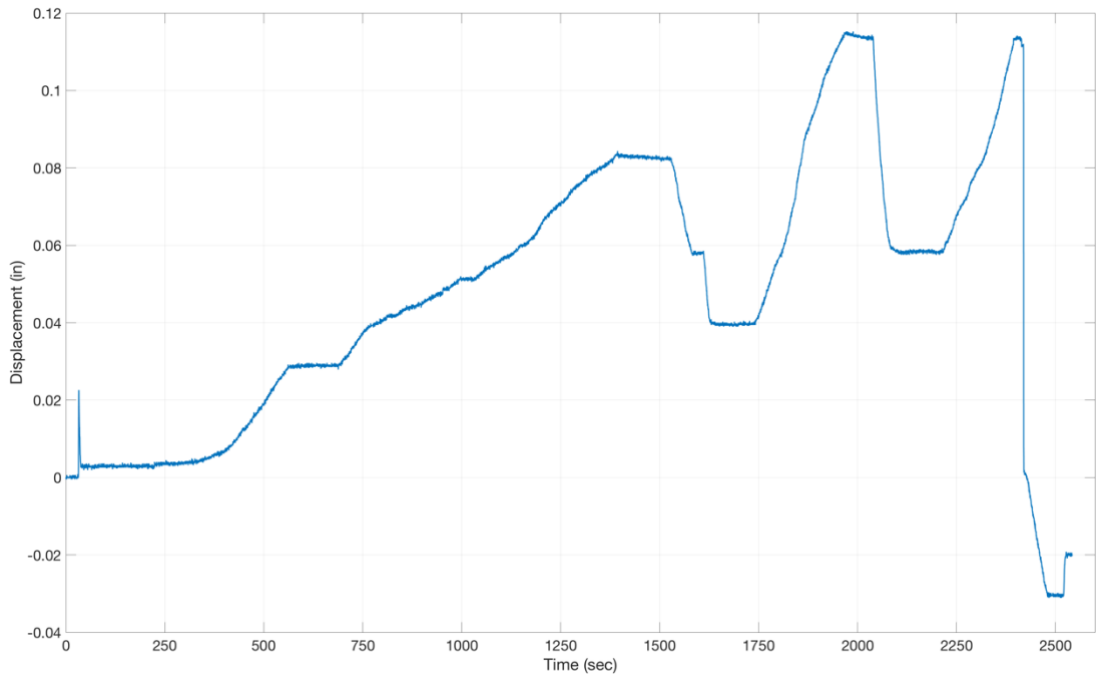

Figure A.24 Corrected displacement-time relationship for string potentiometer SP06 at Specimen 2.

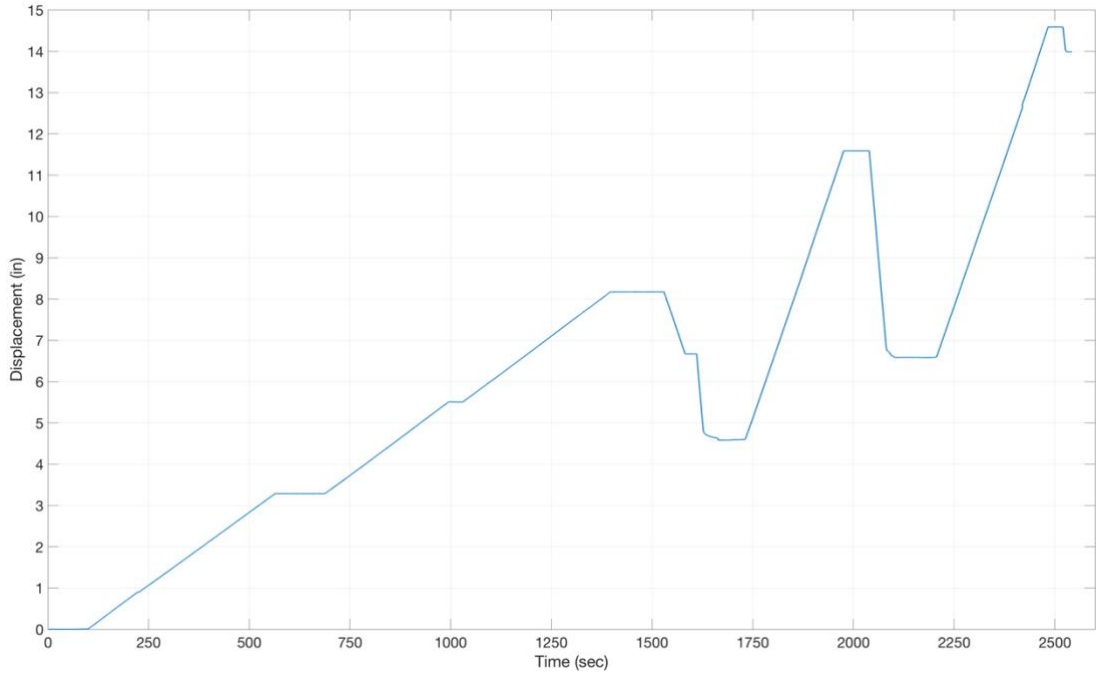

Figure A.25 Corrected displacement-time relationship for string potentiometer SP07 at Specimen 2.

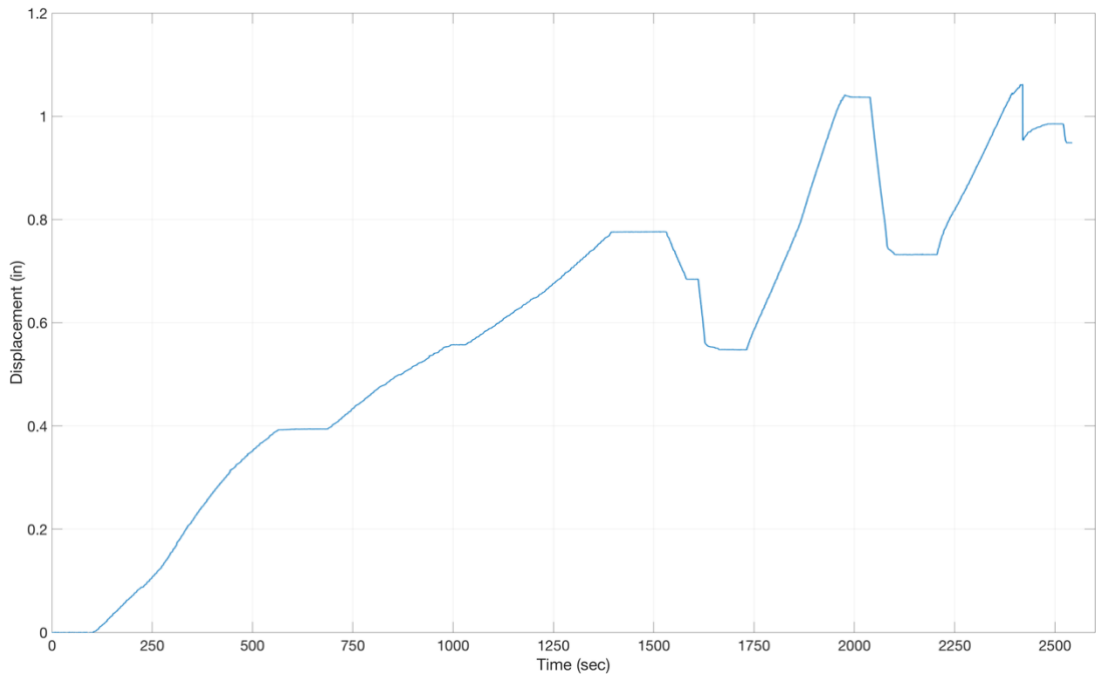

Figure A.26 Corrected displacement-time relationship for string potentiometer SP08 at Specimen 2.

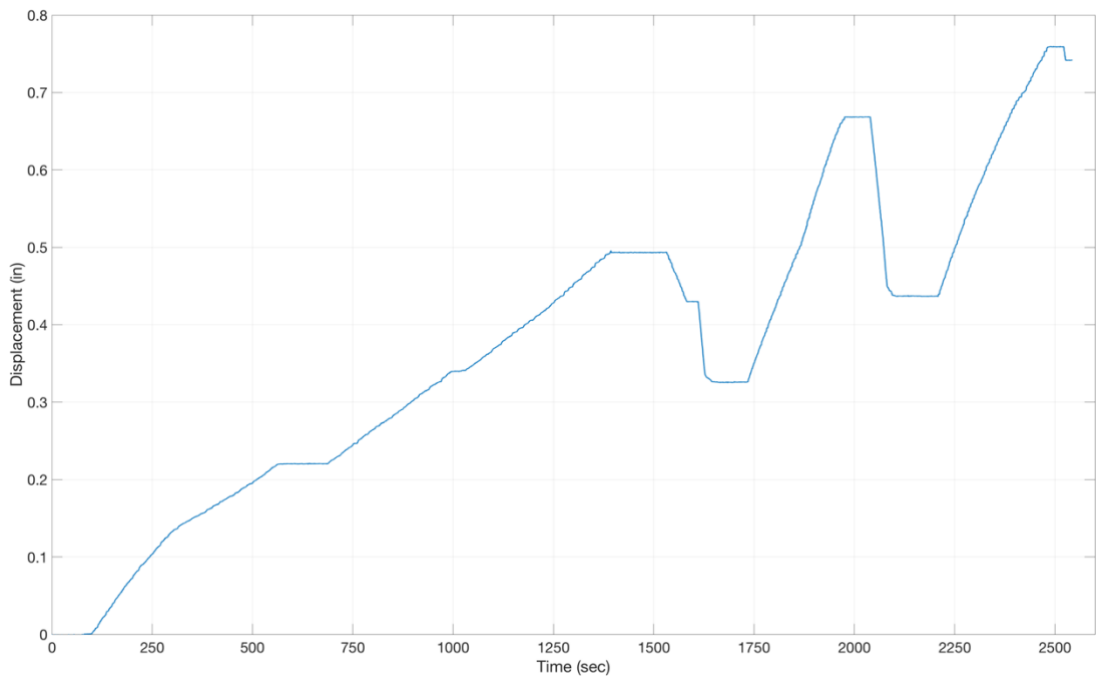

Figure A.27 Corrected displacement-time relationship for string potentiometer SP09 at Specimen 2.

Original (uncorrected) displacement data for each string potentiometer used in Specimen 2.

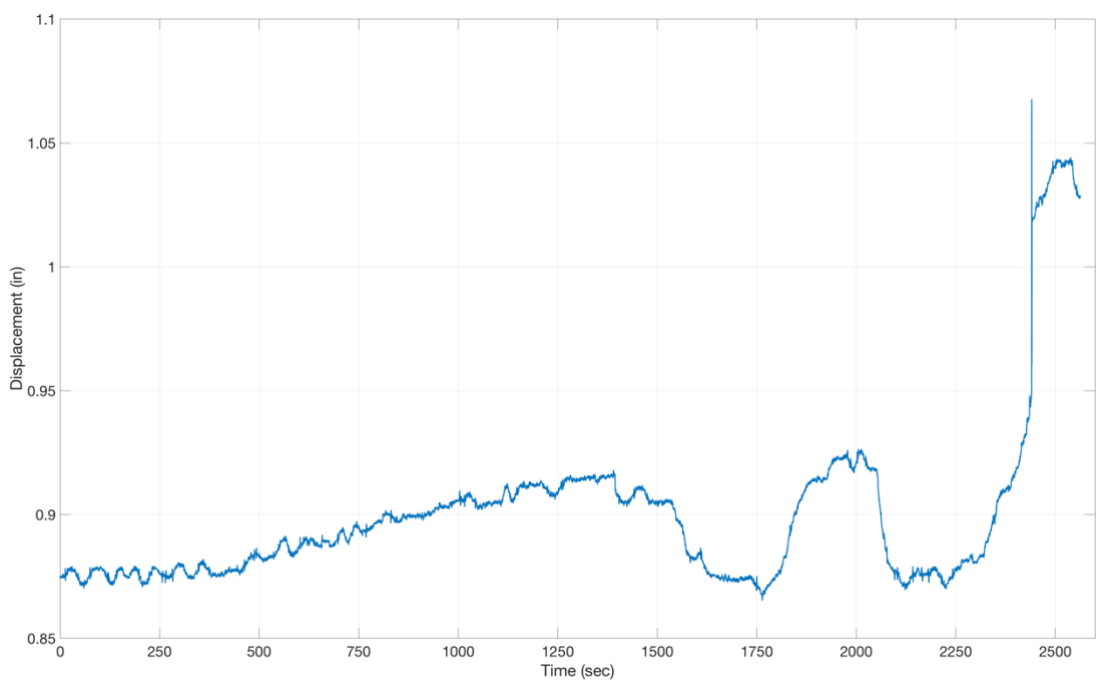

Figure A.28 Uncorrected displacement-time relationship for string potentiometer SP01 at Specimen 2.

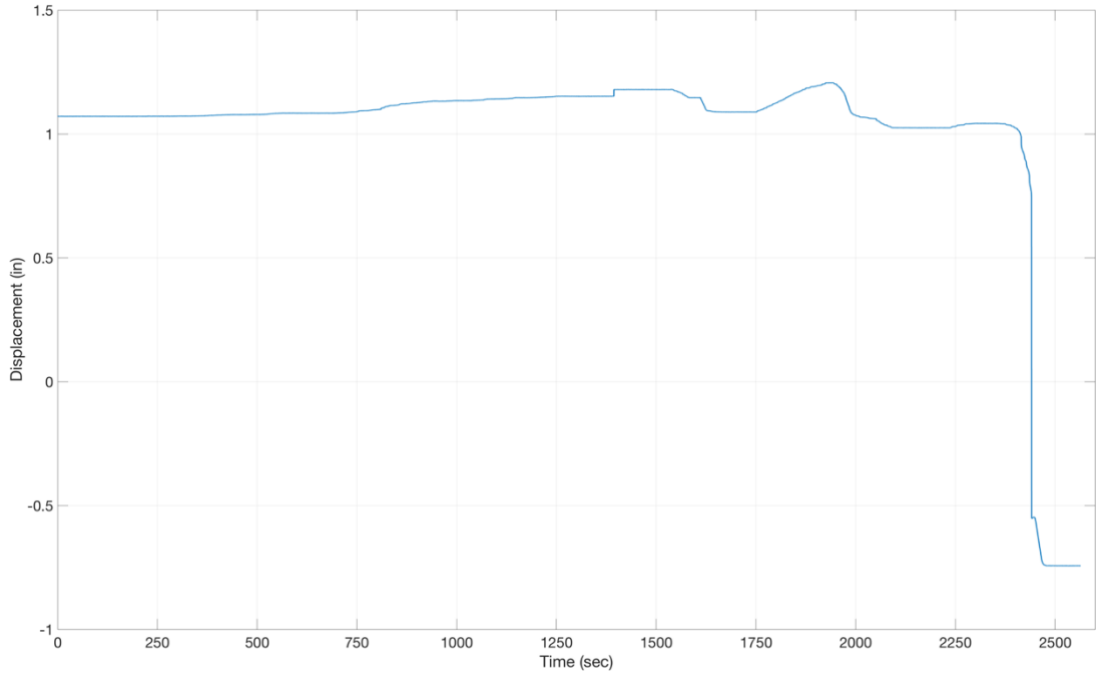

Figure A.29 Uncorrected displacement-time relationship for string potentiometer SP02 at Specimen 2.

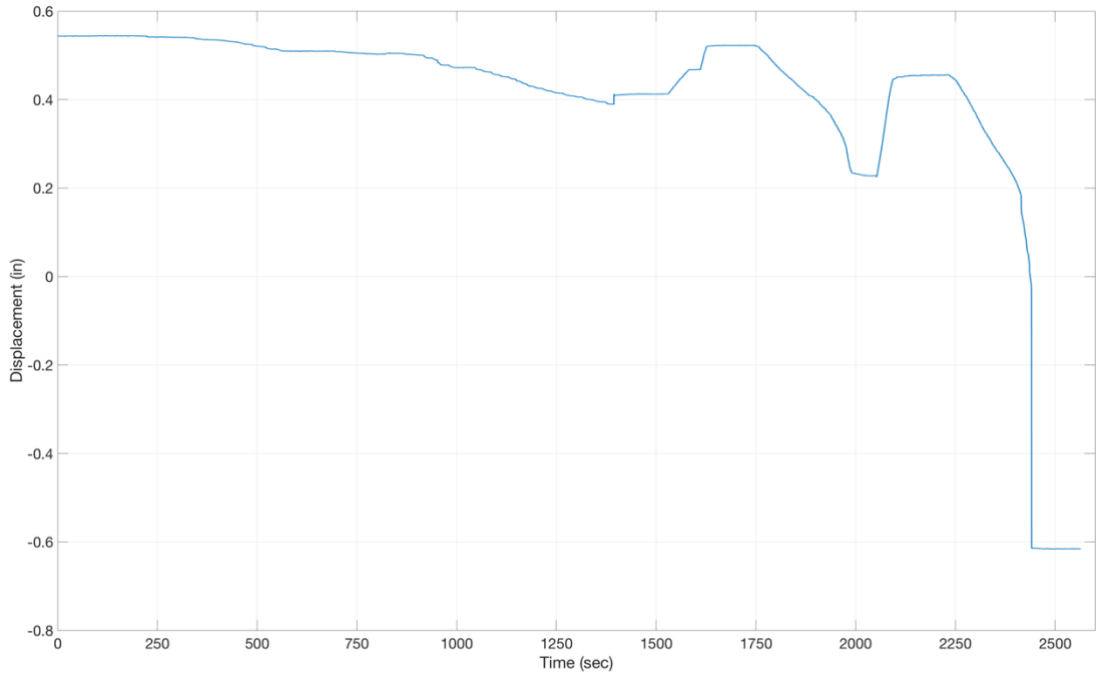

Figure A.30 Uncorrected displacement-time relationship for string potentiometer SP03 at Specimen 2.

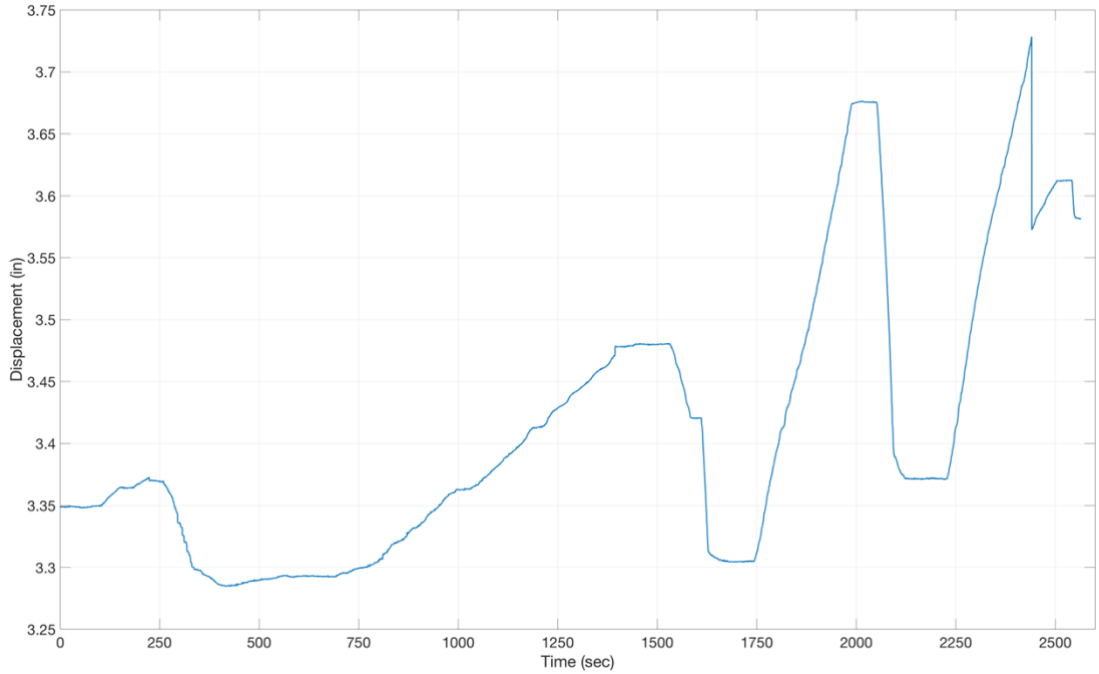

Figure A.31 Uncorrected displacement-time relationship for string potentiometer SP04 at Specimen 2.

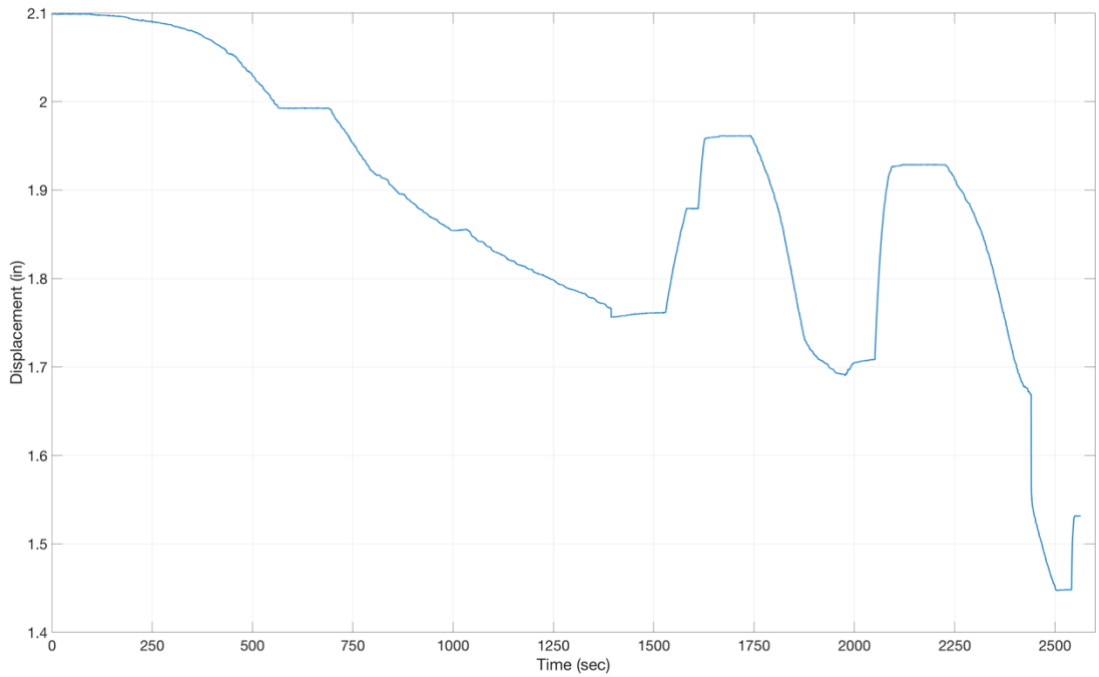

Figure A.32 Uncorrected displacement-time relationship for string potentiometer SP05 at Specimen 2.

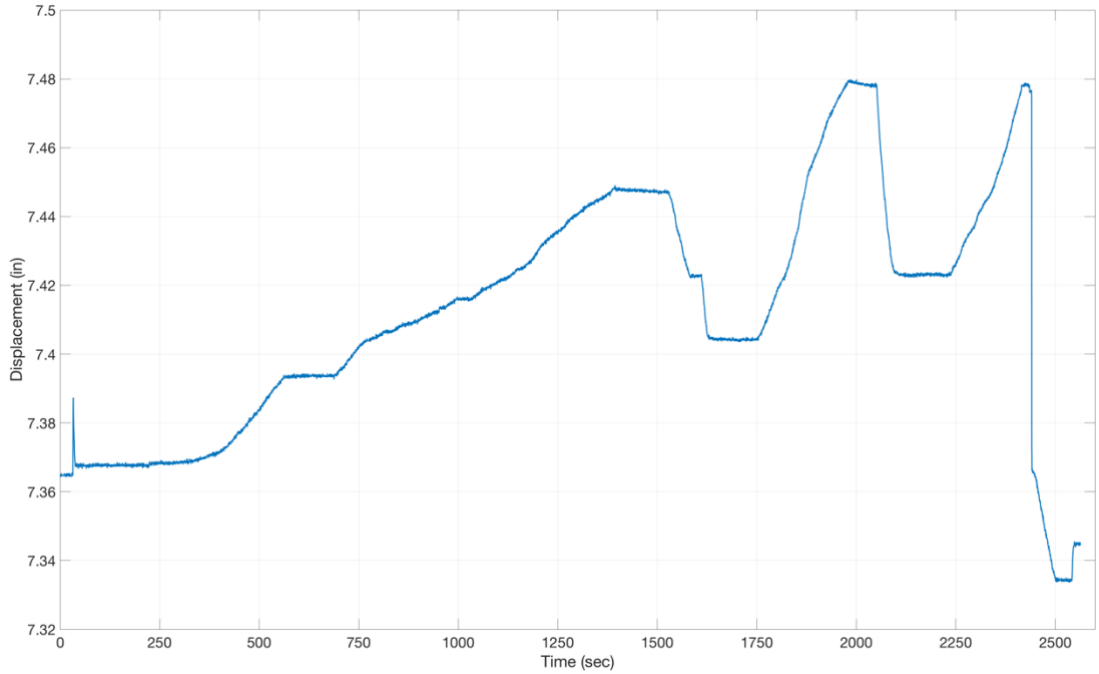

Figure A.33 Uncorrected displacement-time relationship for string potentiometer SP06 at Specimen 2.

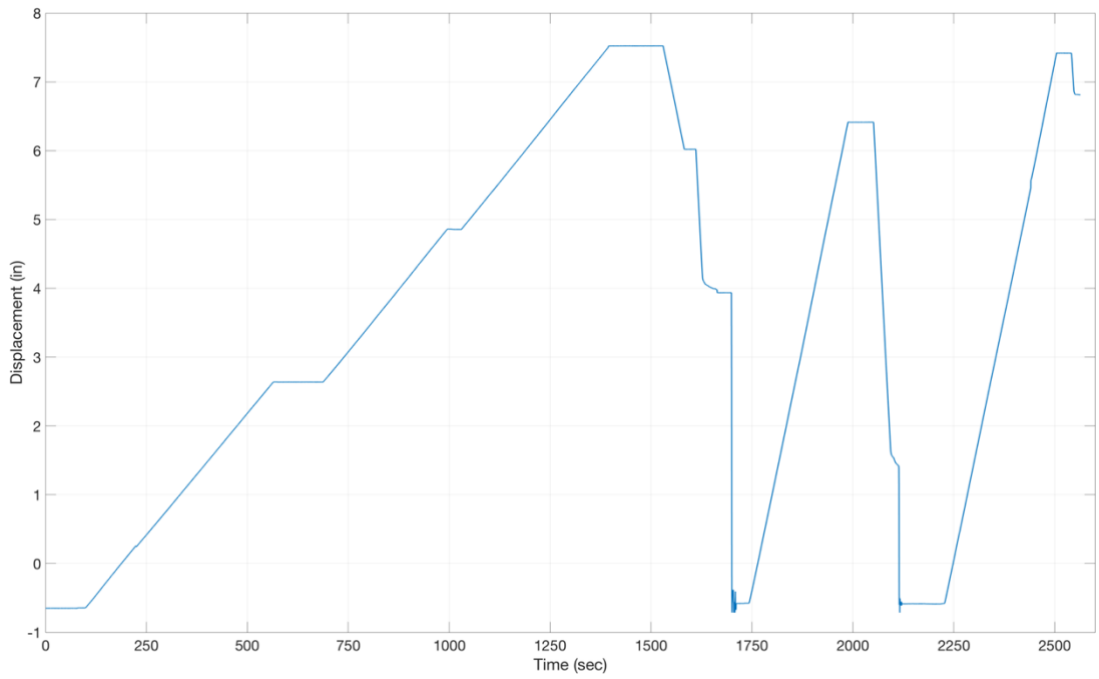

Figure A.34 Uncorrected displacement-time relationship for string potentiometer SP07 at Specimen 2.

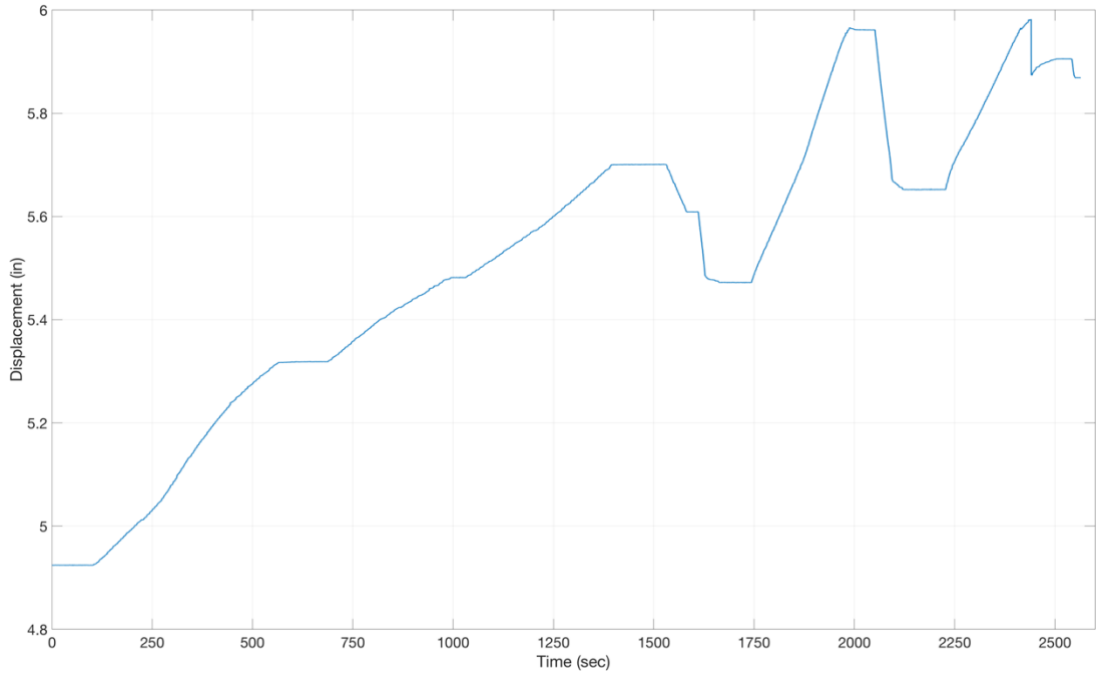

Figure A.35 Uncorrected displacement-time relationship for string potentiometer SP08 at Specimen 2.

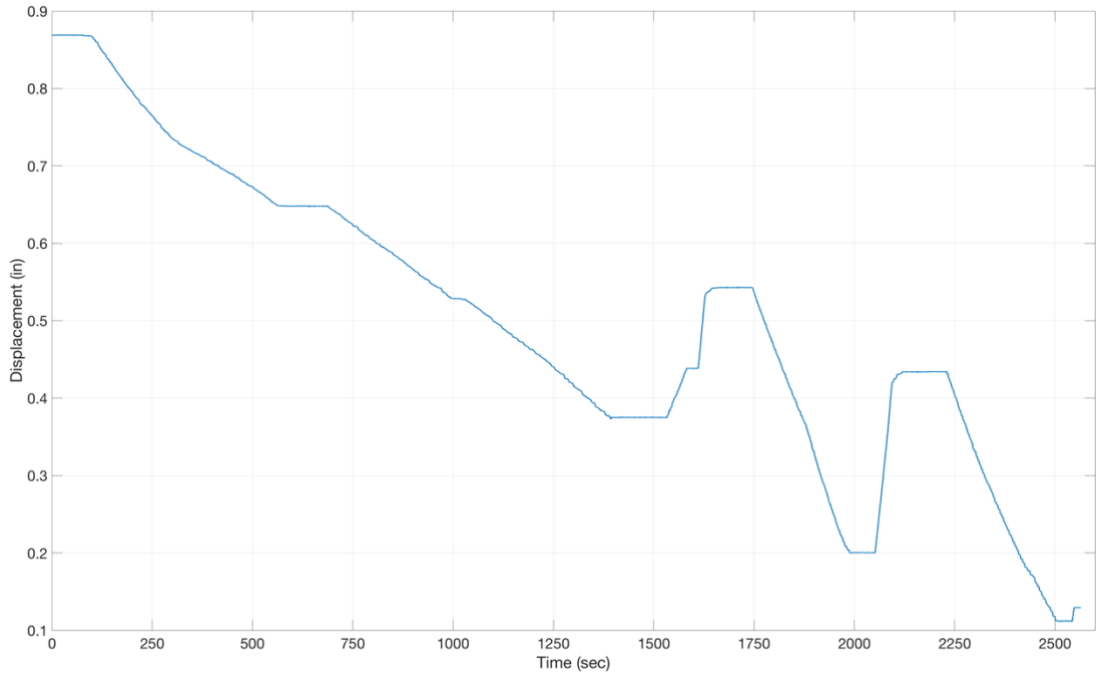

Figure A.36 Uncorrected displacement-time relationship for string potentiometer SP09 at Specimen 2.